METASTABLE MANTLE PHASE TRANSFORMATIONS AND DEEP EARTHQUAKES IN SUBDUCTING OCEANIC LITHOSPHERE

Stephen H. Kirby
U.S. Geological Survey
Menlo Park, California

Seth Stein and Emile A. Okal
Department of Geological Sciences
Northwestern University
Evanston, Illinois

David C. Rubie
Bayerisches Geoinstitut
Universität Bayreuth
Bayreuth, Germany

The author found some earthquakes of different character which occasionally occurred in our country. They are noticed by their particular type showing in the seismograms and giving rise to an abnormal distribution of seismic intensity. The depths of these earthquakes were estimated to be over 300 km, by the time observations of seismic waves.... This is a surprising result comparing with the formerly conceived shallow earthquakes.

Kiyoo Wadati (1902–1995) [*Wadati*, 1928, p. 162]

At the two margins of a downgoing lithosphere, the olivine → spinel transition is so rapid that deep penetration of olivine into the spinel field, which is required to generate deep-focus earthquakes, becomes impossible. However, at the cold interior of the downgoing slab, metastable olivine can penetrate very deeply into the spinel field.

Roger Burns (1937–1994) [*Sung and Burns*, 1976a, p. 25]

Abstract. Earth's deepest earthquakes occur as a population in subducting or previously subducted lithosphere at depths ranging from about 325 to 690 km. This depth interval closely brackets the mantle transition zone, characterized by rapid seismic velocity increases resulting from the transformation of upper mantle minerals to higher-pressure phases. Deep earthquakes thus provide the primary direct evidence for subduction of the lithosphere to these depths and allow us to investigate the deep thermal, thermodynamic, and mechanical ferment inside slabs. Numerical simulations of reaction rates show that the olivine → spinel transformation should be kinetically hindered in old, cold slabs descending into the transition zone. Thus wedge-shaped zones of metastable peridotite probably persist to depths of more than 600 km. Laboratory deformation experiments on some metastable minerals display a shear instability called transformational faulting. This instability involves sudden failure by localized superplasticity in thin shear zones where the metastable host mineral transforms to a denser, finer-grained phase. Hence in cold slabs, such faulting is expected for the polymorphic reactions in which olivine transforms to the spinel structure and clinoenstatite transforms to ilmenite. It is thus natural to hypothesize that deep earthquakes result from transformational faulting in metastable peridotite wedges within cold slabs. This consideration of the mineralogical states of slabs augments the traditional largely thermal view of slab processes and explains some previously enigmatic slab features. It explains why deep seismicity occurs only in the approximate depth range of the mantle transition zone, where minerals in downgoing slabs should transform to spinel and ilmenite structures. The onset of deep shocks at about 325 km is consistent with the onset of metastability near the equilibrium phase boundary in the slab. Even if a slab penetrates into the lower mantle, earthquakes should cease at depths near 700 km, because the seismogenic phase transformations in the slab are completed or can no longer occur. Substantial metastability is expected only in old, cold slabs, consistent with the observed restriction of deep earthquakes to those settings. Earthquakes should be restricted to the cold cores of slabs, as in any model in which the seismicity is temperature controlled, via the distribution of metastability. However, the geometries of recent large deep earthquakes pose a challenge for any such models. Transformational faulting may give insight into why deep shocks lack appreciable aftershocks and why their source characteristics, including focal mechanisms indicating localized shear failure rather than implosive deformation, are so similar to those of shallow earthquakes. Finally, metastable phase changes in slabs would produce an internal source of stress in addition to those due to the weight of the sinking slab. Such internal stresses may explain the occurrence of earthquakes in portions of lithosphere which have foundered to the bottom of the transition zone and/or are detached from subducting slabs. Metastability in downgoing slabs could have considerable geodynamic significance. Metastable wedges would reduce the negative buoyancy of slabs, decrease the driving force for subduction, and influence the state of stress in slabs. Heat released by metastable phase changes would raise temperatures within slabs and facilitate the transformation of spinel to the lower mantle mineral assemblage, causing slabs to equilibrate more rapidly with the ambient mantle and thus contribute to the cessation of deep seismicity. Because wedge formation should occur only for fast subducting slabs, it may act as a "parachute" and contribute to regulating plate speeds. Wedge formation would also have consequences for mantle evolution because the density of a slab stagnated near the bottom of the transition zone would increase as it heats up and the wedge transforms to denser spinel, favoring the subsequent sinking of the slab into the lower mantle.

Reviews of Geophysics, 34, 2 / *May 1996*
pages 261–306
8755-1209/96/96RG-01050*$15.00*
Paper number 96RG01050

1. INTRODUCTION

Definitions of technical terms and mineral names may be found in the glossary at the end of this paper.

1.1. Global Deep Earthquake Setting

Greater interest in deep earthquakes has recently been stimulated by the occurrence of the exceptionally large June 9, 1994, earthquake 635 km beneath northern Bolivia. It was the largest deep earthquake in the modern instrumental record with seismic magnitude of 8.2 and seismic moment of 2.7×10^{28} dyn cm [*Dziewonski et al.*, 1995] (Table 1). Deep earthquakes occur in very restricted environments, in contrast to shallow earthquakes which, although localized mostly at plate boundaries, are distributed over much of Earth's surface (Figure 1). Deep earthquakes typically occur in dipping, planar bands known as Wadati-Benioff zones, which can extend to nearly 700 km depth. Explaining how and why such shocks occur is a classic problem of geophysics [e.g., *Griggs and Handin*, 1960; *Griggs and Baker*, 1968; *Frohlich*, 1987a, 1989; *Kirby et al.*, 1991; *Green*, 1994].

1.2. Deep Earthquakes and Slabs

With the discovery of plate tectonics, it was recognized that Wadati-Benioff zones mark locations where slabs of oceanic lithosphere sink into the deep mantle. Although deep earthquakes represent only a few percent of global seismic activity, estimated from either numbers of earthquakes or seismic moments, they are important because they provide direct information about the subducting lithosphere. Their occurrence supports thermal models showing that slabs subduct rapidly compared to the time needed for heat conducted from the surrounding mantle to warm them up and thus should remain colder, denser, and stronger than "normal" mantle [*Orowan*, 1965; *McKenzie*, 1969; *Minear and Toksöz*, 1970; *Griggs*, 1972]. Consequently, slabs transmit seismic waves faster and with less attenuation than the surrounding mantle [*Utsu*, 1967, 1971; *Oliver and Isacks*, 1967; *Isacks et al.*, 1968; *Mitronovas and Isacks*, 1971; *Sleep*, 1973; *Jordan*, 1977; *Creager and Jordan*, 1986; *Cormier*, 1989], making it possible to derive detailed maps of slabs by seismic methods and to show that deep earthquakes occur within them [e.g., *van der Hilst et al.*, 1991; *Fukao et al.*, 1992] (Plate 1). The focal mechanisms of deep earthquakes, which generally show downdip compression, suggested that negative thermal buoyancy of slabs provides a major source of stress within them [e.g., *Isacks and Molnar*, 1971; *Richter*, 1979; *Davies*, 1980; *Wortel and Vlaar*, 1988; *Vassiliou and Hager*, 1988] and is the primary force driving plate motions [e.g., *Forsyth and Uyeda*, 1975]. The concentration of deep earthquakes near 600 km depth, their focal mechanisms, and results from seismic tomography all suggest that slabs encounter resistance to their descent into the lower mantle and, consequently, often deform at depth [e.g., *Isacks et al.*, 1968; *Giardini and Woodhouse*, 1986; *Bevis*, 1988; *van der Hilst et al.*, 1991; *Tao and O'Connell*, 1993]. Deep earthquakes thus provide important constraints on the downgoing limbs of the mantle convection system where oceanic lithosphere returns to the deep mantle [e.g., *Peltier*, 1989].

That deep earthquakes are restricted to downgoing slabs implies more about slabs than simply that they are colder than normal mantle. Seismic failure in slabs is surprising, because deep earthquakes occur at depths as great as 690 km where pressures approach 24 GPa and temperatures may be 500°–700°C. Because laboratory experiments suggest that such conditions should favor aseismic ductile deformation rather than brittle failure [e.g., *Griggs*, 1972; *Kirby*, 1987; *Kirby et al.*, 1991; *Burnley et al.*, 1991], it has been unclear how deep earthquakes can occur at all.

A crucial observation bearing on this question is that deep seismicity is not only restricted to downgoing slabs, it is restricted to the 300–350 to 690 km depth range within them (Figure 2a). This depth range closely brackets the mantle transition zone, defined by rapid seismic velocity increases at approximately 410 and 660 km, which separates the upper from the lower mantles (Figure 2b) [e.g., *Bina*, 1991]. These velocity discontinuities are presumed to correspond to the near-equilibrium phase boundaries separating the primary upper mantle minerals (olivine (α-phase) and pyroxenes) from the denser minerals in the transition zone (β phase (modified spinel), γ phase (spinel), majorite garnet, stishovite, and/or ilmenite) and those in the lower mantle (perovskites and magnesiowüstite, a Mg-Fe oxide) [*Akaogi et al.*, 1989; *Katsura and Ito*, 1989].

It is thus natural to consider that deep earthquakes are somehow associated with phase changes occurring as peridotite in the subducting slab passes through the transition zone [*Griggs*, 1954; *Isacks et al.*, 1968; *Vaisnys and Pilbeam*, 1976; *Kostoglodov*, 1989]. Because slabs are much colder than their surroundings and reaction rates are expected to be sluggish, *Sung and Burns* [1976a, b] proposed that in the coldest parts of fast subducting slabs the phase transformation rates may not keep pace with the slab descent rate. Hence a wedge-shaped region of metastable olivine would extend considerably deeper in the slab than the 410-km depth of the equilibrium transition of olivine to spinel outside the slab (Figure 2c). This hypothesis is supported by recent theoretical and experimental results, which show that the reaction would be kinetically hindered in the cold interiors of some subducting slabs [*Rubie and Ross*, 1994].

The idea that deep earthquakes result from metastable mantle phase changes was previously rejected because deep earthquake focal mechanisms generally indicate faulting (i.e., localized shear failure) rather than the implosive deformation expected for bulk transformation to denser phases [e.g., *Sykes*, 1968; *Kawakatsu*, 1991]. In the last decade, however, laboratory experiments have shown that under metastable conditions, some minerals partially transform to denser phases by a

TABLE 1. The 10 Largest (for Which Seismic Moment Has Been Well Determined) Deep Earthquakes Sorted by Decreasing Seismic Moment at Depths >400 km, 1921–1994

Rank	*Date*	*Region*	*Depth,[a] km*	*Moment, dyn cm*	*Reference*	*Aftershock Moments,[c] %*
1	June 9, 1994	NW Bolivia	636	2.7×10^{28}	1	0.6
2	July 31, 1970	southern Colombia	648	2.0×10^{28}	2	0
3/4	Jan. 17, 1922	Peru-Colombia	637	7.1×10^{27}	3	ND
3/4	March 29, 1954	southern Spain	626	7.1×10^{27}	4	0
5	Sept. 29, 1973	Sea of Japan	574	6.8×10^{27}	5	~0
6[b]	Aug. 15, 1963	Peru-Bolivia	570	4.2×10^{27}	2, 6	0
7[b]	Nov. 9, 1963	Peru-Brazil	571	3.2×10^{27}	6	0
8	March 9, 1994	Tonga-Fiji	562	2.8×10^{27}	1	1.3
9	July 26, 1958	Peru-Bolivia, South America	600	2.6×10^{27}	6	0
10	Dec. 18, 1921	Peru-Colombia	628	1.5×10^{27}	3	ND

References: 1, Harvard CMT [*Dziewonski et al.*, 1995]; 2, *Gilbert and Dziewonski* [1975]; 3, *Okal and Bina* [1994] (event 10 may be considered a foreshock to event 3; no other well-located deep earthquakes has occurred subsequently in region of their hypocenters); 4, *Chung and Kanamori* [1976]; 5, *Furumoto and Fukao* [1976]; and 6, *Huang et al.* [1994].

[a]*Kirby et al.* [1995a] and unpublished depths from the hypocenter catalogue of E. R. Engdahl.

[b]The large South American shocks of August 19, 1961 and doublet of August 31, 1961 are not included because of uncertainties in inverting their seismograms for moment tensor. They are roughly comparable in size to the two 1963 deep events beneath South America (3 to 5 × 10^{27} dyn cm).

[c]Ratio of the sum of the seismic moments of well-located aftershocks detected at teleseismic distances (>25°) and the moment of the main shock. This ratio is expressed as a percentage. ND indicates that no aftershocks were detected, but that high detection thresholds existed at the time.

localization of transformation and strain into thin shear zones called transformational faults [*Kirby*, 1987; *Green and Burnley*, 1989; *Kirby et al.*, 1991; *Burnley et al.*, 1991]. Hence a phase transformation involving only a small volume change forms a thin, weak shear zone and rapidly releases large shear strains. This mechanism removes the principal objection to a phase-change origin of deep earthquakes because the radiated seismic energy

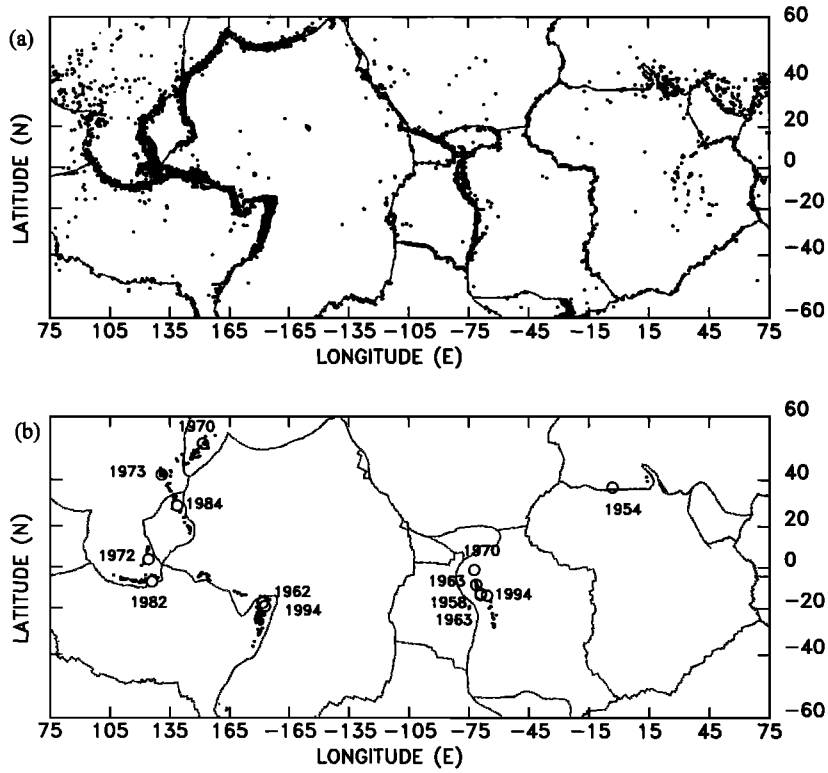

Figure 1. Global epicenter distribution for 1977–1991, taken from the Harvard centroid moment tensor (CMT) catalogue [*Dziewonski et al.*, 1995]. (a) Shallow earthquakes (depths <50 km). (b) Deep earthquakes (depths greater than 300 km). Open circles show the 13 largest deep events from 1954 to 1994 with seismic moments greater than 10^{27} dyn cm (excluding two complex 1961 shocks beneath South America (Table 1)).

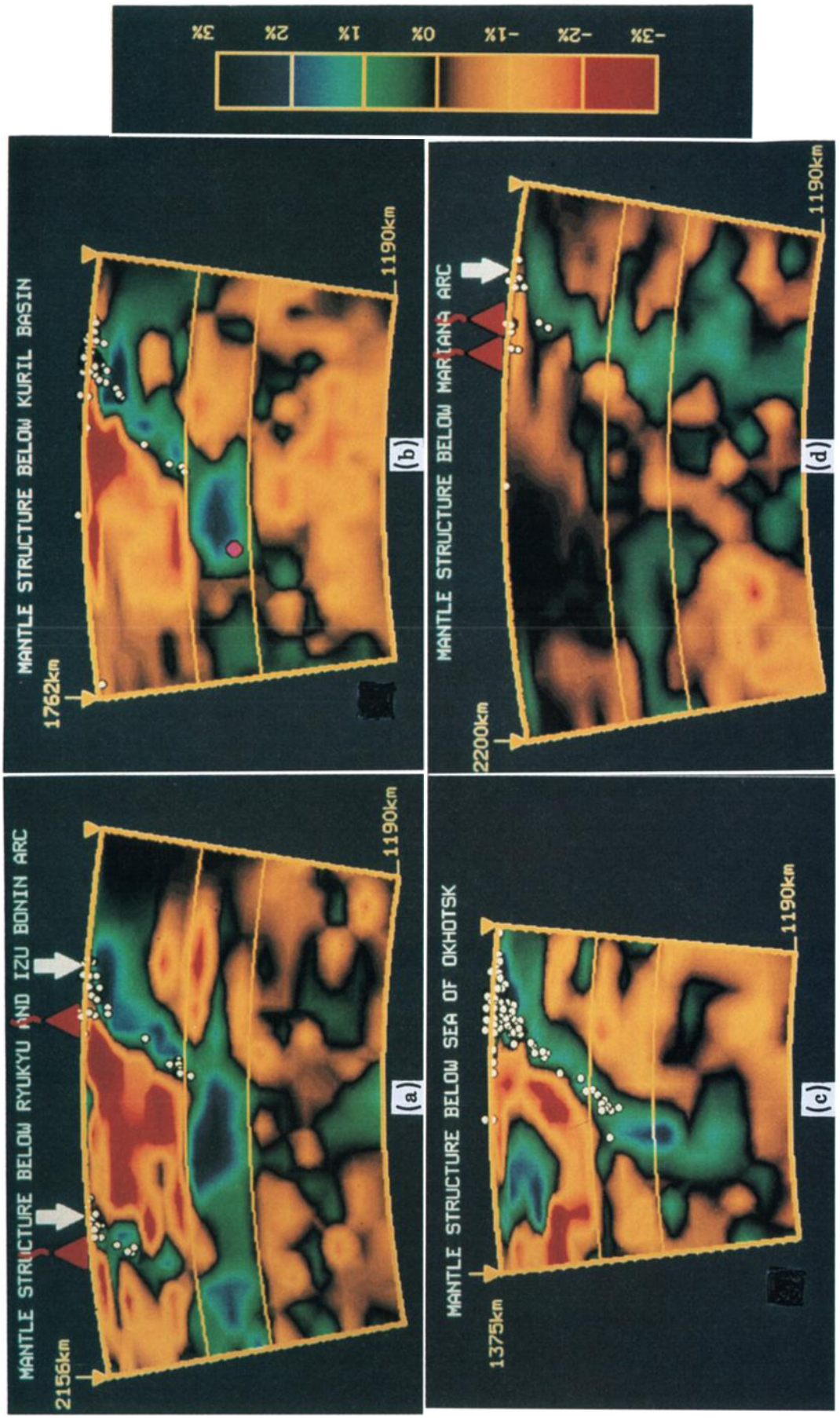

Plate 1. Tomographic images of cross sections across representative northwest Pacific subduction zones with deep earthquakes [from *van der Hilst et al.*, 1991, 1993]. Horizontal lines are at 410 and 660 km depth. White dots are earthquake hypocenters. (a) Central Izu-Bonin. (b) Central Kuriles. (c) Sea of Okhotsk (red dot is hypocenter of a large 1990 deep event). (d) Marianas. The Wadati-Benioff zone earthquakes generally coincide with the high-velocity anomalies that define the subducting Pacific plate. The high-velocity anomalies in Plates 1a and 1b suggest horizontal slab deflection at the bottom of the transition zone, whereas Plates 1c and 1d suggest slab penetration into the lower mantle.

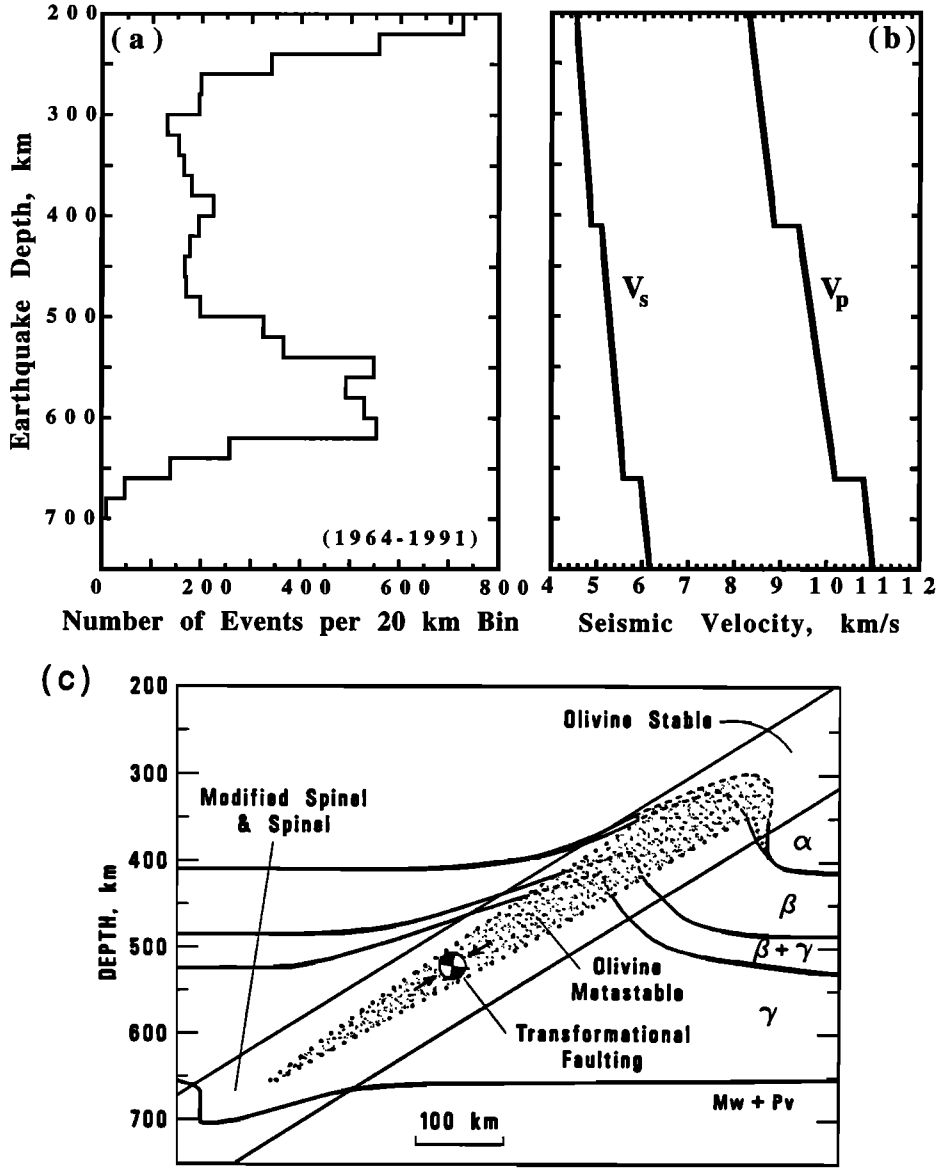

Figure 2. Global variations in deep seismicity, seismic velocity, and mineralogy with depth. (a) Earthquake numbers in 20-km-depth intervals over the time period from 1964 to 1991. (b) Seismic velocities, V_p and V_s, from global velocity model iasp91 [*Kennett and Engdahl*, 1991]. (c) Schematic diagram of the mineralogy in a subducting slab. Pv and Mw denote perovskite and magnesiowüstite [after *Kirby et al.*, 1991].

results from shear across a transformational fault, consistent with the observed focal mechanisms.

1.3. Metastability Hypothesis

In this paper we review and expand on the hypothesis that deep earthquakes occur by transformational faulting in regions of metastable mantle peridotite. We focus on this hypothesis because laboratory results suggest that these changes of state should occur metastably in descending lithosphere and that transformational faulting should result. We will show that this hypothesis makes testable predictions that are in good general agreement with many observed properties of deep earthquakes. In particular, only the coldest slabs have metastable wedges extending into the transition zone, and hence deep earthquakes are restricted to depths corresponding to the transition zone in such slabs, as observed [*Kirby et al.*, 1991].

These predictions result from models of slab thermal structure and reaction kinetics that predict the presence and extent of metastability. Transformational faulting has only been observed in strongly exothermic reactions that are polymorphic. The best candidates for mantle polymorphic reactions are the transformation of olivine to the spinel structure and of clinoenstatite to the ilmenite structure. The region of metastable reaction for olivine, the most abundant phase, begins at the equilibrium phase boundary between olivine and one of its high-pressure polymorphs, spinel or modified spinel (Figure 2c). The equilibrium olivine-spinel boundary may be

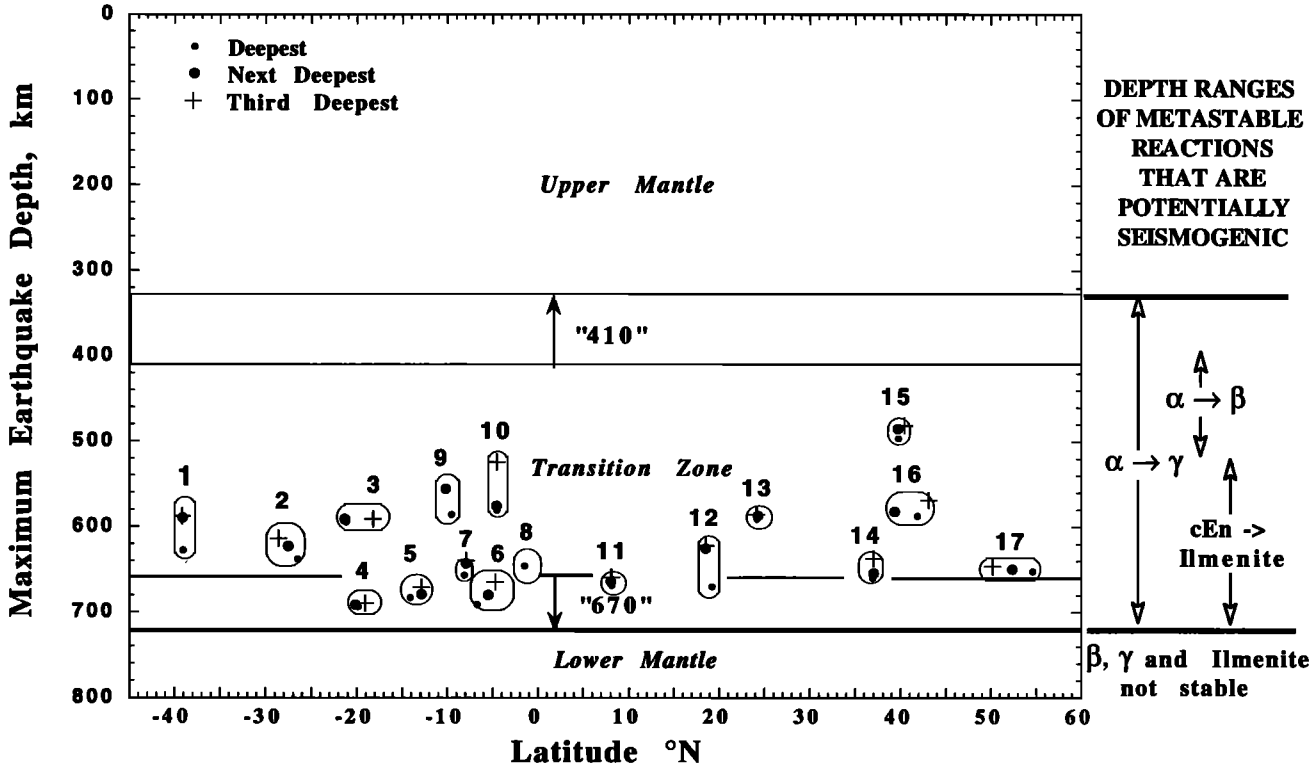

Figure 3. Maximum deep earthquake depths versus latitude for various subduction zones compared to the expected depth ranges of mineral reactions in slabs. Note that over half the examples shown here have maximum depths near the bottom of the transition zone. Depths from an unpublished catalogue of relocated hypocenters (1954–1994) assembled by E. A. Okal, E. R. Engdahl and S. H. Kirby. Legend: 1, New Zealand; 2, South America/Argentina; 3, west of Tonga; 4, Tonga; 5, North Fiji Basin/Vityaz; 6, eastern Indonesia; 7, Peru/Brazil; 8, Colombia; 9, Solomons; 10, Papua New Guinea; 11, Celebes/Mindanao; 12, Marianas; 13, Izu/Bonin; 14, southern Spain; 15, Tyrrhenian Sea; 16, Sea of Japan; 17, Kurile/Kamchatka.

elevated in cold slabs from 410 km in normal mantle to depths as shallow as 350 km because these transitions are exothermic, therefore have positive Clapeyron slopes, and hence occur at lower pressure for lower temperatures [*Turcotte and Schubert*, 1971].

These reactions should not occur in the lower mantle because spinel and ilmenite are no longer stable at those depths, so olivine and clinoenstatite should transform to the more complex multiphase lower mantle assemblage dominated by silicate perovskite. Thus metastable polymorphic reactions should occur no deeper than the maximum depth where spinel and ilmenite are stable in the coldest part of the slab (Figure 3). That depth, about 720 km, should be deeper than the approximately 660-km depth outside slabs, because the reactions forming the lower mantle assemblage have negative Clapeyron slopes. Hence deep earthquakes should be restricted to the depth range 350–720 km, essentially as observed.

In this view, the behavior of a slab depends, in part, on its mineralogical state. We focus here on the region of the slab characterized by the presence of metastable olivine and clinoenstatite. We define this region by the wedge-shaped boundaries bounding the predicted presence of metastable olivine, the primary mineral. The wedge exists at transition zone depths but differs in mineralogy from material at these depths both in the remaining portions of the slab and outside the slab. Deep earthquakes are significant because they indicate the presence of metastable regions, delineate their boundaries, and characterize their deformation. Metastable regions, in turn, differ in temperature, density, and mechanical properties from the rest of the slab and hence have consequences for slab dynamics and evolution.

Large-scale olivine metastability would have major implications for the mantle convection system [e.g., *Silver et al.*, 1988; *Peltier*, 1989]. Although the simplest explanation for the absence of deep earthquakes in the lower mantle (Figure 3) is that slabs do not descend to such depths, seismological observations indicate that many do (e.g., Plates 1c and 1d and *Jordan* [1977], *Creager and Jordan* [1984, 1986], *Fischer et al.* [1988], *van der Hilst et al.* [1991], *Fukao et al.* [1992], *Grand* [1994], *Engdahl et al.* [1995], *Widiyantoro and van der Hilst* [1996]). These observations are consistent with the cessation of deep earthquakes being controlled mineralogically rather than by slab termination. Moreover, the presence of metastability reduces the negative thermal buoyancy of some slabs, with a variety of consequences.

The success of the metastability hypothesis at explain-

ing first-order features of deep seismicity has encouraged us to explore it further. The hypothesis is sufficiently well formulated that we can use thermal and kinetic models to test its implications in detail. Although alternative hypotheses have been offered, they seem to us less successful at explaining the seismological observations and are presently less amenable to quantitative testing. Hence we concentrate on the metastability hypothesis, while briefly summarizing the alternatives.

2. THERMAL MODELS OF DOWNGOING SLABS

2.1. Background

Because deep earthquakes occur only in subducting slabs, which differ from their surroundings largely by being colder, low temperatures seem essential for deep earthquakes (Plate 2). Low temperatures have several effects. Most importantly, for the metastability hypothesis the difference between the pressure-temperature conditions inside the slab and those outside should permit a seismogenic metastable region to form. We therefore consider plausible thermal structures for downgoing slabs.

2.2. Thermal Parameter Concept

Describing the thermal structure in the Earth is challenging because temperatures at depth are not constrained by direct observations but are instead inferred primarily from surface temperature, surface heat flow, and assumed physical properties. As a result, our ideas are based on simple models, which are attractive because the results are relatively insensitive to their details.

Exploration of the metastability hypothesis requires estimates of temperature and pressure inside slabs. A simple analytical model for subduction zones, based on the time required for a slab of finite thickness to heat up by conduction as it subducts into the hotter mantle [*McKenzie*, 1969], illustrates several key ideas. Isotherms within the slab are advected downward, reaching a maximum depth proportional to the product of the vertical descent rate (trench-normal convergence rate times the sine of the dip) and the square of plate thickness. This formulation emphasizes temperature as a function of depth, rather than distance along the slab dip, because mineral reaction rates depend on both temperature and pressure.

The model makes two important predictions. First, the time needed for a slab to equilibrate with the surrounding mantle is much longer than the approximately 10 Myr required for it to reach 700 km depth where earthquakes cease. Second, for a cooling half-space model, in which the thermally defined thickness of the subducting lithosphere is proportional to the square root of its age as it enters the trench, isotherms reach a depth proportional to the product of vertical descent rate and age, a quantity known as the thermal parameter.

This concept is useful for investigating the cause of deep earthquakes, because the maximum depth of earthquakes increases among subduction zones as a function of thermal parameter (Figure 4). *Molnar et al.* [1979] proposed that the maximum depth of seismicity occurs at a critical potential temperature (temperature referenced to the mantle adiabatic gradient), above which the slab is too weak to support seismic failure. This concept has been expanded upon by *Wortel* [1982], *Jarrard* [1986], and *Wortel and Vlaar* [1988].

Although the thermal parameter is useful for comparing average temperature structures between slabs, its

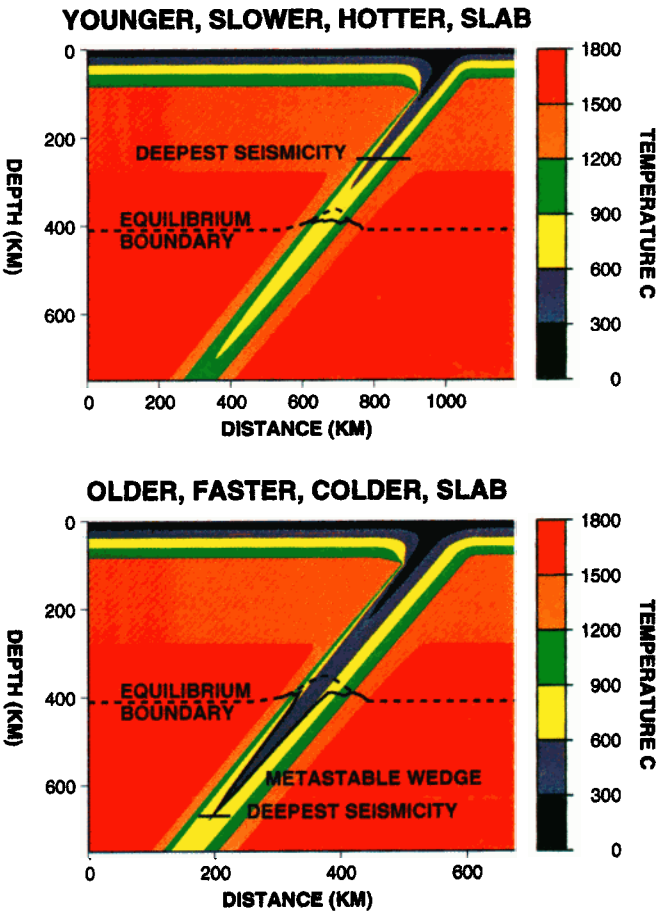

Plate 2. Thermal models approximating the (a) Aleutian slab and (b) Tonga slab. Thermokinetic modeling shows that the younger and slower subducting slab (e.g., the Aleutian slab) is hot enough that transformation of olivine to spinel keeps pace with the descent rate and is completed (solid line) near the equilibrium phase boundary (dashed line). Deep earthquakes should not occur in such a slab because the necessary metastability condition for transformational faulting is not satisfied. The older and faster subducting slab (e.g., Tonga) is colder, such that kinetic hindrance prevents transformation from keeping pace with the descent rate. Metastable olivine thus persists in a region defined by a wedge-shaped lower boundary (solid line) and the equilibrium phase boundary above it. Deep earthquakes could occur inside the metastable wedge provided that slab stresses are sufficient to activate transformational faulting.

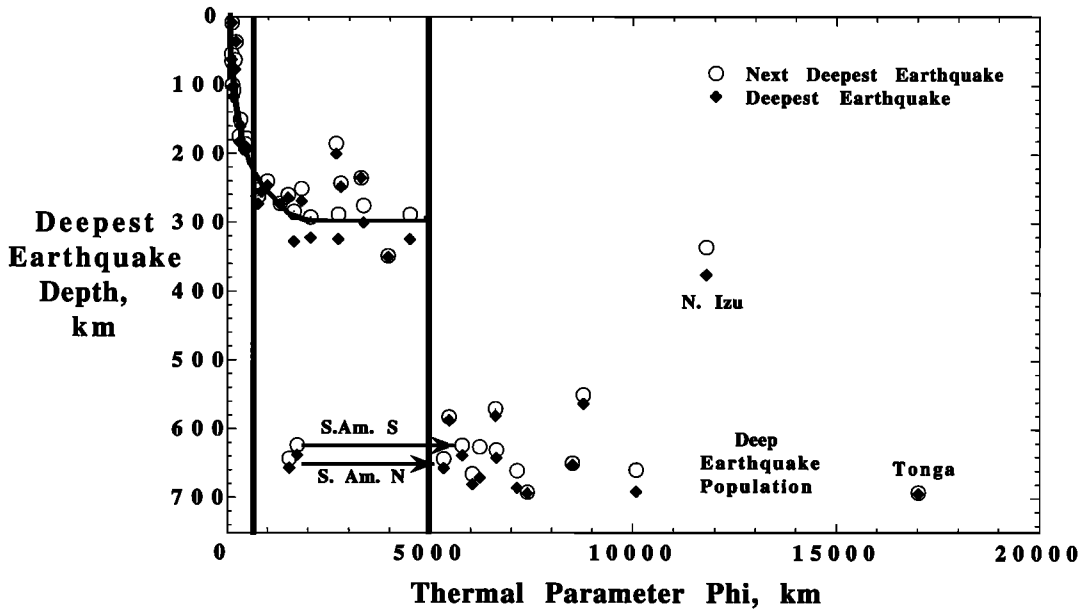

Figure 4. Variation in maximum earthquake depths between subduction zones as a function of thermal parameter (the product of plate age entering trench and vertical descent rate). Depths are shown for the two deepest teleseismically well-located earthquakes for each subduction zone. Depths are determined from the Harvard CMT catalogue [e.g., *Dziewonski et al.*, 1995], the International Seismological Centre (ISC), or our relocations of pre-1964 events based on data from the International Seismological Summary. Convergence rates are from NUVEL-1 [*DeMets et al.*, 1990], augmented when necessary by estimates from various sources of trench migration for the Tonga, Marianas, Izu-Bonin, and South Scotia subduction zones. Slab age is estimated from magnetic anomalies [*Cande et al.*, 1989]. Slab dip taken from the average dip of Wadati-Benioff zone seismicity. Several subduction zones discussed in this paper are labeled. Arrows indicate thermal parameter for the subducting Nazca plate based on evidence that the deep slab is older than the age at the trench [*Engebretson and Kirby*, 1992]. If deep earthquakes were directly temperature limited, their maximum depth would increase continuously with thermal parameter. Instead, the maximum depths seem divided into a group with thermal parameter less than about 5000 km, which do not have deep earthquakes, and a group with higher thermal parameters, which do. This behavior is consistent with the predictions of the thermokinetic model discussed later.

interpretation in terms of a potential temperature limiting deep earthquakes has several shortcomings. Inspection of Figure 4 suggests that maximum earthquake depth is a discontinuous, rather than continuous, function of thermal parameter [*Kostoglodov*, 1989; *Kirby et al.*, 1991]. Maximum depths are divided into a group with thermal parameter less than about 5000 km and lacking earthquakes deeper than 325 km and a group with greater thermal parameters that have earthquakes with depths of 500–690 km. Despite the scatter, both groups remain distinct for reasonable estimates of lithospheric age and plate velocity. Temperature apparently controls maximum earthquake depth in a more complex way than through a critical potential temperature. Another difficulty is that for olivine flow law parameters determined by laboratory experiments, slabs should be strong below the deepest earthquakes [*Brodholt and Stein*, 1988].

The dichotomy between slabs having deep earthquakes and those that do not suggests that different processes control maximum earthquake depths in slabs with thermal parameters less or greater than about 5000 km. We compute thermal structure for different slabs in order to test which, if any, are cold enough that large-scale metastability should occur.

2.3. Representative Thermal Models

We compute thermal models using a code originally developed by N. H. Sleep, based on a finite difference algorithm [*Toksöz et al.*, 1973] and widely used in slab thermal modeling studies [e.g., *Sleep*, 1973; *Hsui and Toksöz*, 1979, *Helffrich et al.*, 1989]. The temperature structure of the lithosphere before subduction and the thermal diffusivity are from the GDH1 thermal plate model [*Stein and Stein*, 1992] in which the geotherm reaches steady state at an age of about 70 Myr. Hence in such a model the thermal structure does not vary greatly with age among old slabs.

We used material parameters within the range typically used in thermal modeling and thought to be appropriate for the upper mantle. Because the actual values in descending slabs are not well constrained, we followed common practice in using temperature- and pressure-independent values. Although the modeling is done for

potential temperatures [*McKenzie*, 1970], the effects of adiabatic heating are relevant for prediction of temperature-dependent effects like reaction kinetics or material strength. We use an adiabatic gradient of 0.27°C km^{-1}. The temperature at 400 km is 1532°C, and that at 655 km is 1600°C in normal mantle with this gradient [*Ito and Katsura*, 1989].

Plate 2 shows the predicted temperature structure for two of the slabs we consider. The colder slab, with old lithosphere subducting very rapidly (Plate 2b), approximates the Tonga subduction zone [*Bevis et al.*, 1995]. The temperature distributions are typical of slab models, though the depth to individual isotherms varies [e.g., *Helffrich et al.*, 1989; *Davies and Stevenson*, 1992]. Successively hotter isotherms penetrate to greater depths. The minimum temperature at any depth is initially near the upper slab surface and moves toward the slab center with increasing depth. In the colder slab, temperatures at 660 km are approximately 600°C. Such temperatures are assumed to permit deep seismicity.

It is difficult to assess uncertainties in the predicted temperatures without independent means of verifying their accuracy. Certainly, many of the model assumptions are idealizations. The temperature in the incoming lithosphere is predicted from a simple plate model. The geometry and uniform thermal diffusivity are also approximations. As the model only allows slab heating by conduction from the surrounding mantle and does not include shear or radiogenic heating, the predicted temperatures are lower bounds. Thus, although we consider these models as sensible approximations to real slabs, we do not regard the predicted temperatures from these (or any other) models as accurate to better than about 200°C. The fact that temperatures from such models predict seismic velocities similar to those inferred from observations [e.g., *Spakman et al.*, 1989] suggests that they are reasonable approximations. Moreover, as we shall see, combining the temperatures with a kinetic model of the phase change (which has its own uncertainties) predicts substantial metastability only for slabs in the age and convergence rate range where deep earthquakes actually occur.

The thermal model does not include the effects of latent heat released by the phase changes, because it differs from earlier ones in which latent heat is released at the equilibrium phase boundary. Because our focus is on the metastable reaction, we use the thermal model in a kinetic calculation to predict where the reaction occurs. Thus slab temperatures will rise by about 40°–200°C due to the latent heat, depending on the degree of metastability. These temperature increments were not incorporated into the heat transport in the thermal model because the distance the slab descends in a time step is generally greater than the computed widths of the reaction zones. Thus the reaction zone is so narrow that the reaction goes to completion before the heat generated by reaction in adjacent regions diffuses back into the wedge.

3. PHASE CHANGES IN SUBDUCTING SLABS

3.1. Background

Subducting slabs can be considered as composed of three layers: a 7-km-thick mafic crust, underlain by a 25- to 30-km-thick layer of harzburgite (a peridotite containing enstatite in addition to the chief mineral olivine), below which is lherzolite, a peridotite containing both enstatite and diopside [e.g., *Ringwood*, 1982]. The harzburgite layer is likely to initially experience the lowest slab temperatures since it is the shallowest and coldest mantle rock entering trenches. We therefore consider phase changes primarily in terms of this basic lithology, which consists of approximately 78% olivine, 22% enstatite, and a trace of garnet [*Ringwood*, 1982].

The upper mantle minerals discussed above become thermodynamically unstable at a depth of about 400 km and begin transforming to higher-density phases, such as spinel, modified spinel, ilmenite, or majorite garnet. If these transformations fail to occur at their equilibrium pressures in cold subducting lithosphere because of sluggish reaction kinetics, these low-pressure minerals will survive as metastable phases to depths determined by the reaction rates [*Sung and Burns*, 1976a, b; *Rubie*, 1993; *Daessler and Yuen*, 1993; *Rubie and Ross*, 1994].

Phase transitions that occur in the transition zone involve major changes in the atomic structure of the minerals. Such changes are normally accomplished by "reconstructive" mechanisms that involve two stages, formation of nuclei of the new phase(s) (normally on grain boundaries in the host rock) and growth of new grains at the expense of the host phase. Although nucleation and growth generally occur simultaneously (Figure 5), the kinetics of the two processes can be considered separately. In general, the overall transformation rate (i.e., the variation of the volume fraction of the new phase(s) with time) depends on the rates of both nucleation and growth and is affected by the impingement of the growing grains.

The mechanisms and, to a lesser extent, the kinetics of the olivine → spinel transformation have been the subject of numerous experimental studies, reviewed by *Rubie* [1993]. We first consider the transformational behavior of olivine, the most abundant phase in subducting lithosphere. In section 3.8, we also review the kinetic behavior of enstatite.

3.2. Kinetics of the Olivine-Spinel Transformation

If equilibrium is maintained at low temperatures (500°–700°C), olivine of mantle composition (α-$Mg_{1.8}Fe_{0.2}SiO_4$) transforms via a sequence of divariant reactions with increasing pressure to the higher-density polymorphs. According to the thermodynamic data of *Akaogi et al.* [1989], the sequence of stable phases with increasing depth in a subducting slab is α, $\alpha + \gamma$, $\alpha + \beta$, β, $\beta + \gamma$, and γ (Figure 6a).

To extrapolate experimental data on the kinetics of a reaction to geological conditions, the transformation

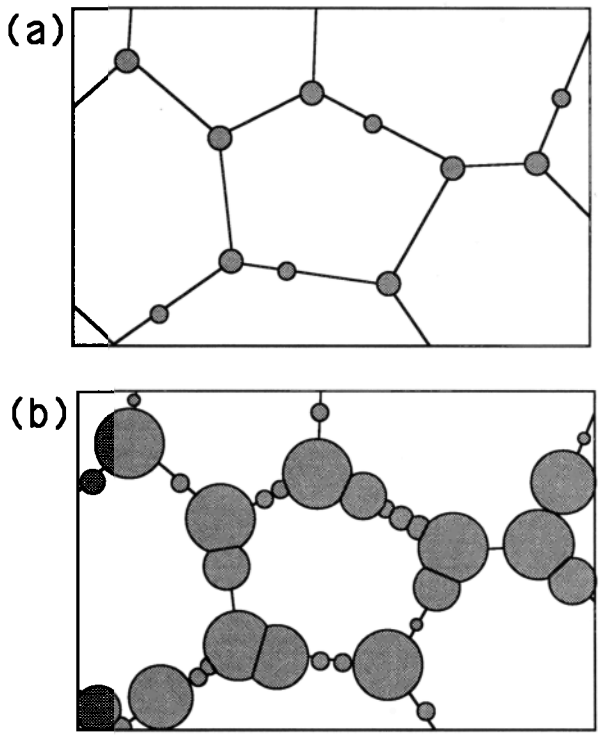

Figure 5. Schematic diagram showing the early stages of a reconstructive phase transformation involving grain boundary nucleation and interface-controlled growth. (a) Grains of the product phase (shaded) nucleate on grain boundaries and at triple junctions in the reactant phase, and grow by consuming the host phase. (b) Following impingement of the growing grains, grains of the product phase grow inward toward the center of the grains of the reactant phase until the reaction reaches completion. The volume fraction of the product phase as a function of time depends on the rates of both nucleation and growth.

mechanism, on which the reaction rate depends, must be understood [*Rubie and Thompson*, 1985]. When differential stress is less than about 1 GPa, the $\alpha \rightarrow \beta$ and $\alpha \rightarrow \gamma$ transformations involve nucleation on olivine grain boundaries [*Boland and Liebermann*, 1983; *Vaughan et al.*, 1984; *Remsberg et al.*, 1988; *Burnley and Green*, 1989; *Brearley et al.*, 1992; *Brearley and Rubie*, 1994]. Growth can involve two possible mechanisms, depending on the pressure. When transformation occurs under near-equilibrium conditions in a two-phase stability field (Figure 6a), the Mg/Fe ratios of the reactant and product phases are different and change as a function of pressure and reaction progress. Growth therefore involves Fe-Mg interdiffusion on the scale of the grain size of the rock [*Rubie*, 1993] and is likely to be "diffusion-controlled" [*Christian*, 1975]. At low temperatures, where the transformation of olivine close to the equilibrium pressure is kinetically inhibited, the two-phase fields can be overstepped and direct transformation to either β or γ can occur without any change in composition and therefore without the need for long-range diffusion [*Rubie*, 1983]. In this case, the growth rate of β or γ is controlled by the rate of short-range diffusion across the narrow interphase boundary and is termed "interface-controlled" [*Christian*, 1975].

Most information on the mechanisms and kinetics of the olivine $\rightarrow$ spinel transformation has been obtained using analog compositions such as Ni_2SiO_4, Co_2SiO_4, and Mg_2GeO_4 [*Rubie and Ross*, 1994]. The transformation to spinel in these compositions is relatively easy to study experimentally because much lower pressures (1–6 GPa) are required than for $(Mg,Fe)_2SiO_4$. Although transformation mechanisms are similar [*Rubie*, 1993], kinetic data for analog compositions cannot be

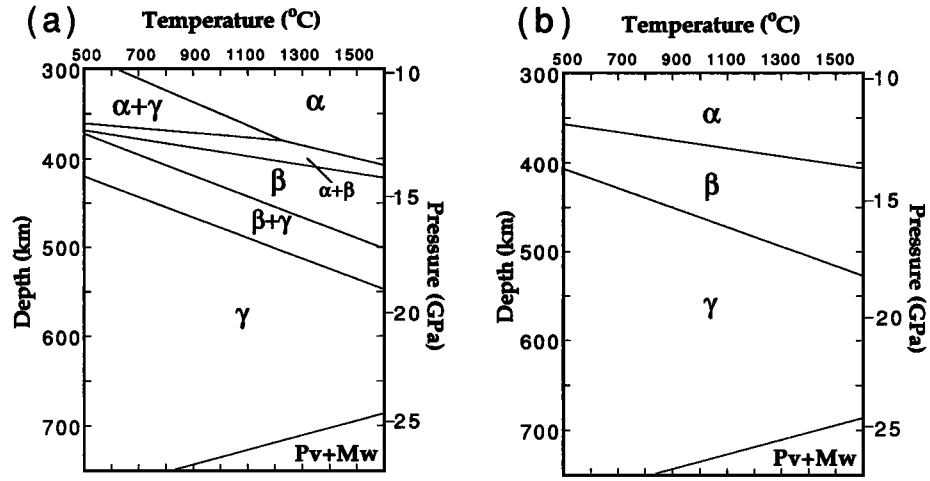

Figure 6. (a) Phase diagram for the composition $Mg_{1.8}Fe_{0.2}SiO_4$ showing stability fields of olivine (α), modified spinel (β) and spinel (γ). In the two-phase fields (e.g., $\alpha + \gamma$) the compositions (i.e., Mg/(Mg + Fe) ratios) of the coexisting phases are different [*Akaogi et al.*, 1989]. (b) Simplified and idealized $Mg_{1.8}Fe_{0.2}SiO_4$ phase diagram in which only univariant reactions are considered. The boundaries shown are metastable phase boundaries separating the stability fields of the α, β, and γ phases, calculated from the thermodynamic data of *Akaogi et al.* [1989].

used directly to predict transformation kinetics in the mantle without considering the effect of composition.

3.3. Growth Kinetics

Although transformation involves both nucleation and growth, we treat only the kinetics of growth in detail, because available data suggest that transformation rates at low temperatures in subducting slabs are controlled entirely by the growth kinetics [*Rubie and Ross*, 1994]. Under such conditions, growth of β or γ is interface-controlled (see above), and the rate of growth (the speed of the interface between phases) is given by

$$\dot{x} = k_0 T \exp\left[-(H^* + PV^*)/RT\right]\left[1 - \exp\left(\Delta G_r/RT\right)\right], \quad (1)$$

where k_0 is a constant, T is absolute temperature, P is pressure, H^* and V^* are the activation enthalpy and activation volume for growth, R is the gas constant, and ΔG_r is the Gibbs free energy change of reaction [*Turnbull*, 1956; *Christian*, 1975]. The first exponential is a kinetic factor describing the thermally activated diffusion of atoms across the interphase boundary. The rate of this process increases rapidly with temperature but (assuming that V^* is positive) decreases with increasing pressure. The second factor (in brackets) depends on the thermodynamic driving potential in the system. ΔG_r can be approximated by $\Delta P \Delta V$, where ΔP is the overstep of pressure beyond equilibrium and ΔV is the transformation volume change at the conditions of the reaction. Hence this factor is zero at equilibrium where $\Delta G_r = 0$ (and therefore the growth rate is zero), and this factor approaches unity as ΔP increases. With increasing pressure at constant temperature the growth rate of spinel during transformation from olivine first increases, due to the thermodynamic factor, and then decreases, due to the kinetic factor.

Experimental estimates of spinel growth rates during the transformation of olivine are available for the α → γ transformations in Ni_2SiO_4 and Mg_2GeO_4 and the α → β transformation in Mg_2SiO_4 [*Burnley*, 1990; *Rubie et al.*, 1990; *Rubie and Ross*, 1994]. On the basis of the observation that grains of both β-Mg_2SiO_4 and metastable γ-Mg_2SiO_4 grow in forsterite at a similar rate at 15 GPa and 1000°C [*Brearley et al.*, 1992], we assume that values of the kinetic parameters in (1) are similar for β and γ and that only ΔG_r differs. In addition to P and T, composition affects the growth rate because the data cannot be described by a single rate law (Figure 7a). *Rubie and Ross* [1994] incorporated an empirical compositional dependence into (1) by expressing the activation enthalpy for growth as proportional to the melting temperature T_m, which also varies with composition:

$$H^* = \alpha T_m, \quad (2)$$

where α is a constant. This relationship seems approximately valid for thermally activated processes such as diffusion and plastic flow in materials of similar structure but different composition [*Frost and Ashby*, 1982].

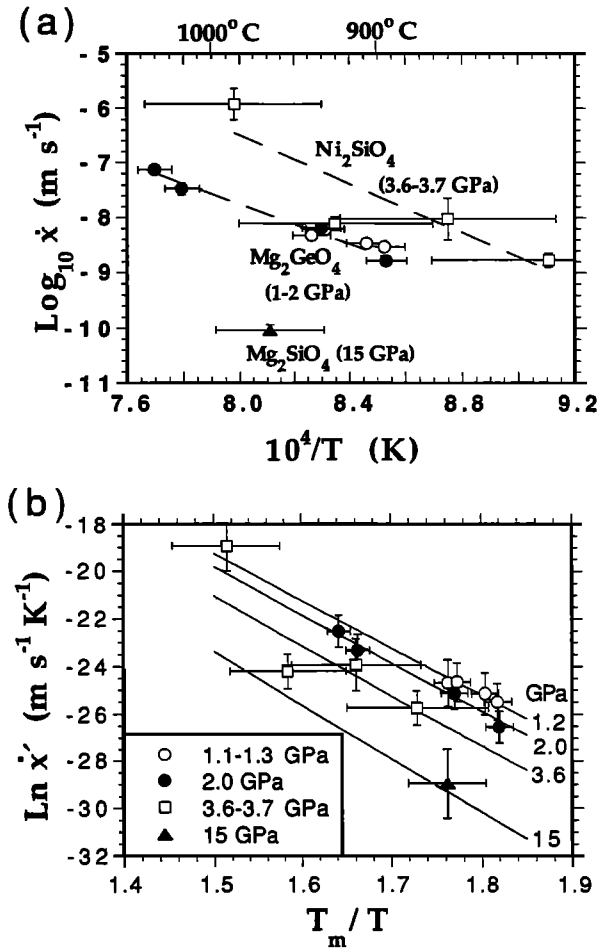

Figure 7. Growth rates as a function of temperature for the following transformations: Ni_2SiO_4 α → γ at 3.6–3.7 GPa (open squares); Mg_2GeO_4 α → γ at 1.2 GPa (open circles) and 2.0 GPa (solid circles); Mg_2SiO_4 α → β (triangle) at 15 GPa. (a) Plot of logarithm of the growth rate against inverse absolute temperature. This plot suggests that growth rates depend strongly on composition because the variations between the different data sets cannot be explained by a dependence on pressure alone. Dashed lines show linear least squares fits to the Ni_2SiO_4 and Mg_2GeO_4 data. (b) Fits of equations (1) and (2) to the normalized growth rate data in Figure 7a at various pressures versus inverse normalized temperature (inverse temperature normalized by the absolute melting temperature T_m). The normalized growth rate, $\dot{x}'$, is the growth rate divided by a term including the free energy change of reaction $\dot{x}' = \dot{x}/\{T[1 - \exp(\Delta G_r/RT)]\}$ (see equation (1)). Parameters used in this fit are $k_0 = 3.7 \times 10^4$ m s^{-1} K^{-1} and α = 159 J mol^{-1} K^{-1}. A pressure-dependent activation volume model is also used [*Rubie and Ross*, 1994].

Equations (1) and (2) can be fit to the data of Figure 7a when the activation volume V^* decreases significantly with increasing pressure. Because there are no estimates of V^* (or its pressure dependence) for diffusion across interphase boundaries in minerals, *Rubie and Ross* [1994] used an empirical model [*O'Connell*, 1977] with

V^* decreasing from 12 $cm^3\ mol^{-1}$ at 1 bar to about 4 $cm^3\ mol^{-1}$ at 15 GPa.

Figure 7b shows a least squares fit of (1) and (2) to the data of Figure 7a. With the exception of one γ-Ni_2SiO_4 data point, the fit is reasonable. Comparison with preliminary growth rate estimates for β- and γ-$Mg_{1.8}Fe_{0.2}SiO_4$ at 1000°C suggests that (1) and (2) can be used to predict growth rates of β and γ in olivine of mantle composition [*Rubie and Ross*, 1994; *Kerschhofer et al.*, 1995]. Although the fit in Figure 7b is based on limited experimental data and extrapolation to low temperatures is not well constrained by the data, this fit is our best current estimate of the growth rate of spinel in subduction zones.

3.4. Transformation Kinetics

Transformation kinetics are described by the volume fraction of the product phase as a function of time, $\xi(t)$, and generally depend on the rates of both nucleation and growth. Growing grains of the product phase eventually impinge on each other; hence growth is impeded, and the reaction rate decreases (Figure 5). A kinetic theory for phase transformations involving grain boundary nucleation and interface-controlled growth, with impingement of growing grains [*Cahn*, 1956] can be modified for nonisothermal, nonisobaric transformations, in which nucleation and growth rates vary with time [*Rubie and Ross*, 1994]. In this formulation,

$$\xi(t) = 1 - \exp\left\{-\frac{6.7}{d}\int_0^{y_{max}(t)} [1 - \exp(-Y_e)]\, dy\right\}, \tag{3a}$$

with

$$Y_e(t, y) = \pi \int_0^{\tau_{max}} \dot{N}(\tau)\left\{\left[\int_\tau^t \dot{x}(\theta)\, d\theta\right]^2 - y^2\right\} d\tau, \tag{3b}$$

where $\xi(t)$ is the volume fraction transformed at time t, d is the grain diameter of the reactant phase, and $\dot{N}(\tau)$ is the nucleation rate at time τ. Here $\dot{x}(\theta)$ is the growth rate of the new phase at time θ, computed using (1) and (2). The dummy variable y is the distance from the grain boundary on which the new grain nucleated and $y_{max}(t)$ is the maximum distance from the grain boundary reached at time t by a grain nucleated at time zero. The variable $\tau_{max}(y)$ is, for any distance $y \le y_{max}(t)$, the time at which a grain originally nucleated which subsequently grows to radius y at time t and is determined iteratively from

$$\int_{\tau_{max}}^{t} \dot{x}(\theta)\, d\theta = y.$$

Finally, the constant 6.7 depends on the relation between d and grain boundary area for a specific grain geometry. The exponentials in (3a) describe the decrease in reaction rate with time due to grain impingement (Figure 5). Note that (3a) is a corrected version of a rate equation derived by *Rubie and Ross* [1994].

We evaluated $\xi(t)$ numerically as a function of time from (3) for a given grain size d, given the dependencies of the nucleation and growth rates on time. Hence by using a thermal model to find the temperature and pressure of a small volume of subducting material as a function of time, the amount of spinel in subduction zones can then be calculated as a function of time and depth.

3.5. Thermodynamic Model

We idealize the transformation of $Mg_{1.8}Fe_{0.2}SiO_4$ olivine to β or γ as a polymorphic reaction which occurs, without changes in composition, by interface-controlled growth. This model is realistic when the two-phase fields (Figure 6a) are bypassed due to sluggish kinetics, and represents a simplification only for near-equilibrium transformation. The Gibbs free energy change for this reaction, on which growth rates depend, is calculated as the free energy difference between α- and either β- or γ-$Mg_{1.8}Fe_{0.2}SiO_4$ from the data of *Akaogi et al.* [1989]. A simplified phase diagram showing metastable equilibrium boundaries between the three phases with this composition is shown in Figure 6b.

There are significant uncertainties in the thermodynamic data for phases in the system Mg_2SiO_4-Fe_2SiO_4. For example, *Bina and Helffrich* [1994] argued that the Clapeyron slope for the Mg_2SiO_4 α → β transformation may be larger than predicted by the data of *Katsura and Ito* [1989] and *Akaogi et al.* [1989]. These uncertainties affect mainly the extent to which the equilibrium phase boundaries are elevated in slabs. Such uncertainties have little effect on the kinetic modeling because the dependence of the growth rate on ΔP and hence ΔG_r is small (see (1)).

3.6. Kinetic Model

To estimate the depths at which olivine (α-$Mg_{1.8}Fe_{0.2}SiO_4$) transforms to either the β or γ polymorphs in subduction zones, we integrate equation (3) along pressure-temperature-time (P-T-t) paths calculated by thermal modeling for representative slabs (e.g., Plate 2). We assume an olivine grain size of 5 mm; varying this value between 1 and 10 mm changes the calculated depth of transformation by only 10–20 km [*Rubie and Ross*, 1994]. The growth rate of either β or γ is calculated from (1) and (2) using parameter values from Figure 7b and the activation volume model of *Rubie and Ross* [1994]. The nucleation rate is estimated using model 2 of *Rubie and Ross* [1994]. Although there are large uncertainties in the calculated nucleation rates, these uncertainties affect the calculated transformation depths only along relatively high-temperature P-T-t

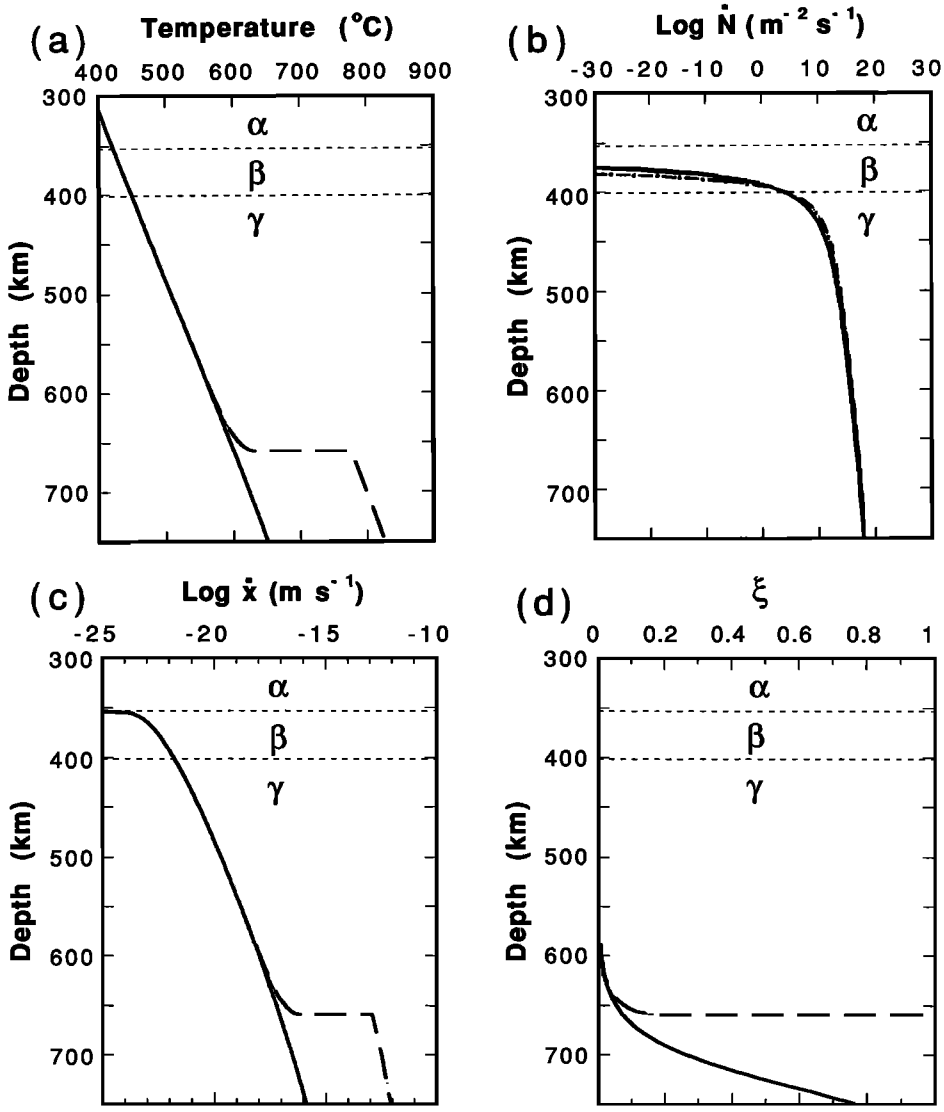

Figure 8. (a) Temperature, (b) nucleation rate for β (solid line) and γ (dash-dotted line), (c) growth rate, and (d) volume fraction transformed as functions of depth, calculated for the coldest temperature-depth path in the coldest thermal model (slab D) (Plates 2b and 3d). Dashed and solid lines show results obtained with and without the release of latent heat, respectively. Typical errors associated with such results are discussed by *Rubie and Ross* [1994].

paths ($T > 600$°C at a depth of about 400 km), as discussed in the next section. Along low-temperature paths, growth is the rate-controlling step according to the calculations, so varying the nucleation rate does not affect the results [*Rubie and Ross*, 1994].

Depths of transformation were calculated both with and without the release of latent heat. To evaluate the latent heat release, the molar heat production of the reaction of α to either β or γ is calculated from

$$\Delta H_{T,P} = \Delta H_{T,1\text{ atm}} + \int_{1\text{ atm}}^{P} \Delta V_{T,P}\, dP \qquad (4)$$

where $\Delta H_{T,1\text{ atm}}$ is the enthalpy change of reaction at temperature T and 1-atm pressure, and $\Delta V_{T,P}$ is the molar volume change at a given T and P. Because of the interaction between kinetics, temperature, and latent heat production the volume fraction transformed (ξ) is evaluated iteratively from (3) over a sequence of small depth increments.

3.7. General Results of the Kinetic Model

Results of the kinetic calculations for the coldest P-T-t path (Figure 8a) of slab thermal model D (Plate 2), with and without the release of latent heat, are shown in Figure 8b–8d. Even though the nucleation rate becomes high by a depth of 400 km (Figure 8b), significant transformation of olivine only begins at about 600 km depth (Figure 8d) because of slow growth rates (Figure 8c). Thus metastable olivine should persist more than 250

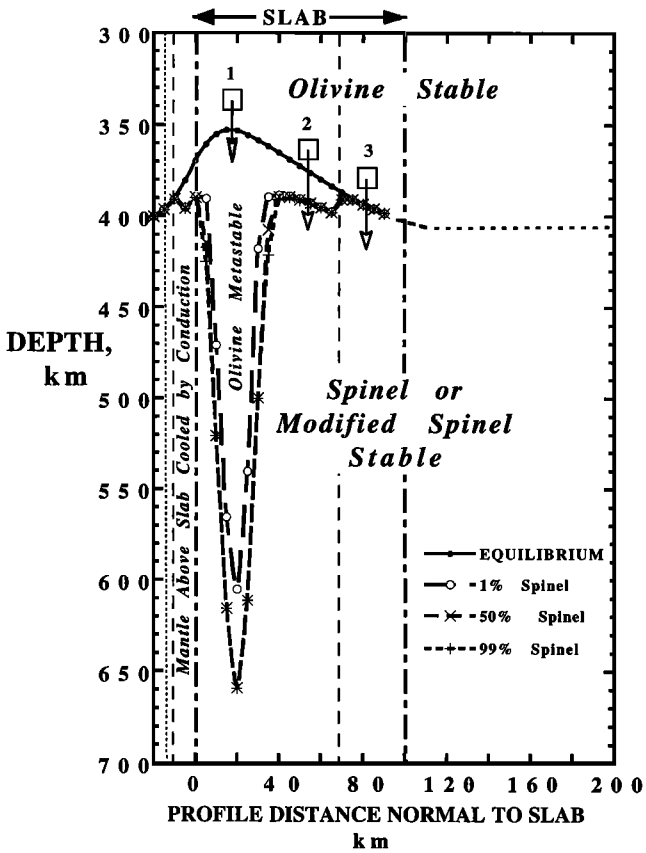

Figure 9. Detailed mineralogical structure predicted by the thermokinetic result for the Tonga slab (thermal model of Plate 2b), including the effects of latent heat release. Three regimes of olivine → spinel reaction are recognized. A volume element of peridotite in the cold slab interior (marked 1) bypasses the equilibrium olivine-spinel boundary and survives metastably until it reacts abruptly by growth-controlled transformation to spinel. In contrast, olivine in element 2 only slightly bypasses the equilibrium boundary and reacts by a nucleation-controlled transformation. Nucleation does not occur in volume element 3, composed of warmer slab material, and passes through the equilibrium boundary without spinel nucleation, but an olivine → spinel reaction front ascends from greater depths to the equilibrium boundary at rates comparable to the slab descent rate.

km below the equilibrium phase boundary in a very cold slab.

Without including the effect of the release of latent heat, transformation occurs gradually over a depth interval of about 100 km (Figure 8d). In contrast, latent heat increases the temperature which, through the effect on kinetics, leads to a runaway reaction rate and a very sharp boundary between unreacted olivine and spinel (Figure 8d).

Different kinetic regimes can be identified from the kinetic model, depending on temperature, as illustrated for slab model D in Figure 9. When the temperature at 400 km depth is less than about 600°C, olivine persists metastably to significant depths below the equilibrium phase boundary. The depth of transformation in this case is controlled by growth kinetics and is independent of the nucleation rate model [*Rubie and Ross*, 1994]. This situation produces the metastable wedge. The reaction occurs over a narrow depth range, so the average thickness of the transitional olivine-spinel zone transverse to the slab is about 5 km. The metastable wedge has a V-shaped lower boundary well approximated by the 600°C isotherm. The wedge is thinner and bounded by a cooler isotherm than was found earlier [*Sung and Burns*, 1976a, b; *Kirby et al.*, 1991].

When temperatures in the slab at 400 km depth are higher (about 600°–1100°C), transformation occurs much closer to equilibrium, at a depth controlled by the nucleation kinetics. The uncertainty in this depth is at least 50 km, due to nucleation rate uncertainties [*Rubie and Ross*, 1994, Figure 5]. Finally, when temperatures exceed 1100°C at 400 km depth, the growth rate can equal the rate of subduction at conditions close to those at the equilibrium phase boundary. In this fast growth case the transformation front moves up the descending slab by growth alone, without the need for nucleation, and transformation occurs very close to equilibrium.

3.8. Enstatite Phase Transformations

Enstatite $(Mg,Fe)SiO_3$ is the second most abundant phase in mantle harzburgite. At high pressure (6–10 GPa) the orthorhomic polymorph, orthoenstatite, transforms to another pyroxene polymorph, clinoenstatite. Under equilibrium conditions in slabs, clinoenstatite, in turn, should transform to garnet at about 400 km depth [*Ringwood*, 1982]. However, at low temperatures (e.g., 600°C) it is likely that the garnet-forming reaction is kinetically inhibited because of slow rates of chemical diffusion [*Hogrefe et al.*, 1994]. Under these conditions and with increasing pressure, clinoenstatite should react in grain size domains of local equilibrium to modified spinel + stishovite or spinel + stishovite, then to ilmenite, and finally to perovskite (Figure 10).

The kinetics of the transformations of $MgSiO_3$ clinoenstatite to high-pressure phases have been studied experimentally [*Hogrefe et al.*, 1994]. Hot-pressed forsterite + clinoenstatite aggregates were reacted in the temperature range 1000°–1650°C at pressures of 16–21 GPa. The transformation of clinoenstatite to β phase + stishovite on a laboratory timescale requires very high temperatures (≥1550°C) at pressures of 18–21 GPa. This reaction is kinetically much more sluggish than the olivine-spinel transformation (which only requires temperatures of 900°–1000°C and lower pressures to occur on a comparable timescale). The large difference in the kinetics of these two reactions is due to differences in both nucleation and the scale of chemical diffusion. The clinoenstatite reaction requires nucleation of two phases (spinel and stishovite) compared with only one phase for the olivine-spinel reaction. Stishovite nucleation appears to be particularly sluggish. The scale of chemical diffusion during clinoenstatite breakdown is large (e.g., a few

micrometers) because during growth, chemical components diffuse to spatially separated spinel and stishovite grains. In contrast, the olivine-spinel transformation only involves diffusion across a grain boundary between the two phases, which should have a width of ≤2–3 nm.

When clinoenstatite is pressurized at temperatures less than 1550°C, it persists metastably and bypasses the β phase + stishovite and spinel (γ) + stishovite stability fields (Figure 10). At higher pressures, clinoenstatite transforms polymorphically to the ilmenite structure at a relatively rapid rate. From these experimental results, clinoenstatite is likely to persist as a metastable phase in subducting slabs to greater depths than olivine and then to transform polymorphically to $(Mg,Fe)SiO_3$ ilmenite at higher pressure [*Rubie*, 1993; *Hogrefe et al.*, 1994]. As discussed later, direct conversion to the ilmenite structure is likely to be important for the process of unstable faulting under stress.

The kinetics of the olivine → spinel transformation are catalyzed by clinoenstatite because olivine-clinoenstatite phase boundaries form preferential nucleation sites for spinel [*Sharp and Rubie*, 1995]. This observation reinforces our view that growth, not nucleation, is the rate-controlling process for the kinetics of spinel-forming reactions in slabs.

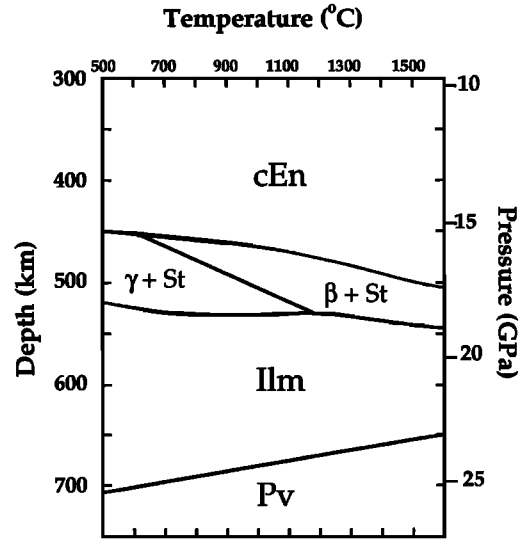

Figure 10. High-pressure phase diagram for $MgSiO_3$ [after *Saxena et al.*, 1993]. Abbreviations are cEn, clinoenstatite; St, stishovite; Ilm, $MgSiO_3$ ilmenite; Pv, perovskite. In a cold slab, cEn should bypass the two-phase fields involving stishovite and then transform directly by the polymorphic reaction: metastable cEn → ilmenite.

4. THERMOKINETIC MODEL RESULTS

These results for olivine → spinel kinetics permit use of thermal models to predict where metastable olivine should occur and hence where a necessary condition for deep earthquake faulting by transformational faulting is satisfied.

4.1. Thermokinetic Models of Various Slabs

Deep seismicity occurs only for slabs with thermal parameters greater than 5000 km (Figure 4). To see if this behavior would be expected, we computed temperature structures and reaction boundaries for four representative slabs with successively increasing thermal parameter (Plate 3 and Table 2). Category A, a young slab, approximates the Cascadia, Mexico, or Nankai Trough subduction zones. Category B, a middle aged slab, approximates the Middle America, northern Chile, or central Aleutians subduction zones. Category C, an old slab, approximates the eastern Indonesia and Kuriles subduction zones. Category D, an old slab subducting rapidly, approximates the Tonga subduction zone.

As expected, the model slabs are progressively colder with increasing thermal parameter. Significant metastability is predicted between the equilibrium boundary and the 50% transformation contour computed including latent heat release. For the warmest slab, A, the olivine → spinel reaction occurs near the equilibrium boundary, and no metastability occurs. Similarly, the somewhat cooler slab B has only minor metastability. Because these slabs are hot enough that the phase transformation keeps pace with the subduction rate, essentially no metastable wedges form, transformational faulting should not occur, and deep earthquakes are not expected.

A distinct metastable wedge is evident for the next colder slab, C, which models the thermal state expected for most old slabs. The wedge extends to approximately 500 km depth. The coldest slab, D, has an even larger wedge extending to 660 km. These two slabs are cold enough that phase transformation cannot keep pace with the subduction rate, a distinct metastable wedge forms, and deep earthquakes are expected.

4.2. Model Predictions and Earthquake Depths

The model predictions are in good accord with observations of earthquake depths. For thermal parameters less than 5000 km, earthquakes occur no deeper than about 350 km, whereas for larger thermal parameter the depths of the deepest shocks are approximately constant at about 650 km (Figure 4). Similarly, in the models a metastable wedge develops for thermal parameters exceeding approximately 5000 km. Slab models B and C (Plate 3) bracket this transition; B has insignificant metastability, whereas C has a well-developed wedge. Model C is representative of the thermal and kinetic structure of most slabs with thermal parameters from about 6000 to 10,000 km because thermal structure does not vary appreciably for slab ages from 80 to 140 Ma, and most deep Wadati-Benioff zones represent slabs that vary in age over this range and vary less in vertical descent rates.

This effect can be seen within a single arc, where the Australian plate subducts beneath Indonesia. Both the

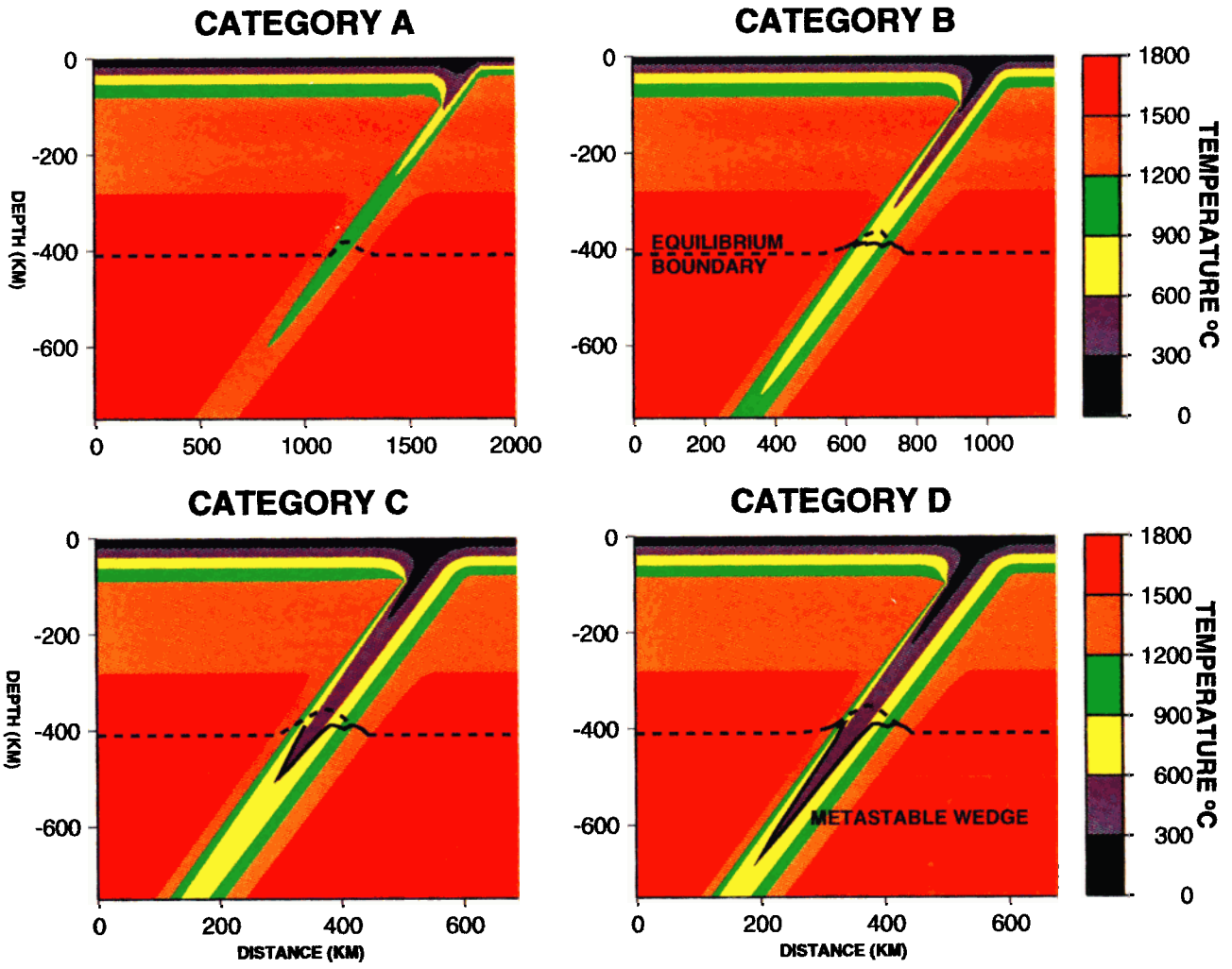

Plate 3. Thermokinetic model results for four slabs representing subducting lithosphere at different trenches. The assumed plate ages, convergence rates, and calculated thermal parameters are given in Table 2. Slabs with successively increasing thermal parameter are colder and thus differ in the predicted region of metastability, delineated above by the equilibrium boundary (dashed line) and below by the 99% transformation contour (solid line). Younger and more slowly sinking slabs (e.g., categories A and B) are hot enough that olivine → spinel transformation essentially keeps pace with the descent rate and is completed near its equilibrium phase boundary. At most a small metastable region forms, so deep earthquakes would not occur. Older and faster subducting slabs (e.g., categories C and D) are cold enough that kinetic hindrance prevents transformation from keeping pace with the descent rate. Metastable olivine thus persists below the equilibrium phase boundary depth, and deep earthquakes occur by transformational faulting within the wedge. These predictions are consistent with the variation in earthquake depths between and along subduction zones, in that deep earthquakes occur only when the thermal parameter exceeds about 5000 km (Figure 4).

age of lithosphere and the convergence rate increase from west to east (Plate 4). Earthquakes deeper than 350 km, however, only occur east of approximately 105°E (Figure 11). A cross section parallel to the arc (Figure 12a) shows that the onset of deep earthquakes from west to east occurs abruptly when the thermal parameter exceeds about 5000 km (Figure 12b). Thus the onset of deep seismicity along this arc is similar to that observed in the global compilation of Figure 4.

TABLE 2. Assumed Plate Ages, Convergence Rates, and Calculated Thermal Parameters

Slab Category	*Age, Ma*	*Convergence Rate, cm/yr*	*Thermal Parameter, km*
A	12	6	360
B	50	7	2,475
C	140	8	9,699
D	140	14	16,974

We regard these results as support for the metastability hypothesis. Although we made no a priori assumptions about the critical thermal parameter in the thermokinetic models, they predict an onset of metastability near the critical thermal parameter where deep events first occur.

4.3. Features and Limitations of the Thermokinetic Modeling

Several points merit additional discussion. First, the exact depth extent of metastability predicted is less significant than the predicted presence of an appreciable metastable wedge within slabs in the age and convergence rate range that have deep earthquakes. The simple models used here do not explain the abrupt onset of deep earthquakes at a thermal parameter of about 5000 km; the bottom of the metastable wedge in model C is at about 500 km, whereas earthquakes for slabs in this thermal parameter range typically extend to depths of 550–690 km. Hence although the model predicts the observed first-order behavior, its simplicity may make it inadequate to predict fine details. In particular, uncertainties in the predicted depth extent of metastability result from simplifications in both the thermal model and the extrapolation of spinel growth rates to temperatures markedly lower than constrained by the experiments.

Second, the maximum depth of metastability and thus the predicted seismicity are ultimately limited because near the base of the transition zone, either metastable olivine or spinel transforms to the stable lower mantle assemblage. As discussed in sections 5.4.2 and 5.4.3, these transformations should not be seismogenic. This ultimate limiting condition is not included in our model because the metastability field for olivine is not predicted to go significantly into the lower mantle.

Third, the sides of the wedge in models C and D approximately coincide with the 600°C isotherm due to the strong temperature dependence of the transformation rate. Hence for old, fast subducting, and hence cold slabs where metastability should occur, the long-suggested approximate relation between the maximum depth of seismicity and a limiting isotherm would be expected [*Kirby et al.*, 1991]. The metastability hypothesis thus reconciles the apparent temperature control of the deepest seismicity with the observation that no such critical weakening is expected from laboratory-based rheological laws for olivine [*Brodholt and Stein*, 1988]. In this view, the temperature effect on metastability, rather than on strength, controls earthquake depth distribution.

Last, this thermokinetic model does not incorporate any internal deformation. Various observations (section 7) suggest that slabs deform at the bottoms of Wadati-Benioff zones, so simple models may be inappropriate there.

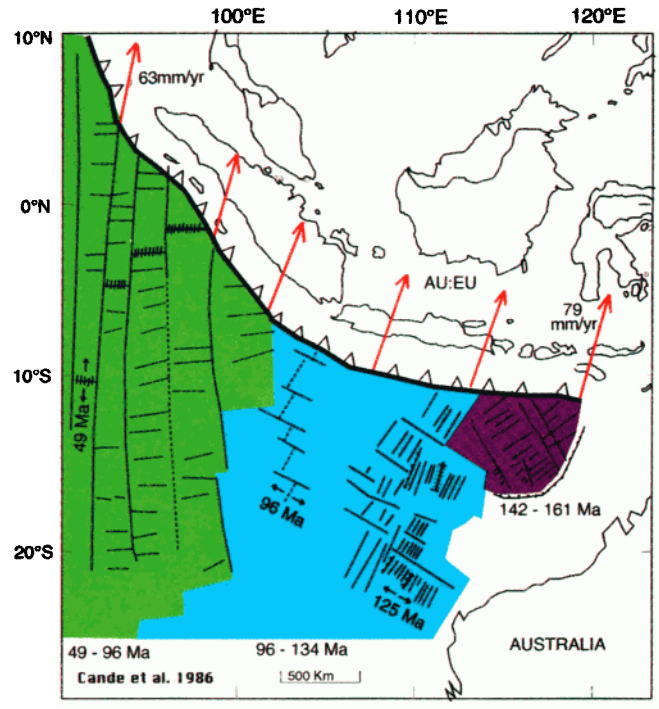

Plate 4. Plate tectonic setting of the Indonesia subduction zone showing magnetic anomalies, fracture zones, and age of the Australian plate being consumed at the Sunda/Java trench (serrated) [*Cande et al.*, 1989; *Veevers et al.*, 1991] and the convergence rates calculated from the NUVEL-1 rigid plate motions of the Australian plate relative to the Eurasian plate [*DeMets et al.*, 1990]. Diverging arrows indicate fossil spreading centers (dashed where inferred) with the approximate ages of cessation of spreading.

5. HIGH-PRESSURE SHEAR INSTABILITIES

The modeling results presented above indicate that significant regions of metastable peridotite would be expected in the coldest interiors of downgoing slabs that have deep earthquakes. Such metastability has implications for various failure mechanisms proposed for deep earthquakes. In this paper, we explore a mechanism, transformational faulting, that requires the presence of this metastability. Before exploring this hypothesis, we review and evaluate some other proposed mechanisms in view of the likelihood that many slabs have significant metastable regions.

5.1. Effects of Initial Pore Fluids

The failure processes responsible for shallow faulting, ordinary brittle fracture and frictional sliding, are unlikely to occur in unmodified form at depths below a few tens of kilometers because the stresses required for fracture and frictional sliding (i.e., brittle strength) increase linearly with pressure [e.g., *Griggs and Handin*, 1960; *Kirby*, 1987]. Hence fracture or sliding would require stresses much higher than the likely ductile strength. Fluids in porous rocks may extend the depth range of brittle fracture and frictional sliding by reducing

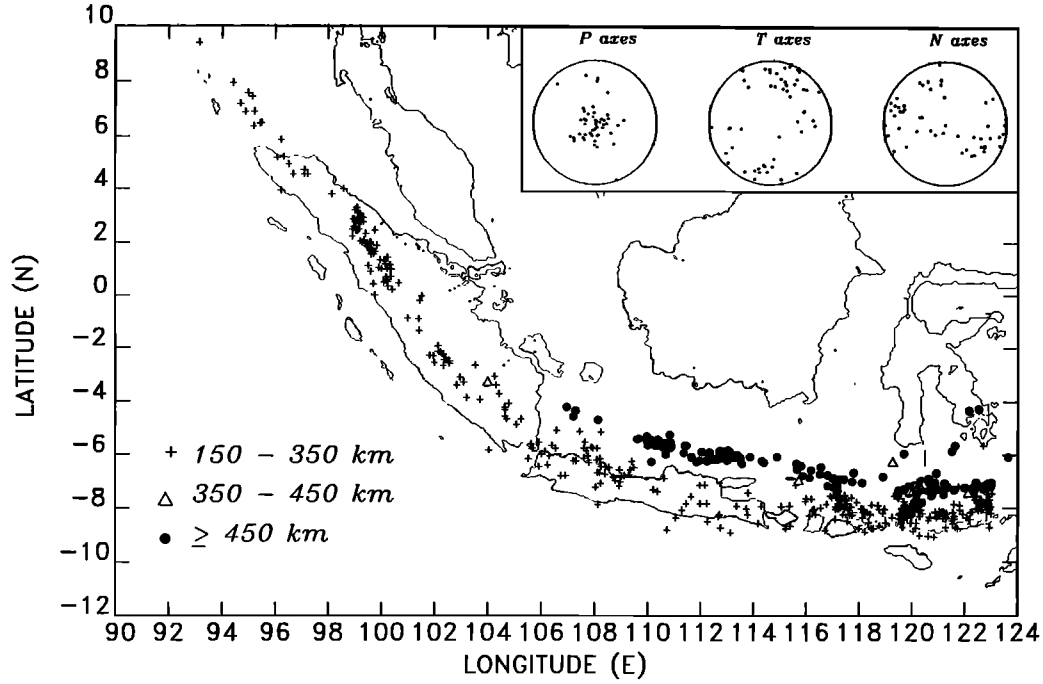

Figure 11. Epicenters of earthquakes with focal depths greater than 150 km along the Indonesia subduction zone. Events before 1964 are relocated using the method of *Wysession et al.* [1991]. Locations of post-1963 events are generally from ISC or National Earthquake Information Center (NEIC) preliminary determination of epicenters (PDE) catalogues. Note the abrupt deepening of seismicity east of 107°E and the spatial separation of deep and intermediate depth events from 107° to 115°E. The focal mechanisms of deep events were assembled from various sources and show a pattern of *P* axes oriented downdip, generally consistent with observations of deep earthquakes elsewhere [e.g., *Isacks and Molnar*, 1971].

the effective normal stress and hence the brittle strength [*Hubbert and Rubey*, 1959; *Handin et al.*, 1963; *Paterson*, 1978]. This faulting process is, however, an unlikely candidate for deep seismic failure because at depth in oceanic lithosphere, free pore water is unstable, reacting with crust and mantle at shallow depths to form hydrous minerals [e.g., *Ulmer and Trommsdorff*, 1995].

5.2. Dehydration Embrittlement

Water may exist at depth in oceanic lithosphere primarily in chemically combined form in hydrous minerals but would not reduce effective stress until the minerals reach sufficiently high temperatures that free water is liberated by dehydration [*Hubbert and Rubey*, 1959]. *Raleigh and Paterson* [1965] discovered that such dehydration weakens serpentine and causes faulting at pressures where serpentine otherwise would be ductile and strong. Subsequent work showed that such dehydration embrittlement is a general phenomenon where unstable hydrous minerals release water and thus reduce effective stress [*Paterson*, 1978].

It has been proposed that dehydration embrittlement may be an important faulting process for intermediate and possibly deep earthquakes [*Raleigh*, 1967; *Green and Burnley*, 1989; *Meade and Jeanloz*, 1991; *Green and Houston*, 1995; *Kirby*, 1995; *Silver et al.*, 1995]. Faulting by this process would be delayed until the hydrated regions of subducting slabs heat up sufficiently to liberate water by dehydration. A recent development in evaluating this candidate for deep seismic faulting has been the recognition that many of the hydrous rocks in oceanic crust (recovered from drilling, dredging, and exposures on land) occur along faults and shear zones created at spreading centers and trench-rise systems [e.g., *Kirby*, 1995]. Thus when these faults are reactivated during dehydration, slip can occur right where pore pressure is high [*Kirby*, 1995; *Silver et al.*, 1995; *Kirby et al.*, 1996]. This hypothesis for the mechanism of intraslab earthquakes by fault reactivation via dehydration embrittlement is an extension of the fault reactivation hypothesis of *Savage* [1969]. Intermediate-depth earthquakes in slabs (i.e., those in the approximate depth range 70–325 km) may thus occur by slip on fossil faults weakened by dehydration embrittlement [*Kirby*, 1995; *Kirby et al.*, 1996]. This earthquake population is distinct from deep earthquakes, because it peaks at about 100–125 km and decays to a relative minimum at about 300–325 km [*Kirby*, 1995] (Figure 2a). The peak corresponds to the average depth of Wadati-Benioff zones beneath arc volcanoes, where large-scale slab dehydration is thought to occur. The subsequent decay of this population to minimal activity at 300–325 km suggests that dehydration embrittlement is exhausted by that depth and hence is not the physical mechanism for deep earthquakes [cf.

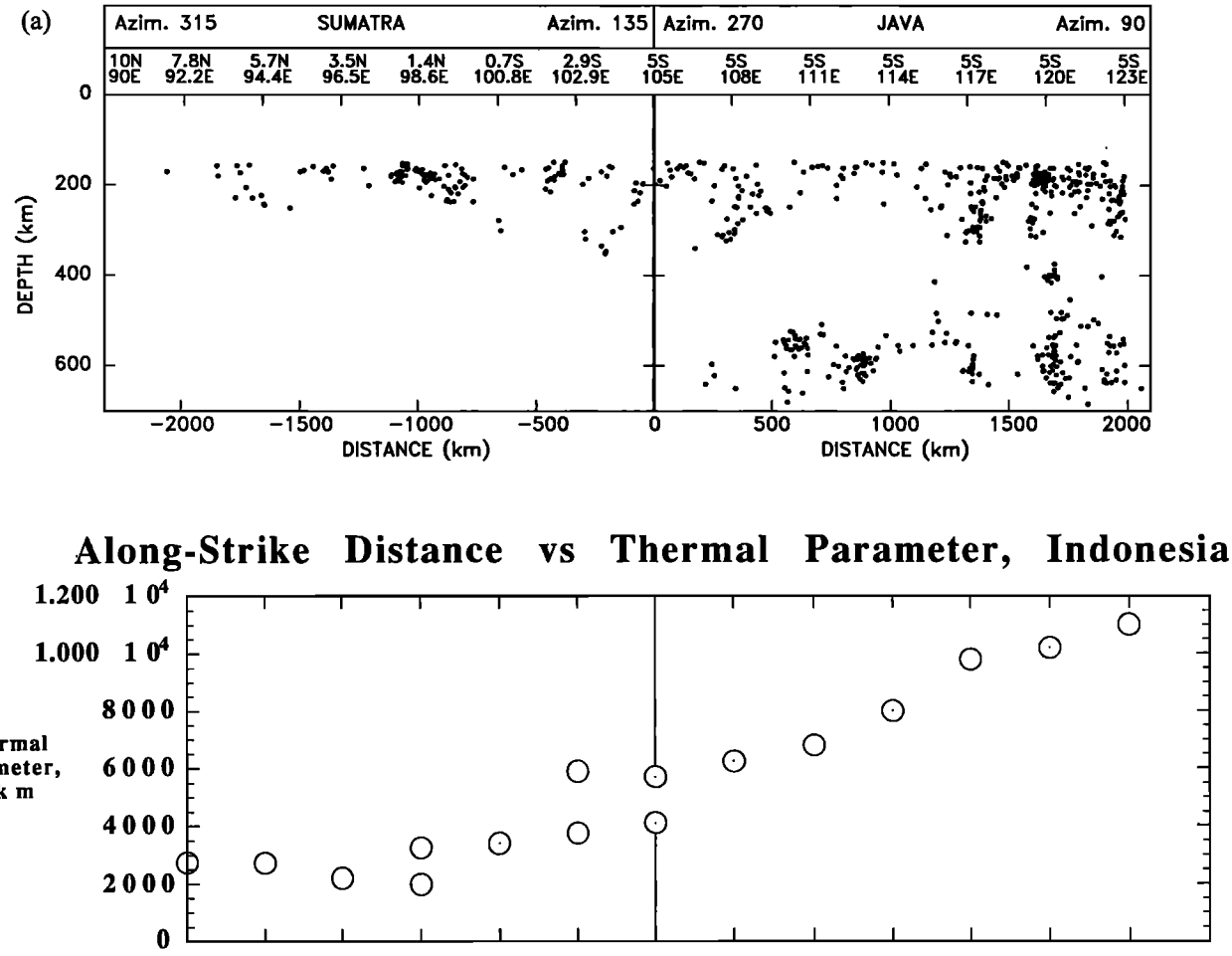

Figure 12. (a) Variation in earthquake depths determined in this study with distance along the Indonesia subduction zone showing clustered nature of slab seismicity and the marked deepening east of 105°E. Earthquake data are the same as in Figure 11. Note that earthquakes are absent at depths between 350 and 500 km from longitude 107° to about 115°E. (b) Along-strike variation of thermal parameter for the Australian slab beneath Indonesia. The double values of thermal parameter indicate uncertainty in the longitudinal position of the boundary between lithosphere created by late Cretaceous/Tertiary spreading (49–84 Ma) and earlier Cretaceous quiet zone and M series spreading (84–161 Ma) (see Plate 4).

Silver et al., 1995]). Recent laboratory studies of the stability of hydrous phases in slabs [*Schmidt and Poli*, 1994; *Ulmer and Trommsdorff*, 1995] support this conclusion. These results are not surprising because hydrous minerals are only stable near the upper surfaces of oceanic plates and hence should be the first part of descending slabs to heat up and dehydrate during slab descent.

5.3. Other Shear Mechanisms

Some other proposed mechanisms for deep earthquakes have similarities to transformational faulting, but seem less likely because metastability is expected in the coldest interiors of the coldest slabs where deep earthquakes occur. *Griggs and Baker* [1968] and *Ogawa* [1987] proposed that deep earthquakes occur via a shear instability that results when the viscosity of a fault zone is reduced by shear heating until the onset of melting. This instability is a positive feedback, in that such heating reduces the fault strength, causes the velocity across the fault to rise, and thus provides faster shear heating, raising the temperature further. However, in metastable material, such heating should favor the formation of the stable high-pressure phases, spinel and ilmenite, rather than partial melt, because internal heating should promote the kinetics of the solid-state reactions at lower temperatures than those required for partial melting. Put another way, transformational faulting should intervene during the temperature runup associated with thermal feedback before the onset of melting.

Similarly, the shear localization mechanism favored by *Post* [1977] and *Hobbs and Ord* [1988] involves grain size reduction by recrystallization of olivine under stress and strain localization by grain-size-sensitive superplasticity in the fine-grained zones. This "ductile-faulting" mechanism is similar to transformational faulting but without the phase change. It is likely, however, that metastable olivine and clinoenstatite in slabs would re-

crystallize to the stable phases (spinel and ilmenite) rather than back to metastable olivine and clinoenstatite. Such a mechanism is, however, more plausible in the relatively cold spinel-rich region outside metastable wedges, perhaps triggered by transformational faulting inside wedges. This may be a viable mechanism for some small aftershocks of large deep events (section 7.3.2).

Lomnitz-Adler [1990] suggested that deep earthquakes are caused by the olivine-spinel transformation via a martensitic (crystallographic shear) mechanism similar to mechanical twinning [*Poirier*, 1985; *Kirby and Stern*, 1993]. Although martensitic transformations [*Meade and Jeanloz*, 1989] and mechanical twinning can produce acoustic emissions in the laboratory, neither process is known to produce macroscopic faulting. S. H. Kirby has conducted dozens of experiments on polycrystalline and single-crystal enstatite under conditions where the martensitic polymorph readily forms and has observed no macroscopic faulting. Crystallographic shear transformations may not form throughgoing shear zones because such shear occurs on prescribed crystallographic planes and directions and so would not propagate between grains of varying orientation. Moreover, the ratio of volumetric to shear strain (0.22) prescribed by the crystallography [*Kirby and Stern*, 1993] is higher than inferred for deep earthquakes (section 7.3.1). It seems more probable that martensitic lamellae could form locally at high strain rates during the propagation of a transformational fault and then serve as nuclei for subsequent growth of spinel [*Burnley*, 1995].

Meade and Jeanloz [1991] noted microacoustic emissions accompanying the disappearance of the X ray lines of crystalline serpentine during pressurization of serpentine in a diamond anvil cell. They proposed that formation of an amorphous phase in serpentine causes deep earthquakes, via localized strength reduction and faulting. These experiments are difficult to interpret because the physical conditions in their samples are poorly known, acoustic emissions do not necessarily indicate faulting, and the very high-pressure phase relations and kinetics of amorphization are not established. As noted in section 5.2, the stability relations for serpentine [*Ulmer and Trommsdorff*, 1995] cast doubt that it would be spared dehydration near the tops of slabs that have descended to depths below about 600 km. However, if serpentine transforms to another hydrous phase, amorphization might occur to greater depths.

5.4. Transformational Faulting

Bridgman [1945] and *Griggs* [1954] speculated that polymorphic phase changes might be important physical processes for deep earthquakes. Experimental deformation of anhydrous minerals that change to denser forms at high pressures was subsequently studied in the laboratory [*Griggs et al.*, 1960]. *Griggs and Handin* [1960] and *Griggs* [1972] noted that none of these experiments produced mechanical instabilities or weakening. Thus, although the subduction process requires the conversion of large volumes of material to denser, higher-pressure phases, the fact that deep earthquakes did not show the expected isotropic implosions (section 7.3.1) suggested that such conversion did not occur rapidly enough to radiate seismic waves.

5.4.1. Experimental studies. Interest in a phase-change mechanism for deep earthquakes revived as a consequence of experiments indicating that rapid phase conversion could occur in a primarily shear, rather than isotropic mode. These studies have shown that under metastable conditions, some minerals partially transform to denser phases by a localization of transformation and strain into thin shear zones called transformational faults. This phenomenon was observed in such transformations as Ice I → II [*Durham et al.*, 1983; *Kirby et al.*, 1985; *Kirby*, 1987; *Kirby et al.*, 1991, 1992; *Stern et al.*, 1994] and tremolite → amorphous phase (isochemical but not polymorphic because the product phase is noncrystalline) [*Burnley and Kirby*, 1982; *Dell'Angelo*, 1993]. Further interest was stimulated by the discovery of transformational faulting in Mg_2GeO_4 olivine → spinel [*Green and Burnley*, 1989; *Burnley et al.*, 1991] and possibly olivine → spinel [*Green et al.*, 1990].

The transformational faulting process showed various features that have potential implications for deep earthquake faulting:

1. Only phase changes in mineral systems that display polymorphism, significant volume changes, and high latent heats produce transformational faulting (Figures 13 and 14). All three factors appear necessary because transformational faulting involves rapid transformation of the metastable host phase to the high-pressure phase as the fault grows. For example, the reaction albite → jadeite plus quartz, which is nonpolymorphic because two minerals are produced, proceeds smoothly under stress without faulting even though it is strongly exothermic with a large volume change (B. R. Hacker and S. H. Kirby, unpublished data, 1995). Such nonpolymorphic transformations have lower limiting rates than polymorphic ones, because the formation of two product phases require long-range diffusion of chemical components. Similarly, the weakly exothermic and polymorphic transformations calcite → aragonite [*Hacker and Kirby*, 1993] and α-quartz → coesite [*Tullis*, 1971] occur smoothly under stress (Figure 13) [*Kirby et al.*, 1991]. Release of latent heat favors transformational faulting by providing destabilizing thermal feedbacks [*Kirby*, 1987; *Kirby et al.*, 1991; *Burnley et al.*, 1991]. The additional heat evidently both speeds reaction kinetics, as in chemical explosions, and weakens the fault zone in a fashion similar to the effect of viscous heating [*Grunfest*, 1963; *Griggs and Baker*, 1968; *Anderson and Perkins*, 1974; *Ogawa*, 1987].

2. Transformational faulting develops only at temperatures low enough that bulk transformation is kinetically sluggish. Under these conditions the low-pressure phase persists metastably well into the P-T stability field

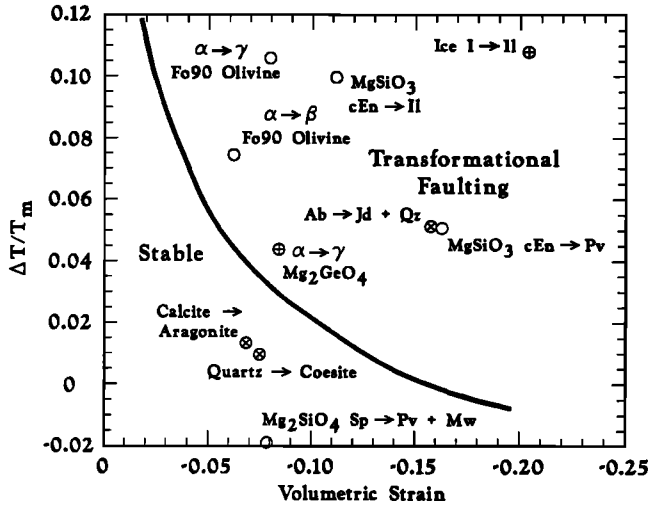

Figure 13. Effects of the thermodynamic properties of phase changes (volumetric strain versus temperature rise from heat of reaction normalized by the temperature of melting, T_m) on the occurrence of transformational faulting. Transformations with crosses do not display transformational faulting, whereas those that do are indicated by pluses. Open symbols denote mantle reactions for which transformational faulting properties are not known. Faulting is restricted to polymorphic transformations with large latent heats, suggesting that the olivine → spinel and clinoenstatite (cEn) → ilmenite transformations both should be seismogenic, whereas the prime lower-mantle-forming reactions in slabs, spinel → Pv + Mw and ilmenite → Pv (not shown), should not.

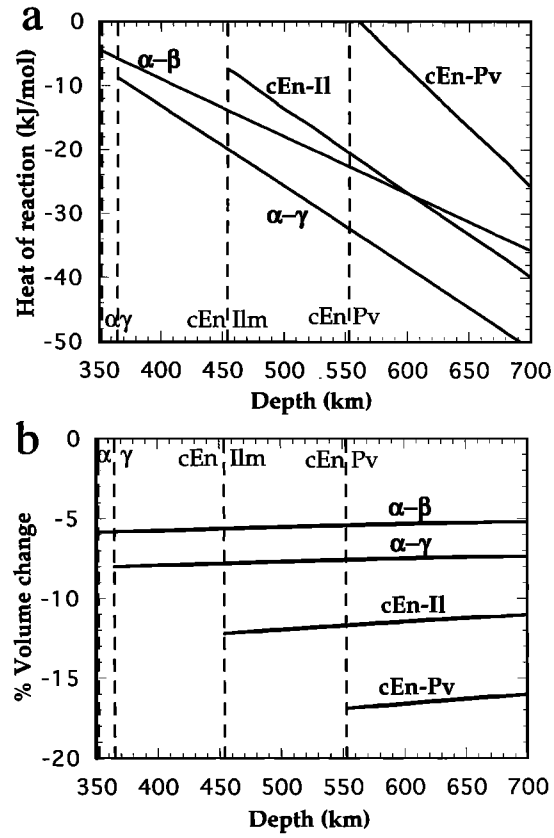

Figure 14. Variations of thermodynamic properties for several mantle phase changes along the coldest temperature profile of the Tonga slab (Plate 2b and Figure 7a). (a) Heat of reaction and (b) volume changes. Both properties are negative, indicating that heat is liberated and volume is reduced. Vertical dashed lines are the depths corresponding to the equilibrium pressures for the indicated transformations. The properties of the endothermic ilmenite → perovskite reaction (Figure 10) are not shown.

of the high-pressure phase before faulting under deviatoric stress.

3. Initial inelastic yielding is followed by sudden stress drops accompanied by loud acoustic reports.

4. Abundant compressional microinclusions of the high-pressure phase are implicated in the nucleation of the faults [*Green and Burnley*, 1989; *Burnley et al.*, 1991] (Figures 15, 16, and 17). Fault growth takes place by the formation of self-propagating arrays of inclusions produced by stresses localized at the edge of a growing zone (Figures 18b–20) [*Kirby et al.*, 1991; *Stern et al.*, 1994].

5. Thin fault zones with appreciable shear offsets develop (Figures 15b and 17). In addition to some host material, the shear zones contain fine-grained high-pressure phase. The fine grain size of the high-pressure phase helps explain why the shear zone is weak relative to its matrix, despite the fact that when the high-pressure phases are coarse grained, they are generally stronger than their low-pressure polymorphs. Fine grain size evidently lowers strength by promoting the superplasticity often displayed by very fine-grained materials [*Poirier*, 1985].

6. The total amount of sample transformed to the denser phase after faulting is small, usually less than a few percent.

5.4.2. Transformational-faulting origin for deep earthquakes. *Kirby* [1987], *Green and Burnley* [1989], *Kirby et al.* [1991], and *Burnley et al.* [1991] argued that deep earthquakes occur by transformational faulting. Two key features make this mechanism plausible: shear occurs suddenly enough to radiate elastic waves, and the faults are thin relative to the shear displacements [*Kirby et al.*, 1991]. Thus transformational faults are fundamentally shear instabilities whose static displacement fields have very small isotropic components. If these static spatial characteristics scale to the dynamic displacements over deep earthquake source dimensions, transformational faults should provide essentially shear (double-couple) earthquake sources.

Although transformational faulting is a shear instability, its energetics have similarities to explosive chemical reactions. Explosive reactions commonly are strongly exothermic, with feedback such that heat released by reaction raises temperatures, speeds reaction, and hence leads to runaway reaction rates [*Dainton*, 1966; *Hodder*, 1984; *Scott*, 1991]. The association of transformational faulting in the laboratory with strongly exothermic mineral reactions suggests that a high heat of

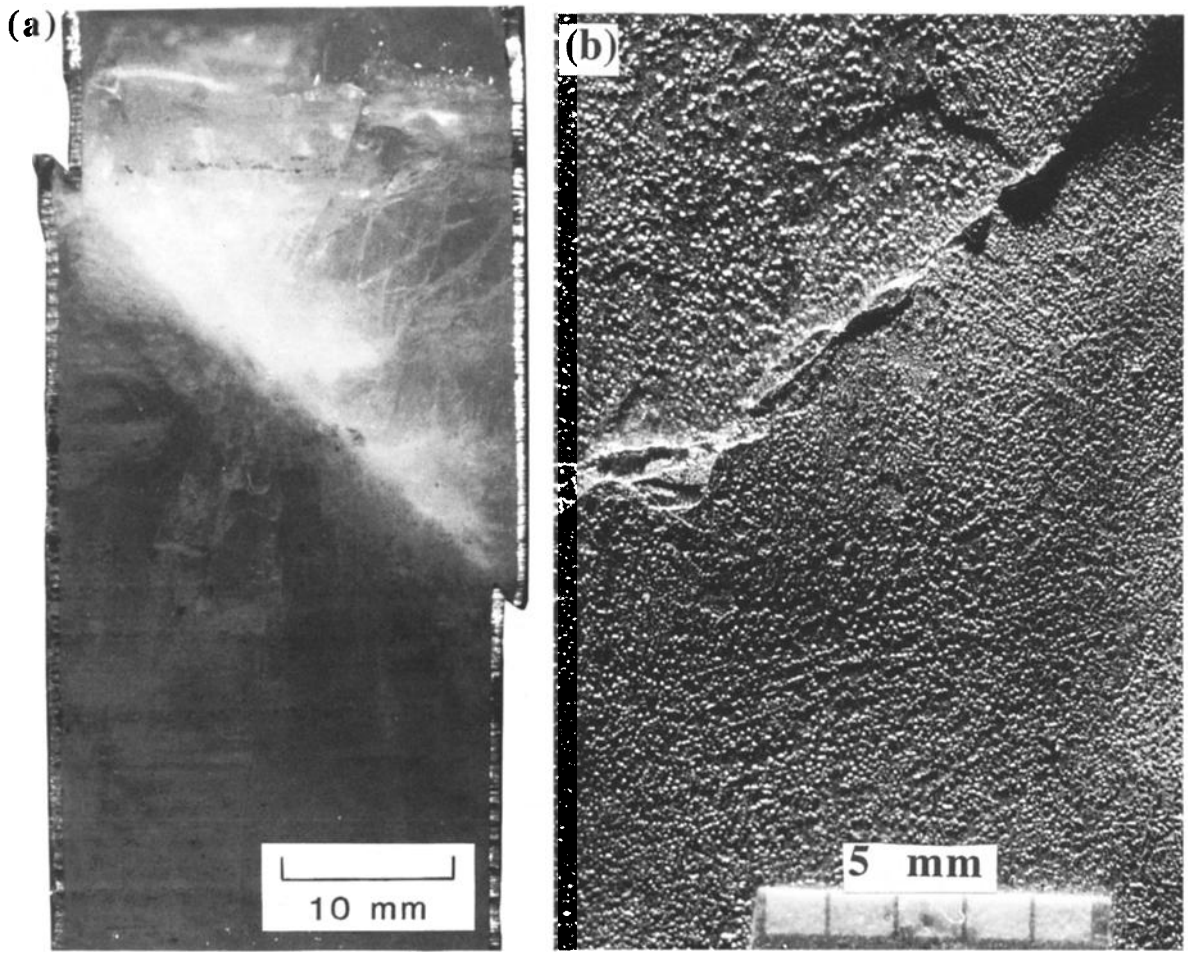

Figure 15. Transformational faults in ice I partially transformed to ice II under metastable conditions. Transformational faulting was discovered in experiments on this material. Shear displacement is several millimeters, but the shear zone is much less than 100 μm thick. (a) Central portion of sample sawcut along original cylinder axis. Note that the fault is cohesive (not fractured). Light areas are believed to be release microfractures that probably occurred during unloading and depressurization. (b) Inside of cylindrical indium jacket of faulted ice sample 308 that replicates surface topography produced by the ice I → II volume change and the shear displacement of the transformational fault. The fault shear zone is very thin (≪1 mm), but the shear displacement is several millimeters. The small, bright features are microinclusions of ice II. Faint streaks inclined to the compression direction are arrays of ice II inclusions that self organize under shear stress and are believed to be prototransformational faults.

reaction is required. With increasing depth and pressure inside a metastable wedge, the driving potential for growth of spinel (which increases with increasing pressure overstep), the heat of transformation to spinel, and, as explained shortly, the stress due to the volume change, all increase to maxima at the wedge tip. Thus the factors promoting transformational faulting should peak at the bottom of the metastable region.

The lack of evidence for rapid implosive reactions for minerals under hydrostatic conditions in the laboratory implies that shear stresses are essential for solid-solid transformations to occur at very high rates. Shear plays at least two likely roles in the instability. Shear heating should occur in transformational faults and thus augment the destabilizing effect of the heats of reaction. Shear probably also increases the rates of transformation during the growth of transformational faults [*Kirby*, 1987; *Wu et al.*, 1993]. Although the effects of deformation on the kinetics of bulk transformation are well documented experimentally [e.g., *Kirby et al.*, 1991, 1992; *Burnley et al.*, 1991; *Wu et al.*, 1993], the mechanisms of kinetic enhancement are not firmly established.

Some limitations of the transformational faulting hypothesis are evident. It has not been demonstrated that transformational faults occur under slab conditions and that such faults would scale up dimensionally and temporally from those in the laboratory. For example, the finite size of laboratory samples is destabilizing in the sense that as a transformational fault grows, the local shear stresses promoting its growth increase with fault size because less and less of the sample supports the load. It is not known whether this potential source re-

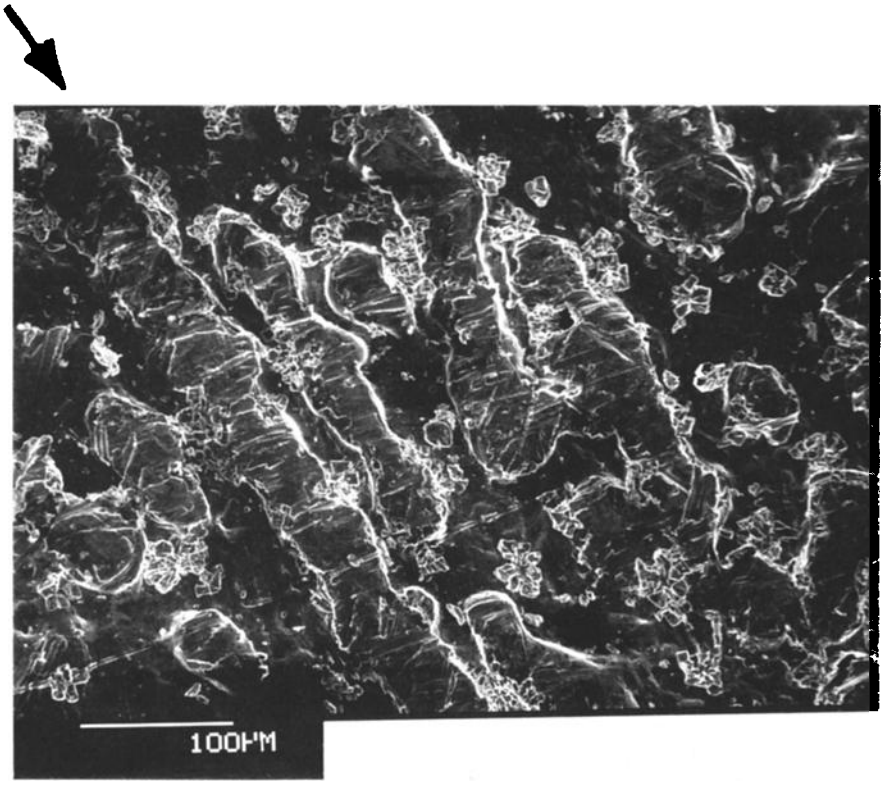

Figure 16. Scanning electron micrograph of inclined arrays of ice II inclusions shown in Figure 15b and also showing an array (arrow) that has grown into a continuous layer of ice II and is believed to represent a prototransformational fault.

gion finiteness is destabilizing in very large earthquakes in slabs.

5.4.3. Depth range of transformational faulting in slabs. The metastability hypothesis for deep earthquakes requires that their depth range correspond to that of metastable phase transformations with the appropriate properties for such faulting. Two of the reactions forming the transition zone mineral assemblage have the properties of mineral systems that display transformational faults in the laboratory. As noted in section 4, large-scale olivine metastability is expected in some subducting lithosphere. In addition, preliminary experiments on the rates of conversion of clinoenstatite to higher-pressure phases show even greater kinetic hindrance than for olivine. Hence, in an old, cold slab, harzburgitic peridotite should persist well below the 350–410 km depth where olivine and clinoenstatite first become metastable. Transformational faulting is expected for reactions where both the latent heat and volume change are significantly negative. Hence, as shown in Figures 14a and 14b, the two major minerals of peridotite in slabs, olivine and clinoenstatite, have properties favoring transformational faulting.

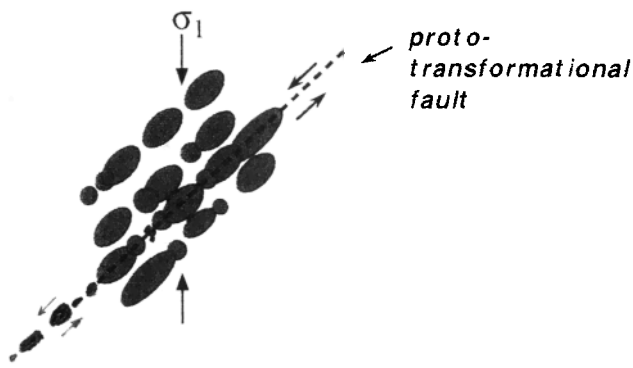

Figure 17. Schematic diagram illustrating how transformational faults form by the in-plane nucleation and growth of ice II inclusions at the edge of the array and by coalescence between ice II inclusions (from material of *Stern et al.* [1994]).

Transformational faulting is not, however, expected for the reactions which transform minerals in slabs to the lower mantle assemblage. Direct conversion of metastable clinoenstatite to perovskite and metastable olivine to magnesiowüstite plus perovskite both have positive latent heats. Hence even if metastable olivine and clinoenstatite survive to the bottom of the transition zone in slabs, they should not undergo transformational faulting. Moreover, the reactions that convert the slab transition zone phases to lower mantle phases (ilmenite → perovskite and spinel → magnesiowüstite plus perovskite)

absorb heat. Therefore transformational faulting should not occur in the lower mantle.

6. DEEP SLAB SEISMIC DEFORMATION

6.1. Earlier Ideas

The hypothesis that deep earthquakes occur in metastable material within cold slabs gives a new perspective on questions which earlier ideas about deep earthquakes could not resolve. The condition for earthquakes to occur is that stresses reach the seismogenic faulting strength. Thus the distribution of deep earthquakes maps the intersection of two spatially varying quantities: stresses in slabs and the faulting stress required by the unknown failure mechanism. Deep earthquakes do not occur outside slabs, because material there is too weak to store enough elastic strain energy to cause a significant earthquake. Within slabs, deep earthquakes occur only in regions with either lower strength than the aseismic regions, higher stress, or a combination thereof.

Prior treatments of deep seismicity focused on the role of low slab temperature in controlling both the stresses and the ductile strength [*Isacks et al.*, 1968; *McKenzie*, 1969; *Molnar et al.*, 1979; *Richter*, 1979; *Davies*, 1980; *Wortel*, 1982, 1986; *Wortel and Vlaar*, 1988; *Vassiliou and Hager*, 1988]. Cold slabs should be denser than their surroundings, so a negative buoyancy body force interacts with viscous forces resisting slab motion, producing higher stresses in slabs compared to their surroundings. The cold slabs should also be strong enough to support and transmit much higher stresses than the surrounding mantle. Modeling studies based on these assumptions produce stresses generally consistent with inferences from the depths and focal mechanisms of deep earthquakes [e.g., *Wortel and Vlaar*, 1988]. It has also been assumed that slab temperatures control the spatial distribution of seismicity, with earthquakes occurring only in portions of slabs where the temperature is low enough that high strength is predicted by a ductile flow law. This strong region should bound the potentially seismogenic region, because the faulting strength must be less than the ductile strength for faulting rather than flow to occur (Plate 5a).

This thermomechanical approach, though successful at explaining many aspects of deep seismicity, is clearly incomplete. This incompleteness is shown by the fact that it leaves at least three major issues unresolved. First, it does not adequately explain the coincidence of the depths of deep earthquakes with the transition zone in slabs. Deep earthquakes form a distinct population ranging in depth from about 350 to 690 km, whereas seismological observations suggest that some slabs extend deeper into the mantle. Hence earthquakes stop at depths where laboratory results predict that slabs should continue to have considerable strength [e.g., *Brodholt and Stein*, 1988]. Second, it does not identify the failure process responsible for deep earthquakes. As noted earlier, the brittle strength of slab material should be enormous, far in excess of likely slab stresses, so deep earthquakes should not occur. Dehydration embrittlement seems unlikely to resolve this issue because it is unclear why this mechanism would be restricted to the transition zone in slabs (section 5.2). Third, it is insufficient to explain the earthquakes, which we consider later, that occur in detached portions of slabs that appear to have foundered at the bottom of the transition zone. In this geometry the stresses derived from thermal bouyancy seem inadequate to explain the seismicity and focal mechanisms.

6.2. Incorporation of Metastability

We have seen that large-scale metastability is predicted in slabs by thermokinetic modeling, and that laboratory results indicate that metastability should cause transformational faulting. Consideration of these effects of the mineralogical state of the slab provides a fuller description of slab processes than consideration of thermal effects alone. In particular, consideration of the effects of metastability provides useful insight into the three major issues listed in the last section.

First, because transformational faulting is expected only within the metastable region, the restriction of deep earthquakes to the transition zone in slabs is a natural consequence. Second, because transformational faulting in slabs occurs at lower stresses than for brittle fracture, transformational faulting provides a plausible failure mechanism. Third, as we shall see, the distribution of metastable material should give rise to stresses within slabs even if mechanically isolated.

Thus, as explored in later sections, the effects of metastability augment those expected from the purely thermomechanical perspective. The metastable wedge forms a distinct portion of the slab where earthquakes occur because it can fail seismically at lower stress than the surrounding, already transformed, portions of the slab. Moreover, as shown later, the reaction boundaries of the wedge provide a secondary source of stress reinforcing those due to thermal buoyancy. Hence the seis-

Plate 6. (opposite) Perspective diagram showing the deep earthquakes beneath the North Fiji Basin as viewed from the NW toward the SE. Blue dots indicate events from 1957 to 1992 with depths greater than 400 km. This isolated population of earthquakes is distinct from other earthquakes, shown as red and green symbols in the Vanuatu subduction zone (viewed approximately along strike). The isolated deep events extend under the downdip projection of the Vanuatu Wadati-Benioff zone, a relationship that argues against the deep zone being related to Vanuatu subduction. The isolated band of deep earthquakes is parallel to the fossil Vityaz trench and is thought to result from detachment of a slab that subducted at that trench and subsequently foundered to the bottom of the transition zone of the mantle [e.g., *Hamburger and Isacks*, 1987].

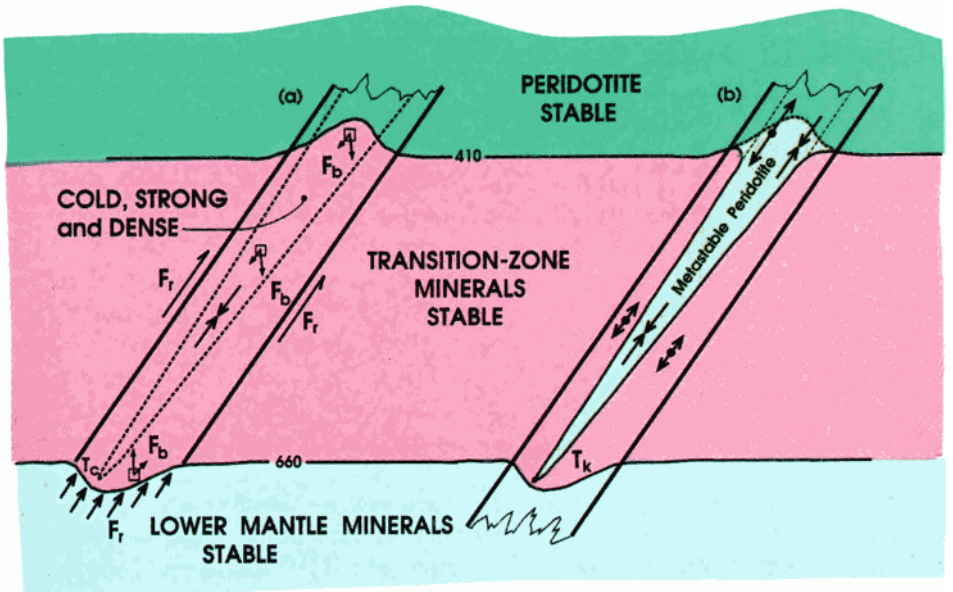

Plate 5. Schematic diagrams of slabs sinking into the transition zone showing the direct effects of cold slab temperatures, and the indirect effects of such temperatures in producing sluggish reaction kinetics. (a) Cold, strong and dense slab descends to the bottom of the transition zone and transforms to the transition zone assemblage at near-equilibrium conditions. High slab strength is sustained at temperatures below a critical temperature T_c. Stresses resulting from the downward thermal buoyancy forces (F_b) and the viscous forces (F_r) resisting slab descent are assumed to cause deep earthquakes at temperatures below T_c by some unspecified faulting process. (b) The cold thermal structure of the slab causes peridotite to bypass the equilibrium olivine → spinel boundary because of sluggish reaction rates. This condition produces a wedge-shaped region of metastable peridotite, which persists to some critical temperature T_k, where transition zone reactions take place. The net negative buoyancy of the slab is reduced by the relatively low-density wedge, reducing the stresses that derive from thermal buoyancy. Internal stresses occur in the slab in addition to those discussed in Plate 5a because of the mechanical effects of the volume change that accompanies the conversion to spinel. These internal stresses include both wedge-parallel compressive stresses in the wedge and slab-bending stresses in the vicinity of 410 km (opposed arrows). Deep earthquakes occur by transformational faulting in metastable peridotite where slab stresses satisfy the criterion for such failure. Earthquakes occur neither in portions of the slab that have transformed to spinel nor in the lower mantle, because subsequent reactions, if they occur, do not have the properties that produce transformational faulting.

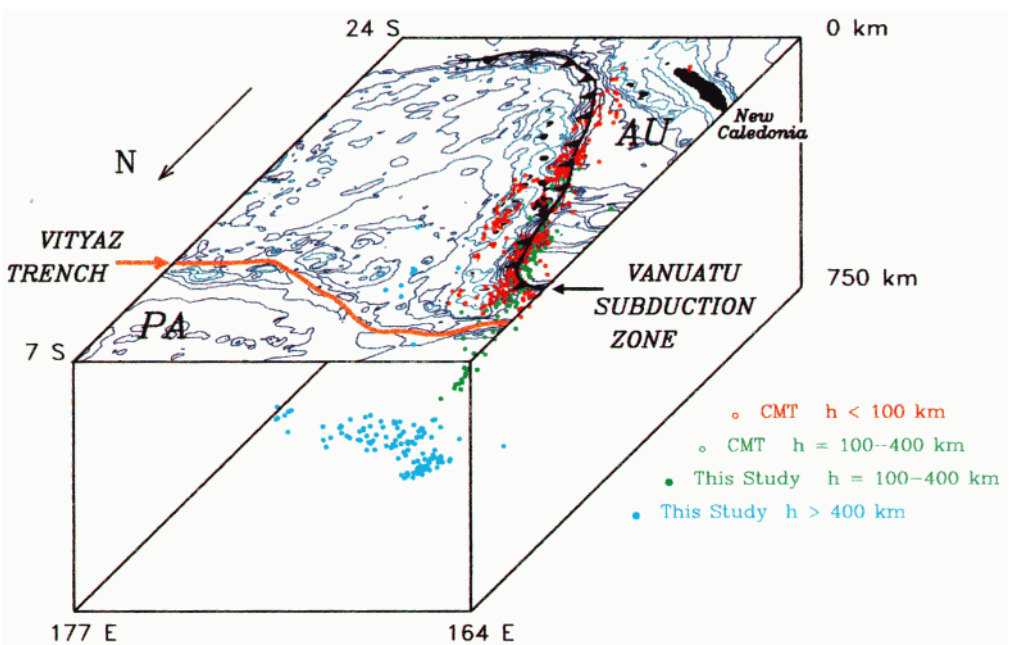

micity is controlled ultimately by temperature, via the kinetics of the phase changes.

To illustrate, consider the three peridotite blocks within a downgoing slab (Figure 9). Olivine in the region outside the cold slab core (block 2 or 3) transforms to spinel near the equilibrium boundary because the transformation rate keeps pace with the descent rate. In contrast, olivine in the block in the cold slab core (block 1) cannot transform rapidly enough relative to the descent rate and so persists metastably to depths below the equilibrium boundary. Within the metastable wedge, localized transformation can occur because the olivine is metastable and will occur by transformational faulting under the appropriate stress conditions, causing deep earthquakes. Eventually, the block reaches a depth where the bulk transformation rate keeps pace with the descent rate, and all the olivine transforms rapidly over a short distance. Below this depth, which is the lower wedge boundary, metastable olivine no longer exists, and deep earthquakes should not occur. Thus deep earthquakes within the metastable wedge result from localized transformations involving only a small fraction of the peridotite, most of which eventually transforms aseismically at the wedge boundaries.

In some cases, such as the Tonga slab, the wedge geometry may be such that metastable olivine persists to 670–700 km and then transforms directly to the stable lower mantle assemblage. This aseismic transformation should occur close to the equilibrium boundary, because most of the slab, i.e., the material outside the wedge, has already transformed to spinel and released considerable latent heat and/or is finer grained, favoring more rapid kinetics.

6.3. Slab Stresses

Metastability affects stresses within slabs in a number of ways. Although the basic stress pattern is that due to thermal buoyancy and resistive forces, interesting additional effects are expected. We discuss these effects here and later show that many are consistent with seismological observations.

First, the metastable wedge changes the density of the slab, which governs the distribution of gravitational body forces. Density differences arise both because of the temperature contrast (the wedge is about 750°C colder than the surrounding slab and about 1000° colder than the mantle outside) and the 8% higher density of spinel. Thus metastable olivine in the wedge, which makes up about 1/5 of the slab (Figure 9), should be about 100 kg/m^3 less dense than the spinel outside the slab. Outside the wedge, however, the slab is about 100 kg/m^3 denser than its surroundings. Hence the density structure differs from that previously assumed for two reasons (Plate 5b). The relatively low-density wedge is present, and the previously assumed high-density region below the elevated equilibrium phase boundary [e.g., *Turcotte and Schubert*, 1971] is not present but instead forms the top of the wedge. The net negative buoyancy of the slab should be reduced, and the average downdip compressive stresses deriving from the balance between that buoyancy and the resistive forces due to the surrounding mantle should be less than previously assumed.

In addition to changing the buoyancy-derived stresses, the metastable wedge causes internal or "self" stresses due to volume changes associated with the bulk transformation (Plate 5b) [e.g., *McGarr*, 1976; *Woodward*, 1977; *Goto et al.*, 1987; *Kirby et al.*, 1991]. These self-stresses, which do not result from external forces, are generated locally by the heterogenous volume change. They are analogous to the thermoelastic stresses that cause fracture due to inhomogeneous expansion accompanying temperature changes, as occurs in an ice cube dropped into hot water. Even larger stresses and deformation result when a phase transformation varies spatially, because the volume changes are much larger than those for thermal expansion. Thus the sharp kinetic boundary defining the metastable wedge should produce significant self-stresses [*Goto et al.*, 1987; *Kirby et al.*, 1991].

The roughly layered structure of the metastable wedge should produce coherent stresses oriented parallel to the wedge, and hence slab, boundaries. This stress state is similar to that in a bimetallic strip where a layered stress state results from differential thermal expansion across a compositional boundary. In this situation, compression parallel to the interface occurs on the side where contraction is smallest, and the stress level depends upon the relative thicknesses and rheologies of the layers [*Boley and Weiner*, 1960]. In the descending slab, slab-parallel deviatoric compression should occur in the wedge, and deviatoric tension should occur in the transformed mantle outside the wedge (Plate 5b) [*Kirby et al.*, 1991]. Because differential contraction occurs across both the top and bottom boundaries of the wedge, as the wedge thins with depth, the net compressive stresses within it increase to a maximum near the tip where the stresses from both boundaries superimpose [*Goto et al.*, 1987]. Thus these self-stresses should be highest near the maximum depth of metastability, which in our models ranges from about 500 to 700 km. In addition, slab-bending stresses may result from an asymmetry in the transformation (R. Denlinger and S. H. Kirby, personal communication, 1995). Because material below the cold core is hotter and therefore transforms sooner than material above, flexural stresses arise with the lower portion of the wedge under compression and the upper part under deviatoric tension (Plate 5b). Such flexural stresses should occur between about 350 and 450 km depth, where the asymmetry in bulk transformation is greatest, and be most significant in shallowly dipping slabs (R. Denlinger, personal communication, 1995).

Further complexities would also be expected because real slabs are more complicated than the idealized two-dimensional thermokinetic models. For example, we used a simple planar geometry and included no variations in the thermal or mineralogic structure of the lithosphere entering the trench and no lateral variations

in physical properties within the slab. In real slabs, these and other effects could cause complexities in the geometries of kinetic phase boundaries, the stresses accompanying heterogeneous phase changes, and the geometries of regions where transformational faulting can occur. In section 7 we speculate that such complexities in the geometry of metastable olivine regions cause various peculiar and enigmatic aspects of deep earthquakes.

7. DEEP EARTHQUAKE PHENOMENOLOGY AND MANTLE PHASE CHANGES

We now turn to various features of deep earthquakes that have implications for their origin. These features can be divided into three broad categories: the global distribution and tectonic settings of deep earthquakes, the fine structure of individual Wadati-Benioff zones, and the source properties of deep events. We briefly review each feature in a sequence that roughly reflects its relative significance and argue that some of its characteristics are difficult to explain without invoking the effects of metastability and transformational faulting. We review in some detail those features which have not already been introduced and refer to earlier discussions for features already noted.

7.1. Global Distribution and Tectonic Setting

7.1.1. Wadati-Benioff zones. Deep earthquakes generally form curvi-planar Wadati-Benioff zones associated with surface manifestations of subduction and with high seismic velocities. This points to failure in cold, strong, subducting slabs. As noted earlier, without invoking metastability and transformational faulting it is hard to see how earthquake failure can occur at transition zone depths.

7.1.2. Depth distribution of earthquakes. We consider deep earthquakes to be those forming the distinct population of earthquakes at depths below 300–325 km evident on seismicity-depth histograms (Figure 2a). Deep seismicity is restricted to depths bracketing the transition zone. The distribution is not uniform; the number of deep earthquakes peaks at about 600 km and declines steeply to an apparent limit at about 690 km [*Gutenberg and Richter*, 1954; *Gutenberg*, 1956; *Sykes*, 1966; *Isacks et al.*, 1968; *Stark and Frohlich*, 1985; *Rees and Okal*, 1987]. Viewed either by number of large earthquakes or seismic moment, the population is bimodal (Figure 18), with peaks at depths near 400 and 600 km and a relative minimum at about 500 km. The depth cutoff at about 600–690 km is shown well by the deepest earthquakes in individual Wadati-Benioff zones (Figure 3). Thus the four key aspects of the depth distribution are the onset of deep seismicity at 325–350 km, the secondary peak at 330–430 km, the major peak at about 600 km, and the cessation at about 650–700 km.

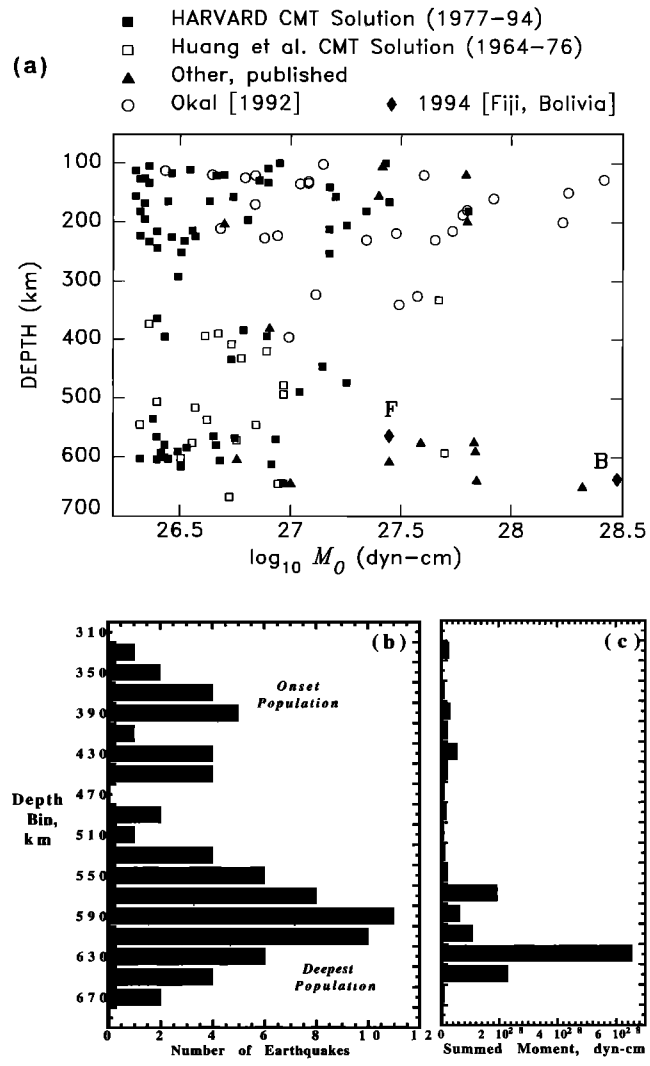

Figure 18. (a) Seismic moments of large intermediate and deep earthquakes plotted against depth (modified and updated from *Okal* [1992]). Note the relative minimum in activity at about 300 km depth, the sporadic activity at 325–400 km, and the steep rise at depths greater than 450 km in maximum moments and numbers of events. (b) Depth histogram for large earthquakes (moments greater than 1.5×10^{26} dyn cm) that are deeper than 300 km (January 1954 to July 1994). Many of the events at depths between 420 and 540 km occurred in the Izu-Bonin Wadati-Benioff zone (Plate 6). This histogram shows a small peak in deep activity near 330–430 km depth and a larger one near 600 km. Seismic moments binned in 20-km depth intervals of the large deep earthquakes shown in Figure 18b. This histogram shows that most of the deep seismic moment release occurs near the bottom of the transition zone in connection with a few of the largest events (see Table 1).

Historically, the variation in stress with depth was assumed to result largely from the balance between the negative buoyancy and resistive forces (Plate 5a). Modeling studies show that the peak in seismicity near 600 km can be a consequence of high stresses due to resistance to slab penetration into the lower mantle [e.g., *Richter*, 1979; *Vassiliou and Hager*, 1988; *Tao and*

O'Connell, 1993]. Seismological studies (e.g., Plate 1) indicate that some slabs are deflected or distorted at 660 km, whereas others penetrate to substantially greater depths and in some cases deform. It is thus plausible to relate the peak in seismicity at 600 km to slabs encountering resistance to penetration into the lower mantle.

It is not, however, appropriate to assume that seismicity ceases near 660 km because slabs somehow end or fail to enter the lower mantle. The failure of thermomechanical arguments alone to provide a physical mechanism for the cessation of seismicity at about 700 km, despite seismological evidence for slab descent into the lower mantle, strikes us as a major limitation.

In contrast, the metastability hypothesis provides a natural explanation for the depth range and plausible explanations for the two peaks in deep seismic activity. The correspondence of the depths of deep earthquakes with those over which metastable reactions should produce transformational faulting (Figures 2 and 18) is an argument for metastability. Deep earthquakes can first occur at a depth corresponding to the onset of metastability at the elevated α-β or α-γ equilibrium phase boundary in the slab, at about 350 km. Earthquakes cannot occur deeper than about 690–720 km, because the spinel- and ilmenite-forming reactions will not occur where these minerals are no longer stable. Instead, the upper mantle assemblage should transform directly to the lower mantle assemblage, via reactions that should not give transformational faulting (section 5.4.3). The peaks in seismicity near 350 and 600 km correspond to depths where metastability should cause high stresses (section 6.3). The predicted self-stresses are largest near the wedge tip and thus may augment the effects of resistance to descent into the lower mantle in causing the seismicity peak near 600 km. The flexural stresses expected from the asymmetry of the transformation may explain the secondary peak near 330–430 km.

7.1.3. Variation in maximum earthquake depths with slab thermal parameter. The increase in the maximum depth of deep earthquakes as a function of thermal parameter (Figures 4 and 12) is a first-order feature for which metastability provides a clear explanation (section 4).

7.1.4. Earthquakes in recumbent slabs. Some deep earthquakes occur in unusual locations above the downdip extension of the main Wadati-Benioff zone (Figure 19) [*Lundgren and Giardini*, 1994]. For example, several dozen events since 1963 occurred west of the main Tonga Wadati-Benioff zone at depths between 500 and 670 km, above the downdip projection of the main zone. Seismic tomography [*van der Hilst*, 1995] shows a continuous slab connecting these "outliers" to the main Wadati-Benioff zone. Similarly, in the Izu-Bonin subduction zone, travel time anomalies indicate that outlier earthquakes occur in a flat-lying high-velocity zone at the bottom of the Wadati-Benioff zone [*Zhou*, 1988, 1990; *Okino et al.*, 1989; *van der Hilst et al.*, 1991] (Plates 1a and 1b and Figure 19). Continuous slabs with outlier earthquakes also occur in the central Kuriles (Plate 1 and Figure 19), South America [*Engdahl et al.*, 1995], and Indonesia [*Widiyantoro and van der Hilst*, 1996].

The focal mechanisms of outlier earthquakes differ markedly from those of the deepest earthquakes in the main Wadati-Benioff zone, which typically show downdip compression [*Lundgren and Giardini*, 1994]. The orientation of the *P* axes for the outliers differ from the slab-parallel orientation expected if the tomographically imaged, and thus presumably mechanically continuous, slab acted as a stress guide or a bending plate (Figure 19). In our view, the seismogenic stresses result from phase changes, because such slabs should still be significantly colder than the ambient mantle and have not entered the stability field of lower mantle minerals. The resulting self-stresses do not depend on forces transmitted along the slab because they are derived locally from the volumetric strain change [*Kirby et al.*, 1991]. The stress state will probably be more complicated than in a normal slab because the isotherms in recumbent segments are perpendicular to the pressure gradient. Furthermore (section 7.2.2), this situation would be even more complex if the slab is disrupted and penetrated by hot material, complicating the reaction boundaries and resulting stresses.

7.1.5. Deep events in detached slabs. Some deep earthquakes occur in slabs apparently detached from near-surface manifestations of active subduction. Beneath the North Fiji Basin a WNW trending band of 116 deep earthquakes have been located between 12.0° and 15.5°S during the period 1957–1991 (Plate 6 and Figure 20) [e.g., *Hamburger and Isacks*, 1987; *Okal and Kirby*, 1993a]. These events occur predominantly at depths from 600 to 670 km and are well separated from those in the nearby Vanuatu and Tonga subduction zones. Nowhere else do so many deep earthquakes occur that are not obviously related to active subduction. This group approximately parallels the Vityaz trench, a fossil trench with no associated shallow or intermediate-depth seismicity and no active magmatic arc. These relationships suggest that the earthquakes occur in a slab subducted at the Vityaz trench and later detached. Most of these events occur in a tabular zone with an apparent thickness of less than 50 km. It thus appears that the shocks occur in a detached slab which foundered to a recumbent attitude to the top of the lower mantle. Focal mechanisms show unusual variability compared to deep events in continuous deep slabs (Figure 20) much like the variability for events in recumbent slabs discussed in section 7.1.4.

The third largest deep earthquake with an accurate estimate of scalar moment, which occurred beneath southern Spain in 1954 (Table 1), is analogous. Only two other small nearby deep events are known. Evidence is lacking for present-day shallow subduction, and the intermediate-depth earthquake zone appears unrelated to the deep shocks [*Buforn et al.*, 1991]. Deep failure is likely to have occurred in a slab detached after an earlier

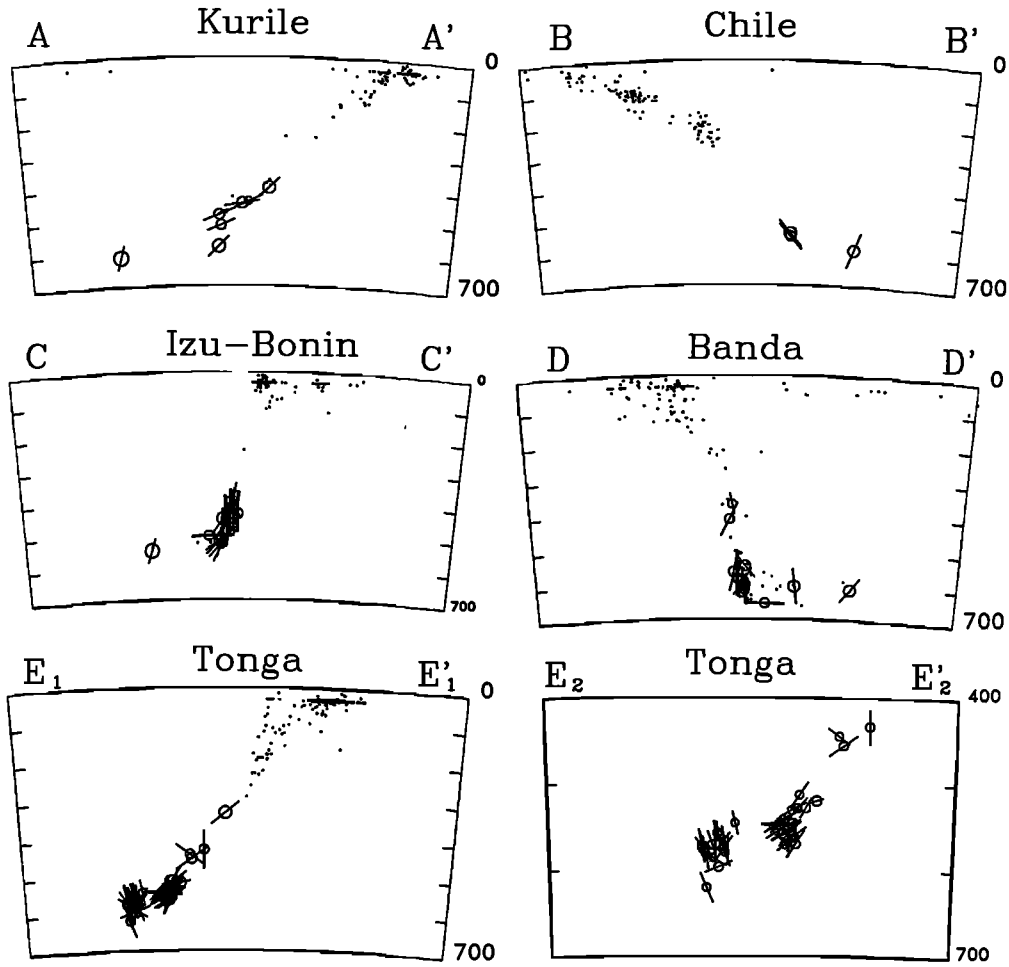

Figure 19. Cross sections of selected Wadati-Benioff zones showing the occurrence of "outlier" earthquakes above the downdip extrapolation of the main Wadati-Benioff zones. Lines through the symbols indicate the projection of the compression direction of the Harvard CMT focal mechanisms [*Lundgren and Giardini*, 1994]. Tonga section E2-E2′ is a blow up of section E1-E1′.

regime of subduction between the Africa and Eurasia plates [*Chung and Kanamori*, 1976; *Grimison and Chen*, 1986; *Royden*, 1993]. Evidence for a detached slab is found in tomographic images [*Blanco and Spakman*, 1993] showing a velocity anomaly including the hypocenters of the three deep earthquakes.

These examples indicate that large earthquakes occur in the dying remnants of detached slabs without mechanical continuity to the surface. This configuration is difficult to interpret in terms of earlier ideas because thermal bouyancy should not produce high deviatoric stresses in those settings. Instead, we believe that recently detached slabs are analogous to recumbent slabs, in that complex self-stresses can result because of the survival of regions of metastable peridotite with complex geometries.

7.2. Fine Structure of Deep Wadati-Benioff Zones

Individual Wadati-Benioff zones have intriguing internal structure that hypotheses for the origin of deep earthquakes should explain. We briefly review some of these features and note that some may be consequences of metastability. In particular, we suspect that many peculiar features of individual subduction zones result from the geometry of metastable regions in deformed slabs. The simple model presented here represents idealized slabs. However, the complex shapes of Wadati-Benioff zones, the heterogeneous release of seismic moment, and seismic tomography indicate that real slabs are deflected, thickened, and otherwise distorted three-dimensional objects.

7.2.1. Large isolated deep earthquakes. Large deep earthquakes tend to be distant from others in a Wadati-Benioff zone [*Wiens and McGuire*, 1995]. For example, the great 1970 Colombian earthquake (Table 1) occurred at the northern limit of South American deep seismicity, about 250 km north of the nearest deep earthquakes [*Okal and Bina*, 1994] (Figure 1). Farther south, in the 900-km region at about 13°–14°S offsetting the main zones of deep earthquakes, a band of four large events occurred (Table 1 and Figure 1). Except for a few small aftershocks of these events, no other well-located deep earthquakes have occurred in this 800-km zone in

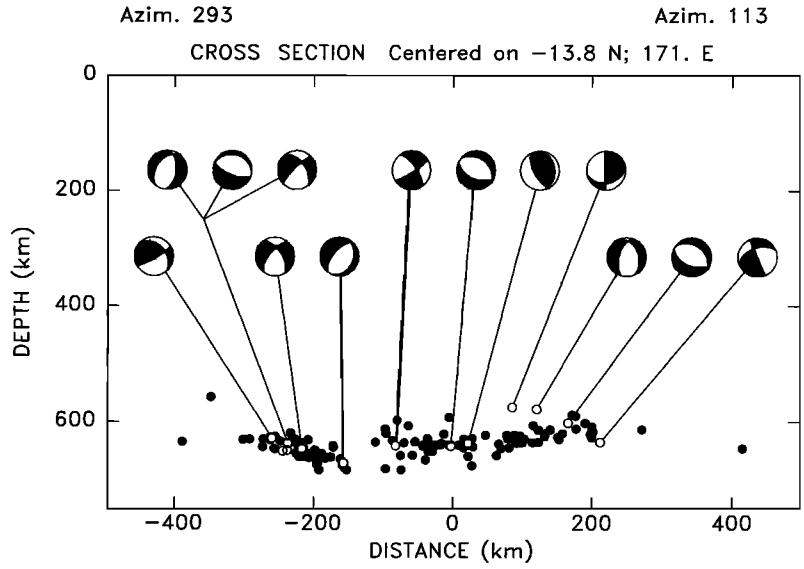

Figure 20. Depth cross section of the deep events shown in Plate 6 projected along the azimuth 203°, normal to the trend of the Vityaz trench. Note the tight clustering with depth. Focal mechanisms of the larger of these deep events (open circles) are highly variable. (Data sources are Harvard CMT catlogue [*Dziewonski et al.*, 1995] and unpublished first-motion mechanisms by E. A. Okal).

nearly 80 years of instrumental record. The great 1994 Bolivian deep earthquake was 180 km east of the others near this latitude. The E-W trend of the group and their focal mechanisms suggest that this segment of the Nazca slab has an orientation differing markedly from the N-S trend of the deep seismic zones in the Nazca slab to the north and south (Figure 1). *Kirby et al.* [1995a] propose that these large deep shocks occurred in regions of intense deformation where slab geometry abruptly changes in the along-strike direction.

Thus the largest four deep events known (Table 1), including the 1954 Spanish earthquake (section 7.1.5), are largely isolated and occur at 625–650 km depth, near the maximum depth of seismicity. The fact that the two biggest shocks occurred near the spatial limits of deep seismicity or where Wadati-Benioff zone geometry changes radically suggests to us that these earthquakes occur in isolated regions of metastable peridotite with a complex three-dimensional geometry, not connected to nearby metastable wedges. Hence although stresses could be high in adjacent regions where peridotite has already transformed, seismic failure by transformational faulting could not occur.

An extension of the metastability hypothesis may also explain why these isolated earthquakes are so large. Metastable peridotite which survives to about 650 km would be under huge overpressure, up to 10 GPa [*Kirby et al.*, 1995b]. As a result, the dynamic shear stress from even a small transformational faulting earthquake could trigger transformational faulting over the entire region. Earthquake fault areas could thus grow to the maximum size permitted by the metastable region, so large deep earthquakes would have few nearby smaller companions. Shear wave triggering of a shear instability would be analogous to shock wave detonation of solid explosives, materials that are also extremely metastable.

7.2.2. Along-arc variations in deep seismic deformation. Marked variations in seismic moment release occur along strike in many deep subduction zones that may be related to lateral variations in slab thermal structure, peridotite metastability, and hence slab stresses and faulting mechanism. We noted (section 4.2) that along the Indonesian arc, deep earthquakes begin abruptly where the thermal parameter reaches a value of about 5000 km. Curiously, the largest deep events in this subduction zone in the past 50 years (April 16, 1957, and December 15, 1963) occurred near this transition [*Okal and Kirby*, 1993b; *Okal et al.*, 1993]. The metastability hypothesis offers some insight into why the largest earthquakes occur at the edges of a region of deep seismicity. In areas where the metastable region should have a distinct lateral edge, the arguments (section 6.3) for high stress and seismic moment release near wedge tips should apply to their lateral edges.

A possibly related phenomenon occurs for the northwest Pacific, where deep seismicity is not uniform along the arcs (Figure 21). In particular, seismicity shallows dramatically at the cusps between the Mariana, Izu-Bonin, NE Japan, and Kurile-Kamchatka arcs. Moreover, large earthquakes occur at the edges of the regions of deep seismicity. These deep seismic reentrants may indicate "tears" in the downgoing lithosphere at the junctions between arcs [e.g., *Burbach and Frohlich*, 1986]. Hot mantle material could reach the edges of such tears, giving a sharp lateral edge to a metastable wedge, high stresses, and thus large earthquakes.

Furthermore, most of the deep seismic moment release beneath South America occurs in two narrow sec-

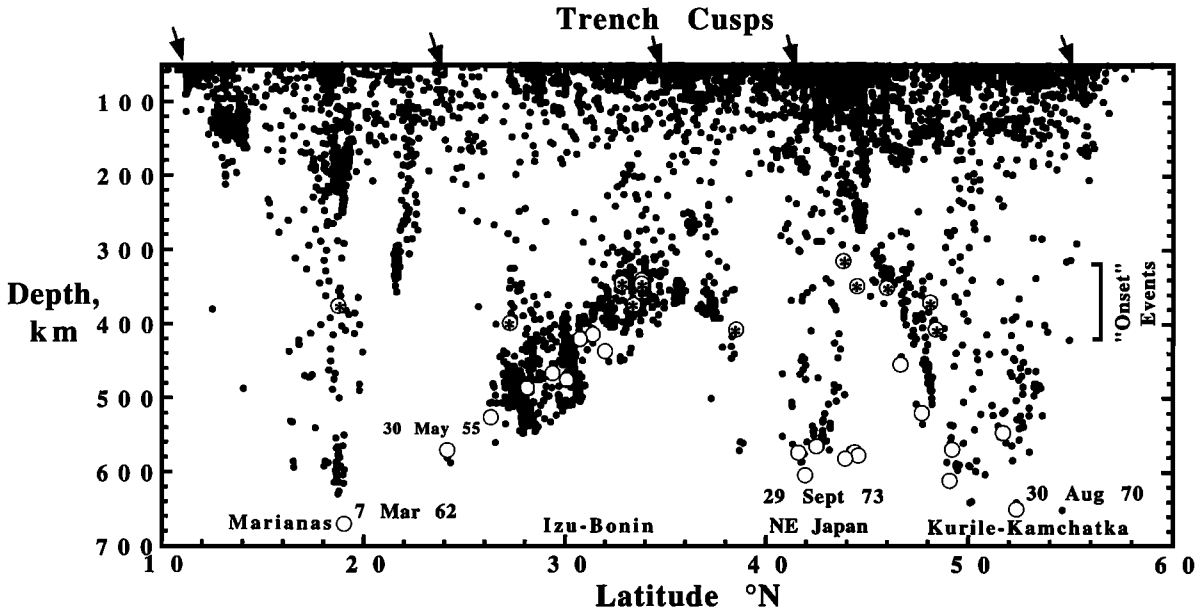

Figure 21. North-south cross section showing seismic activity in the subduction zones of the NW Pacific. Small dots are events relocated from ISC arrival time observations from 1964 to 1991 (courtesy of E. R. Engdahl (unpublished data, 1994)). Large open circles represent large (moments greater than 1.5×10^{26} dyn cm) deep events from 1924 to 1992, relocated from pre-1964 historical and modern arrival time data. Seismicity shallows toward the cusps where arcs meet (i.e., the individual Wadati-Benioff zones are tongue shaped). Large events tend to be near the bottoms or lateral edges of deep seismicity or are isolated from the main Wadati-Benioff zone seismicity. Note also the events at depths between 325 and 425 km that represent "onset" shocks in the deep population (Figure 18b).

tors. As noted in section 7.2.1, the largest two deep earthquakes (1970 Colombia and 1994 Bolivia) occurred in regions "downstream" of kinking distortions in the Nazca Wadati-Benioff zone. *Kirby et al.* [1995a] propose that these slab kinks thicken the metastable regions as they sink to the bottom of the transition zone, thickening the potential seismogenic region and permitting very large earthquakes.

7.2.3. Alignment of deep hypocenters into quasi-planar surfaces. A number of observations suggest that at least some deep earthquakes occur on large-scale faults. High-resolution studies reveal thin, approximately planar bands of hypocenters with numerous events sharing an approximately common nodal plane (Plate 7a) [*Isacks et al.*, 1967; *Fukao*, 1972; *Billington and Isacks*, 1975; *Giardini and Woodhouse*, 1984; *Lundgren and Giardini*, 1992]. These bands commonly crosscut Wadati-Benioff zones and occasionally display short-term temporal clustering and progressive failure along the band [e.g., *Isacks et al.*, 1967]. These zones are commonly conjugate, with approximately mutually perpendicular planar zones coinciding with nodal planes of the larger events [e.g., *Giardini and Woodhouse*, 1984; *Lundgren and Giardini*, 1992]. Although fault-like seismic zones might previously have been considered inconsistent with a phase-change source, transformational faulting could cause a planar earthquake source geometry.

7.2.4. Deep double Wadati-Benioff zones. Recent studies indicate that some Wadati-Benioff zones may at least locally be composed of two parallel planes of deep seismicity. *Wiens et al.* [1993] found two places in the Tonga Wadati-Benioff zone where there were paired inclined zones. These zones overlapped in the depth range 300–500 km and were separated by about 25 km perpendicular to the zones (Plate 7b). Focal mechanisms of earthquakes in the upper zones show largely in-slab *T* axes which is atypical for deep events, whereas the lower zones show the common in-slab *P* axes. In contrast, only a single very thin Wadati-Benioff zone occurs near the bottom of seismicity in Izu-Bonin at 380–510 km (Plate 7c), a more typical structure for deep Wadati-Benioff zone. In the Izu-Bonin SZ, *Iidaka and Furukawa* [1994] detected a double zone similar to, but somewhat shallower than, those in Tonga. Such double zones may result from bending stresses due to the asymmetry in the phase transformation (section 6.3, Plate 5b) (R. Denlinger, unpublished data, 1995). The signs of the predicted stresses are consistent with observed focal mechanisms.

7.3. Source Parameters

The hypothesis that deep earthquakes result from transformational faulting provides a conceptual framework for organizing and evaluating ideas about deep earthquake sources. It largely explains the long-recog-

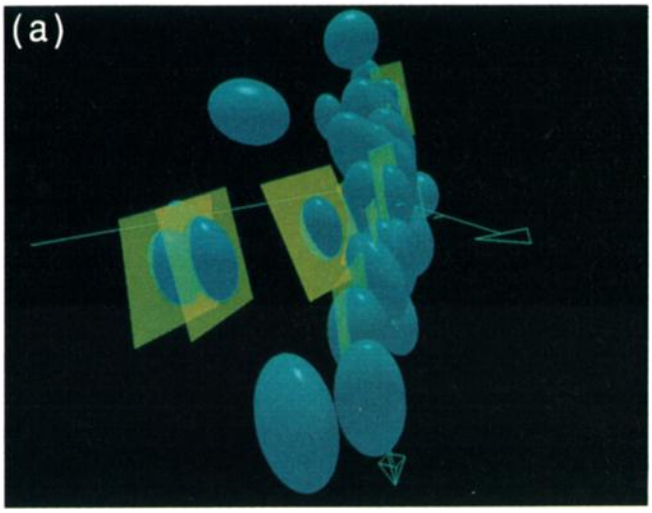

Plate 7a. Fine structures in deep Wadati-Benioff zones. Hypocenters are determined by a high-resolution relocation procedure described by *Wiens et al.* [1993]. Section is through a planar cluster of deep earthquakes in the Tonga subduction zone. The blue figures represent the 95% confidence ellipsoids of the hypocenter inversion, and the yellow squares indicate the orientations of nodal planes closest to that of the planar cluster. The axes are 30 km long and oriented north, east, and down (three-dimensional arrow). Alignment of the hypocenters with the nodal planes suggests a fault-like seismic zone (D. Wiens, unpublished figure, 1994).

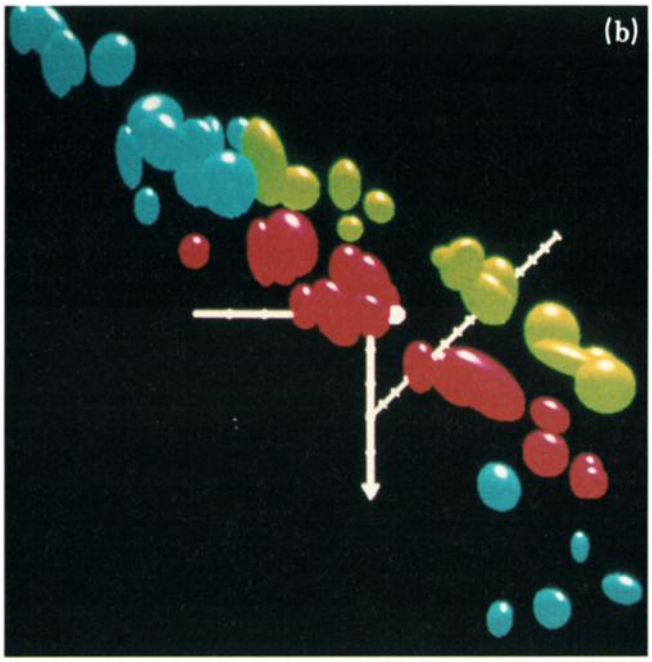

Plate 7b. Depth cross section through one of the deep Tonga double Wadati-Benioff zones, centered at a depth of about 420 km [*Wiens et al.*, 1993]. Scale bar has 5-km tic marks, and box is about 200 × 200 km. The two zones (indicated in yellow and red) are well separated relative to confidence ellipsoids of the hypocenter positions. Earthquake hypocenters that are not differentiated into a double zone are indicated in blue.

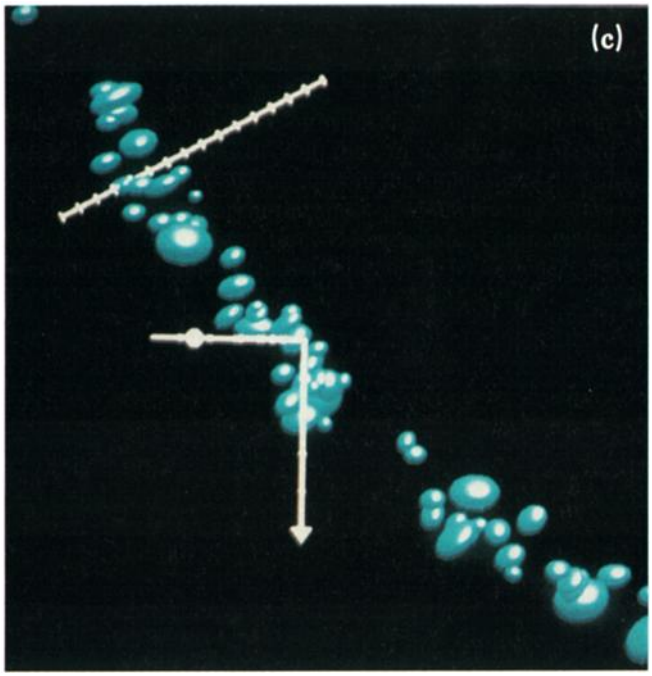

Plate 7c. View along strike of hypocenters near the bottom of the Izu-Bonin Wadati-Benioff zone in a section centered at depth of 450 km and 300 km thick in the along-strike direction. The zone has an apparent thickness of 15–20 km and shows no evidence of a double structure. This structure is more typical of Wadati-Benioff zones than that of Plate 7b [*Wiens et al.*, 1993].

nized but surprising fact that deep earthquake source properties inferred from seismological data are almost indistinguishable from those for shallow earthquakes. Laboratory results for transformational faulting (section 5.4.1) suggest that seismic waves are generated largely by slip across a quasi-planar surface, like that for frictional sliding on shallow faults. Thus, although shallow and transformational faulting involves different microphysics during fault nucleation and growth, the resulting seismic wave fields are generated by slip on a fault and are thus similar.

7.3.1. Isotropic moment tensor components. The observation that deep earthquakes show little or no evidence for isotropic compression is consistent with them occurring by transformational faulting. Isotropic components of the seismic moment tensors for deep earthquakes, which might indicate implosive phase changes, have proved elusive. Although, in principle, isotropic components could be detected by moment tensor inversion [*Gilbert and Dziewonski*, 1975], such detection is difficult [*Mendiguren and Aki*, 1978; *Okal and Geller*, 1979; *Kawakatsu*, 1991]. Numerical experiments suggest that more than 10% of the mechanism would have to be isotropic for detection by conventional methods of inversion of moment tensor [*Vasco and Johnson*,

1989]. *Kawakatsu*'s [1991] study of 19 large deep earthquakes found none with a significant (>10%) isotropic component and that the apparent isotropic components showed no preference for implosion or explosion, further arguing that they have no real significance. Most strikingly, inversion of long-period data for the 1994 Bolivian deep earthquake, the largest instrumentally recorded and thus that with the highest signal-to-noise ratio, indicates that its moment tensor had no significant isotropic component down to detectibility thresholds of as low as a 1.3% [*Ekström*, 1994; *Kikuchi and Kanamori*, 1994a, b; *Hara et al.*, 1995; *Okal*, 1996]. The failure to detect a significant isotropic component is consistent with the large shear displacement compared to the small isotropic compression expected in a transformational fault.

7.3.2. Aftershocks. Because deep and shallow earthquake sources appear similar in their most important aspect, shear faulting, it is natural to ask whether other possible differences in their source parameters offer insight into the faulting process. Such differences have proved elusive, however, except for aftershock occurrence [*Page*, 1968; *Frohlich*, 1987b, 1989]. Shallow earthquakes typically have many aftershocks with magnitudes up to one unit less than the main shock. In contrast, aftershocks for deep earthquakes generally are much smaller and rarer. For example, a shallow earthquake on the San Andreas Fault with the same moment as the great 1994 Bolivian deep earthquake should have more than 1000 aftershocks with magnitude greater than 4 in the first 100 days, including some with magnitude up to 7.3, and net moment release of about 10% of the main shock [*Reasenberg and Jones*, 1990; P. Reasenberg, personal communication, 1994]. The 1994 Bolivian earthquake had only four small teleseismically recorded aftershocks within the first 100 days (National Earthquake Information Center Preliminary Determination of Epicenters (NEIC PDE) catalog), with total moment release only about 0.6% of the main shock. Thus aftershock activity for this earthquake is about 5% of that expected for a comparable shallow earthquake. The same phenomenon is observed for aftershocks of other large deep earthquakes (Table 1). Even more strikingly, no teleseismically recorded aftershock of the great 1970 Colombian deep earthquake has been detected, despite adequate instrument coverage.

A distinct exception to the pattern of deep earthquake aftershocks occurs for the large 1994 deep earthquake in the Tonga subduction zone [*Wiens et al.*, 1994] (Table 1). The aftershocks form the richest deep earthquake aftershock sequence known (with the possible exception of that for the May 26, 1932, Tonga earthquake). The best located aftershocks define a steeply dipping planar zone containing the mainshock and approximately paralleling one of its nodal planes. This zone cuts across the main deep Wadati-Benioff zone into heretofore aseismic mantle. It is unclear why this deep earthquake had so many aftershocks or why the aftershocks cut across the main zone of activity. This unusual behavior may somehow be related to the fact that the deep northern edge of the Tonga Wadati-Benioff zone shows intense seismicity and seismic moment release, indicating intense deformation [*Giardini and Woodhouse*, 1984] of what may be the oldest, coldest, and fastest subducting slab in the world. The aftershocks may also represent failure by ductile faulting in parts of the slab which has already transformed to spinel (section 5.3).

Although aftershocks for the largest and best studied deep earthquakes appear to occur on the fault plane of the main shock, *Willemann and Frohlich* [1987] find that this is not generally the case from a study of smaller deep earthquakes. Given that aftershocks for shallow earthquakes are sometimes on the fault plane and sometimes not, interpretation of the analogous situation for the smaller deep earthquake data set has not yet been forthcoming.

The metastability hypothesis offers a qualitative explanation for the lower aftershock activity after deep earthquakes [*Kirby*, 1987; *Kirby et al.*, 1991]. First, transformational faulting can only produce slip once in a given transformed shear zone, whereas frictional sliding can recur on shallow brittle faults. For deep earthquakes, small aftershocks may still occur if patches of untransformed material survive along the transformational fault zone. Second, although for shallow earthquakes aftershocks may occur as the slip zone grows around that of the main shock, the rupture area of the largest deep earthquakes may be limited to the zone of metastability. Teleseismically located aftershocks of the 1994 Bolivian earthquake form a roughly east-west line at the southern limit of slip defined by subevents of the main shock [*Kikuchi and Kanamori*, 1994a, b; *Kirby et al.*, 1995a], which may also mark the southern limit of metastability at this depth. The fact that the largest isolated deep earthquakes have few aftershocks may reflect the same phenomenon causing them to have few nearby small events. Large events may trigger transformational faulting throughout the region of metastability, essentially exhausting the region's moment release potential (section 7.2.1).

7.3.3. Source dimensions. Consideration of aftershock geometries for large deep earthquakes leads to the important question of whether the predicted regions of metastability are consistent with the inferred earthquake fault dimensions. More generally, because the predicted region of metastability is thermally controlled, the question is whether the fault geometry is consistent with any mechanism in which the seismogenic region is thermally controlled [*Stein*, 1995].

Part of the answer may come from the often assumed (though not rigorously demonstrated) idea that deep earthquake sources are more spatially compact than shallow events of comparable size. Because the seismic moment is the product of the shear modulus, fault displacement, and fault area, and the shear modulus is

about 3 times higher at 600 km than at the surface, deep earthquakes of a given moment would have smaller source dimensions for a given moment and displacement. Whether deep earthquake sources are more compact is unknown due to the difficulties in estimating rupture properties discussed later.

Whether or not deep sources are more compact, the question of whether their dimensions are consistent with metastability remains [*Houston*, 1993, 1994]. If our simple modeling assumptions are generally appropriate, the geometry of the isotherms restricts transformational faulting to a thin, steeply dipping, and essentially planar zone. Hence earthquakes with fault dimensions exceeding a few tens of kilometers could occur only within a limited range of orientations (Figure 9). Testing for such a relation between slab geometry and fault geometry is often difficult because of the need to compare two poorly known three-dimensional geometries: that of the rupture zones for the largest deep earthquakes and that of the downgoing slab and the inferred metastable region in which they may have occurred. Both these geometries are uncertain on a scale of tens of kilometers, a scale comparable to the wedge dimensions predicted by simple models.

Source geometries are poorly known because deep earthquakes generally lack the numerous aftershocks that provide the best estimates of the fault dimensions of shallow earthquakes. Hence although some information can be derived from the relative positions of subevents, the detailed fault geometry is still essentially unknown for most deep earthquakes. Fortunately, the situation is improving due to advances in broadband seismic instrumentation and its deployment in sites of interest, such as for the 1994 Tonga and Bolivian deep earthquakes.

In addition, because the largest deep earthquakes are generally isolated, slab geometry is difficult to map. In some cases (section 7.2), slabs may be significantly distorted or thickened, either along-strike or as they interact with the lower mantle. As a result, the predicted temperature structure in the slab is uncertain for reasons even beyond the limitations imposed by the simple thermal model's uncertainties. Thus the geometry of a possible metastable region, or any temperature-controlled seismogenic region, is not easily predicted in detail.

This situation is illustrated by the 1994 deep Bolivian earthquake, which appears to have ruptured on a near-horizontal fault with north-south dimension about 40 km [*Kikuchi and Kanamori*, 1994a; *Silver et al.*, 1995; *Beck et al.*, 1995]. Although alternative interpretations are possible [*Chen*, 1995], this fault dimension is significantly larger than the narrowest dimension of the metastable wedge predicted from a simple thermal model. Because little is known about the deep slab geometry, owing to the sparse regional deep seismicity, it seems premature to regard this result as evidence against the earthquake resulting from metastability or any similar thermally controlled process [*Stein*, 1995]. *Kirby et al.* [1995a] argue that the slab in the source region is highly deformed, based on the pattern of moment release rates and on results from seismic tomography showing slab thickening and deflection of the slab velocity anomaly near the bottom of the transition zone. Because wholescale thickening of the low-density wedge would make the slab positively buoyant [*Silver et al.*, 1995], any such thickening would have to be relatively local and could deflect the slab toward the horizontal.

This "fault too big" problem, which is also indicated by the aftershocks of the 1994 Tonga earthquake (section 7.3.2), may be problematic for the metastability hypothesis or any other in which the seismogenic region is thermally controlled. The hypothesized failure mechanism may be incorrect, or the temperature structure in the source region may be sufficiently complicated that simple thermal models are inadequate. It is also possible that multiple mechanisms operate. For example, transformational faulting in the metastable wedge may trigger ductile faulting outside.

The possibility that deep earthquake sources are generally confined to a restricted and narrow volume is suggested by the frequency distribution of seismic moments. *Okal and Kirby* [1995] noted that the falloff in deep earthquake numbers with increasing seismic moment in the Tonga Wadati-Benioff zone points to their population having a fractal dimension of three rather than two. They argue that because the fast subducting Tonga slab is probably the coldest on Earth, the metastable wedge is thicker and more three-dimensional than in other deep slabs. At high seismic moments, a change in the falloff of earthquake numbers with increasing size suggests a small transverse dimension for the seismogenic zone (~10–15 km on average for Tonga and as low as 5 km for most other deep seismic zones). These small average dimensions, however, would not apply where the slab is intensely deformed and the largest deep earthquakes occur, as in the northern portion of the Tonga Wadati-Benioff zone (section 7.3.2).

7.3.4. Rupture history. Efforts have been made to find differences in rupture histories between deep and shallow earthquakes that might indicate differences in faulting processes. Unfortunately, only a few simple parameters can be estimated from the seismic waves radiated from a deep earthquake, and these parameters yield only indirect information about the faulting process [e.g., *Choy and Boatwright*, 1981]. Moreover, these parameters are more difficult to estimate for deep earthquakes than for shallow ones. The fault orientation and seismic moment, the parameters most directly derivable from seismograms, tell little about the process causing slip. Additional information is thus sought from the rise time required for slip at a point on the fault to reach its maximum value, from the velocity of rupture propagation, and from the stress drop during the earthquake [*Geller*, 1976; *Aki and Richards*, 1980]. For large shallow earthquakes one can estimate the rupture velocity from the relative location and timing of subevents and the fault area from the distribution of subevents, after-

shocks, surface rupture, and geodetic data. Slip in an earthquake, as inferred from the seismic moment divided by the estimated fault area and shear modulus, may be used, in turn, to calculate the stress drop from the ratio of the slip to the fault dimension. For most deep earthquakes (and many shallow ones) this approach is difficult because there are insufficient well-located subevents and aftershocks to define the rupture velocity and fault area. The primary seismological observable, the duration of the pulse emitted from an earthquake, reflects the time required for rupture propagation and thus the ratio of the fault dimension to the average rupture velocity. Consequently, inferred stress drops have large uncertainties because they depend on an unknown fault geometry, an assumed rupture velocity, and the cube of an estimated duration [*Chung and Kanamori*, 1980; *Stein and Kroeger*, 1980].

Some of this difficulty can be overcome by dividing the moment by duration cubed, a ratio of observables proportional to stress drop. Such studies [*Stein and Pelayo*, 1991] and those using the relation between moment and magnitude [*Ekström and Dziewonski*, 1988] indicate differences between shallow earthquakes in different tectonic settings which may result from differences in either stress drop or source geometry. The situation is even more complicated for deep earthquakes, in that this method has been reported to show stress drops either higher than [*Chung and Kanamori*, 1980; *Kikuchi and Ishida*, 1993] or comparable to [*Vidale and Houston*, 1993] shallow earthquakes. Stress drops measured by other approaches also show no significant difference between deep and shallow earthquakes [*Wyss and Molnar*, 1972; *Green and Houston*, 1995]. Differences in source duration [*Vidale and Houston*, 1993], rise time [*Houston and Williams*, 1991], and pulse shape [*Houston and Vidale*, 1994] between deep and shallow earthquakes have also been reported, though their physical interpretation is unclear. Initial results for the large 1994 Bolivian event suggest that rupture was complex and had an average rupture velocity far lower than the likely shear wave velocity at the source depths [*Kikuchi and Kanamori*, 1994a; *Silver et al.*, 1995; *Beck et al.*, 1995; *Chen*, 1995]. It is not known if slow rupture velocity is a general feature of smaller deep events. In summary, it is not yet established whether deep and shallow earthquakes differ significantly in rupture processes or whether, given our state of understanding, any such differences can provide useful information about the physical mechanism of faulting.

7.3.5. Source complexity. Other differences between deep and shallow earthquake rupture processes have been hypothesized but not demonstrated. Although it is sometimes thought that deep earthquake sources may be simpler than shallow ones, this apparent difference may simply result from the fact that source complexity is seen best for the largest earthquakes, which are typically shallow. The latter possibility is suggested by detailed studies which find source complexity even for small deep earthquakes [e.g., *Choy and Boatwright*, 1981]. It appears that deviatoric non-double-couple components of the source (i.e., that portion of the source not associated with either a volume change or slip on a single fault [*Frohlich*, 1994a]) are no more common for deep earthquakes than for shallower ones [*Kuge and Kawakatsu*, 1993]. *Houston* [1993], however, suggests that the largest and deepest deep earthquakes may have larger non-double-couple components, perhaps due to the restricted source volume in the metastable wedge. The 1994 Bolivian earthquake was a nearly pure double-couple source [*Kikuchi and Kanamori*, 1994a; *Hara et al.*, 1995; *Dziewonski et al.*, 1995], casting doubt on the generality of this association of source size and depth with that aspect of source complexity.

In summary, deep earthquake sources are very similar to those for shallow earthquakes. This observation is consistent with their being due to transformational faulting, because although the micromechanics of faulting differs from that of shallow earthquakes, the radiated seismic waves are generated by slip on a fault.

8. DISCUSSION

8.1. Chemical Reactor Analogue

Some interesting implications of the metastability hypothesis can been seen by considering a chemical reactor analogue for subducting slabs. Subduction brings a flux of cold shallow minerals into the depth and pressure conditions of the transition zone, where these phases are no longer thermodynamically stable (Figure 22). If this flux is fast enough relative to the rate of heat conduction and the material is cold enough as it enters the transition zone, minerals survive metastably below their equilibrium boundaries with the transition zone mineral assemblage. This situation is in many ways like a nonequilibrium chemical reactor in which a flux of reactants enters the reactor, which is maintained at specified pressure and external temperature, and the outgoing flux of chemical products is measured. If the flux is too fast and/or the reactor is maintained too cold, the reaction products fluxing out (i.e., the compounds produced by the reactions inside) are not at equilibrium with the conditions inside the reactor, and hence their outflow is not necessarily proportional to the flux of material into the reactor. We will use the reactor analogue shortly in considering the energetics of phase transformations in slabs.

8.2. Energetics of Deep Seismicity

In the metastability hypothesis, phase transformations largely occur aseismically at the metastable wedge boundaries, with only a small fraction occurring within the wedge by transformational faulting during deep earthquakes. This assumption is supported by a comparison of the total useful energy liberated by metastable conversion of olivine to spinel with the energy radiated

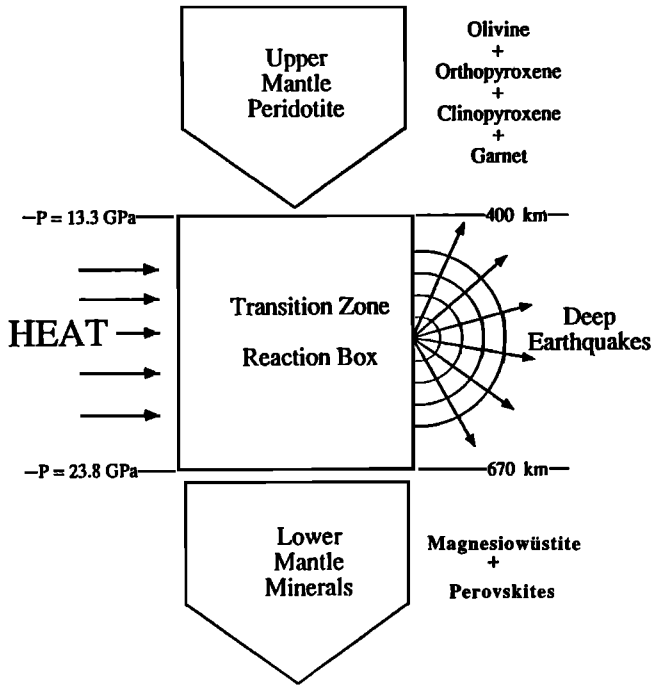

Figure 22. Schematic chemical reactor analogue for slabs subducting through the transition zone. As peridotite descends, it is slowly heated and pressurized, causing upper mantle minerals to be converted by metastable reactions to the transition zone slab mineral assemblage of spinel, ilmenite and possibly Ca perovskite. As a result of these slab reactions in the reaction box, deep earthquakes occur by transformational faulting and radiate seismic energy, latent heat is released, and mineral grain sizes are probably reduced. At greater depths the transition zone minerals convert at near-equilibrium conditions to the lower mantle assemblage of magnesiowüstite, (Mg, Fe) perovskite, and Ca perovskite without causing earthquakes.

by deep earthquakes. Figure 23 illustrates schematically the changes in enthalpy, H, and Gibbs free energy, G, for equilibrium and nonequilibrium conversion of olivine to spinel. If there is no kinetic hindrance (Figure 23a), olivine converts to spinel at the equilibrium pressure where the Gibbs free energy per unit volume is the same for both minerals, so $\Delta G_v = 0$, the thermodynamic criterion for equilibrium at constant pressure and temperature. The maximum useful "mechanical" energy or recoverable work available from the reaction is also given by ΔG_v and so is zero at equilibrium. ΔG_v is an upper limit on the useful energy because in nonequilibrium systems much of this energy is typically dissipated as heat. The change in enthalpy at a given pressure equals the latent heat liberated during conversion and is nonzero at equilibrium. In contrast, if olivine fails to transform at the equilibrium pressure and persists metastably to greater depths and pressures (Figure 23b), its eventual conversion to spinel liberates both heat and useful energy, which can be in part stored as elastic strain energy and later radiated as seismic waves by transformational faulting. Thus deep earthquakes are a small but observable manifestation of disequilibrium in the slab chemical reactor (Figure 22).

A natural test of these ideas is whether the phase transition can provide the amount of energy radiated in deep earthquakes. The maximum global energy release rate ΔW for the conversion of olivine to spinel in slabs can be estimated from the product of ΔG_v and the volume rate of metastable olivine-to-spinel conversion. To a good approximation, $\Delta G_v = (P_a - P_e)\Delta V/V_0$, where P_a and P_e are the pressures at conversion and equilibrium and $\Delta V/V_0$ is the fractional volume change, approximately -0.085 at transition zone conditions. Assuming that the average conversion pressure is the mean of the pressures at the slab olivine-spinel equilibrium depth (350 km; 11.8 GPa) and the maximum earthquake depth (690 km; 23.8 GPa), the average pressure overstep $\Delta P = (P_a - P_e)$ is 6 GPa and $\Delta G_v = -5.1 \times 10^8$ J/m^3 (the negative sign indicates that energy is released).

We estimate the global flux of slab mantle into the transition zone as about 110 km^3/yr, using the along-strike lengths of deep Wadati-Benioff zones, their deep dips, and an average slab thickness of 100 km (because most of the deep seismogenic slabs are old and hence of essentially constant thickness). We used an average vertical rate of slab descent calculated from the NUVEL-1 relative plate velocities. Where significant (e.g., Tonga), we augmented the convergence motion by the rate of back arc spreading and associated trench migration. The volume fraction of olivine converted metastably to spinel can be estimated from the ratio of the thickness of the predicted metastable wedges in our models and the starting plate thickness. Because this fraction ranges from about 1/4 to 1/6, the global rate of metastable peridotite conversion is about 22 km^3/yr. This estimate assumes a constant metastable conversion rate proportional to the rate at which olivine enters the transition zone, an assumption discussed shortly. The annual rate of Gibbs free energy release is thus $\Delta G_v = (-5.1 \times 10^8$ J/m^3) $(22 \times 10^9$ m^3/yr) $= -1.1 \times 10^{19}$ J/yr.

This estimated available energy far exceeds the annual seismic energy radiated by deep earthquakes, about 1.9×10^{15} J/yr. This figure is computed from the average yearly deep seismic moment release for the earthquakes listed in the Harvard CMT catalogue [*Dziewonski et al.*, 1995] from 1977 through 1994 (2.9×10^{20} N m/yr) and from the relationship between seismic moment and seismic wave energy determined by G. Choy (unpublished data, 1995) for deep earthquakes from 1987 to 1993, with a correction for the higher shear modulus at deep earthquake depths (~94 GPa) compared to that for shallow earthquakes (33 GPa)]. Thus the fraction of the energy available from the phase transition which is released seismically is very small, ~0.01%. Considerable uncertainties beset this estimate, such as that in the relationship between seismic moment and radiated energy [see *Choy and Boatright*, 1995]. Moreover, some of the energy available for faulting may derive from thermal buoyancy and would be available were no metasta-

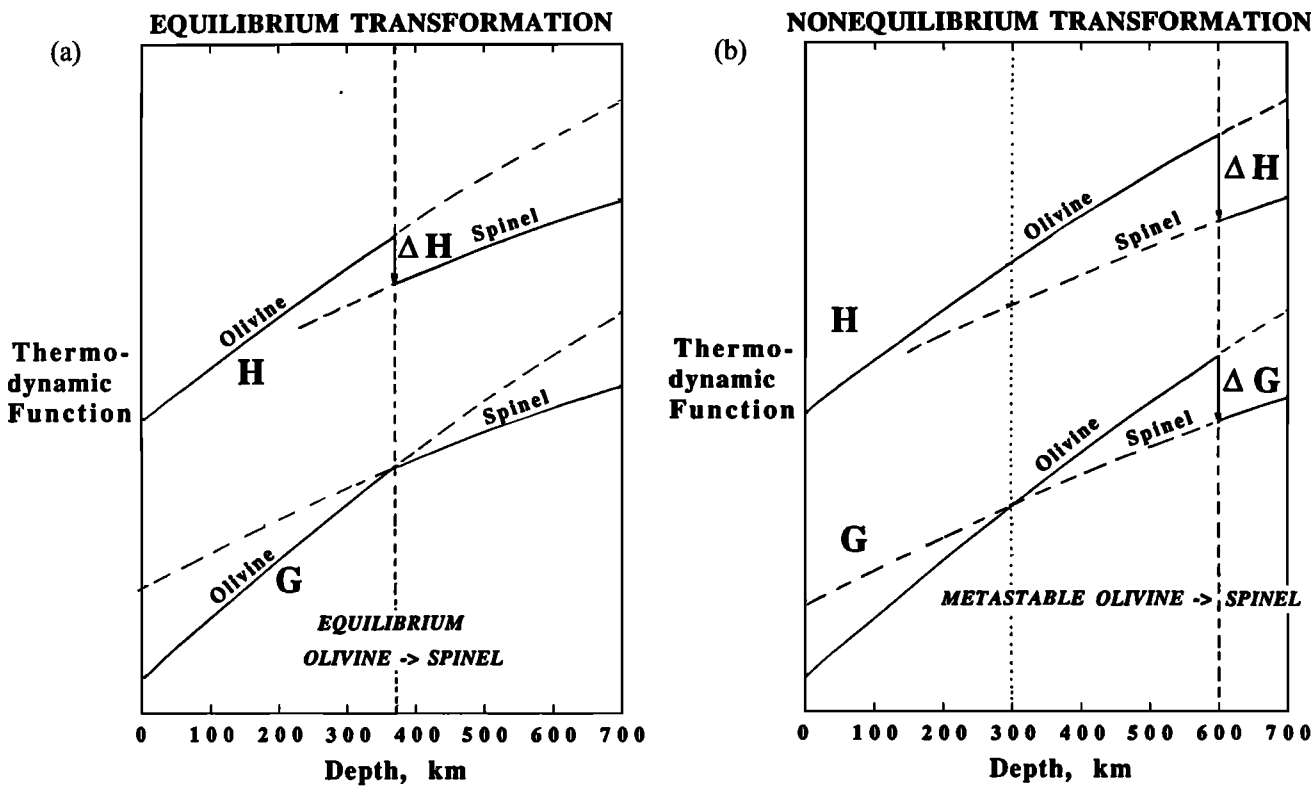

Figure 23. Schematic diagram showing variation of enthalpy, H, and Gibbs free energy, G, for olivine and spinel, as a function of depth. ΔH is the heat released or absorbed by the reaction at constant pressure, and ΔG is the maximum useful energy available from the reaction at constant pressure and temperature. (a) Situation in which reactions occur in normal mantle near the equilibrium olivine-spinel boundary and, consequently, only heat is liberated. (b) The situation within cold slabs in which the spinel-forming reaction is kinetically hindered and both heat and useful energy are released when spinel does form from metastable olivine. The reaction is simplified to a first-order polymorphic conversion as shown in Figure 6b.

bility present. The important point, however, is that deep earthquakes are almost certainly only minor elements in the nonthermal energy budgets of deep slabs. *Liu* [1983] reached a similar conclusion for intraslab earthquakes based on a general comparison of available thermodynamic energies from metastable reactions and earthquake energies.

It seems ironic that deep earthquakes, which radiate a minuscule fraction of the energy available from phase transitions in slabs, are our primary source of information about these transitions. The earthquakes provide the strongest evidence that metastability and transformational faulting occur and offer insight into their distribution among slabs. In the chemical reactor analogy, we know the input material (oceanic lithosphere) and its flux into the transition zone. However, although the bulk chemistry of the material is unaffected by the reactor, the forms of the reaction products (minerals) are unknown because they are not directly observable. We can, however, infer that for certain fluxes (old, fast, and thus cold slabs), reactions occur metastably, as indicated by the noises (earthquakes) they produce. For other fluxes (young, slow, and hot slabs), metastable reactions do not occur and no earthquakes happen. This analogue is plausible: sounds from explosive reaction bursts are often used to study nonequilibrium processes in gas combustion reactors [*Scott*, 1991].

Because deep earthquakes radiate only a small fraction of the energy released from the phase transition, most of this energy is dissipated as heat in slabs or stored in defects, such as grain boundaries or dislocations. As noted earlier, this internal heat source can raise the interior temperature by up to 40°–200°C and thus speed the thermal and hence mechanical equilibration of slabs to ambient mantle conditions and facilitate the phase transformations to the lower mantle assemblage. Similarly, the energy liberated could reduce grain size and thus weaken slabs [*Rubie*, 1984; *Ito and Sato*, 1991]. These consequences of dissipation of energy from metastable reactions at wedge boundaries may contribute to the mechanical and thermal equilibration of deep slabs.

8.3. Variation of Seismic Moment and Energy Release Between Slabs

The fraction of the total energy available that is released seismically is not only small but appears to vary among subduction zones. Such a variation is suggested from a comparison of seismic energy release to the volume flux of subducting lithosphere into the transition zone for individual subduction zones. We estimated the

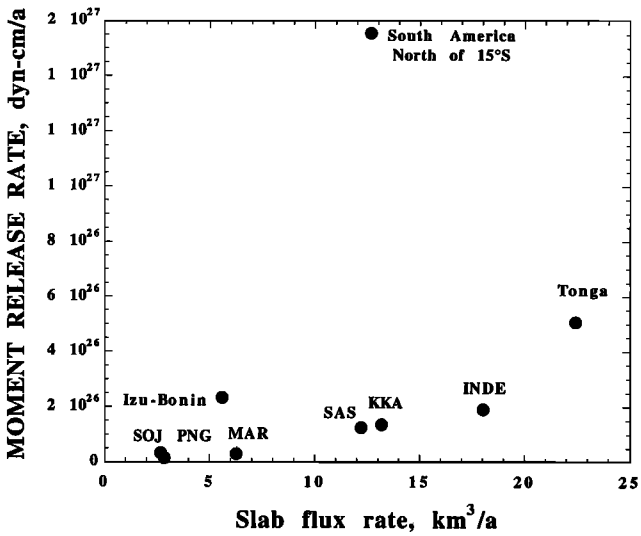

Figure 24. Comparison of the variation of annual seismic moment production for different subduction zones with the estimated slab volume flux of mantle material into the transition zone. Seismic moments taken from the Harvard CMT catalogue (January 1, 1977, to December 31, 1994) [*Dziewonski et al.*, 1995]. Slab flux determined as described in the text. Abbreviations are SOJ, Sea of Japan; PNG, Papua New Guinea/Solomons; MAR, Mariana; SAS, South America south of 15°S; KKA, Kurile-Kamchatka; INDE, eastern Indonesia.

annual volume flux of mantle into the transition zone for each subduction zone producing deep earthquakes from the product of the arc-normal convergence rate from NUVEL-1 [*DeMets et al.*, 1990], the sine of the average angle of dip of the deep Wadati-Benioff zone, and the thickness of the lithosphere (taken to be 100 km). This product was integrated over the length of trench segment with deep earthquakes. There is no clear relation between the annual volume flux and the seismic moment release rate (Figure 24). Although Tonga has a high flux and moment release rate, suggesting a crude correlation, the results for the other subduction zones show marked scatter. Some of the scatter may be due to the difficulty in estimating moment release rates, because deep earthquakes are sufficiently rare that the short history of instrumental seismology provides an inadequate sample. The sampling problem is illustrated by the observations that since 1950 there have been only two deep earthquakes with moment greater than 10^{28} dyn cm and that the largest, the 1994 Bolivian earthquake, had a moment higher than the total of all other deep earthquakes since 1977, including the large 1994 Tonga-Fiji event (Table 1).

Our sense is, however, that this lack of correlation is real and results from the complexity of slab metastability and/or the transformational faulting process. We have assumed that the production of metastable material can be predicted deterministically from the thermal structure and convergence rate, via kinetic modeling. Thus although we can predict where transformational faulting and deep earthquakes can occur, we cannot predict the precise conditions (stress, temperature, composition, etc.) controlling whether a particular volume will undergo transformational faulting. Hence although we can predict which arcs or portions thereof can have deep earthquakes, we have no way at present of predicting the observed variations in deep seismic moment release between arc segments expected to have similar thermal structure.

The complexity of the moment release pattern is illustrated by the fact that both the Izu-Bonin and South American slabs produce much more moment than other arcs with comparable volume flux. This relatively robust and long-lived discrepancy is illustrated by the distribution of deep earthquakes in the subducting Pacific plate in the NW Pacific (Figure 21). Although the nominal age, probable initial thermal structure, and descent rate for the Pacific plate do not vary grossly along strike, the overall modern seismicity and the number of large deep events in the time interval 1924–1992 are markedly higher for the Izu-Bonin arc. This arc is also unusual in that seismicity systematically deepens from north to south and is unusually active in the depth range from 350 to 500 km relative to other Wadati-Benioff zones except Tonga (e.g., Indonesia in Figure 12).

Such large-scale variations in seismicity suggest a complex mode of behavior intermediate between a purely deterministic one (seismicity controlled exclusively by the presence of metastability) and a purely stochastic one (seismicity controlled by random transformational faulting). This complexity may indicate variability of the rates of metastable reactions at constant mantle flux rates. Perhaps the kinetic boundaries defining metastable wedges are unstable when the slab thermal structure varies subtly. Although for simplicity the thermokinetic models did not include a feedback of latent heat into the conduction of heat, the fact that temperature has strongly nonlinear effects on reaction rates (equation (1), Figures 7 and 8) could produce complex time dependence and geometrical complexities in kinetic boundaries [*Kirby and Stein*, 1992; *Daessler and Yuen*, 1993]. In the chemical reactor analogy, constant input fluxes can yield time-dependent behavior ranging from chaotic to periodic to steady state depending on the details of the feedbacks [*Prigogine and Strengers*, 1984; *Nicolis and Prigogine*, 1989; *Coveney and Highfield*, 1990; *Scott*, 1991]. Hence there can be "loss of control" where the slab system's internal evolution is governed by internal feedbacks, rather than by the rates of external inputs or slab descent rates.

8.4. Implications of Metastability for Slab and Mantle Dynamics

Metastability would have significant consequences for the dynamics of slabs and for plate motions. Even a simple steady state metastable wedge affects the slab's density structure. Thus the resulting plate-driving force will depend on the slab age and subduction rate in a

more complex way than expected for purely thermal effects because the formation of a metastable wedge varies nonlinearly with age and rate (Figure 4). Moreover, because wedge formation occurs only for old, fast subducting, slabs, it may act as a "parachute" and contribute to regulating plate speeds by reducing their density and driving force. In a similar fashion, the evolution of metastable wedges would permit plate-driving forces to change with time more rapidly than expected from purely thermal effects, so metastability may play a role in changing plate motions. Such changes might be especially complicated if the metastable wedge geometry varied simultaneously in several plates.

Large-scale metastability could also affect the evolution of the mantle. A major issue for understanding the evolution of the mantle is the extent to which downgoing slabs return material to the lower mantle. Analyses of this issue generally focus on the extent to which slabs are sufficiently dense to penetrate into the lower mantle. Slabs with significant metastability will be less dense than expected on purely thermal grounds, and hence more likely to stagnate above 660 km, as apparently illustrated by the foundered Vityaz slab (Plate 6 and Figure 20). Eventually, such slabs will heat up sufficiently that metastable peridotite will transform to denser spinel, favoring subsequent slab penetration. This effect should be significant for some slabs and may play a role in the proposed large-scale "flushing" events where volumes of stagnant slab material sink into the lower mantle [e.g., *Honda et al.*, 1993].

Although these consequences of large-scale metastability are speculative, they suggest a possible source for spatial and temporal complexity in slab density structure, stresses, and driving forces beyond those expected from purely thermally based ideas. Even steady state metastability gives some of these complexities, and the possibility of thermal and mechanical feedback (e.g., stress effects on transformation kinetics) offers an even greater richness in possible behavior.

9. PROSPECTS

The hypothesis that deep earthquakes result from transformational faulting in metastable peridotite is already providing an impetus and organizing framework for a wide variety of investigations [*Frohlich*, 1994b]. Because the hypothesis has clear and testable implications, it suggests natural lines of inquiry including deep earthquake phenomenology, laboratory investigations of reaction kinetics and transformational faulting, slab properties, and dynamic modeling.

As reviewed earlier, the metastability hypothesis has given new impetus to studies of deep earthquake source properties. The issue of whether a wedge is seismologically detectable is also being investigated [*Vidale*, 1987; *Iidaka and Suetsugu*, 1992]. The data set for deep earthquakes is also growing, both by the fortuitous recent occurrence of large deep earthquakes and by application of modern seismological techniques to historic seismograms [*Huang et al.*, 1994, 1996].

Laboratory studies also should provide important constraints on the inner workings of deep slabs by improving our ability to model the progress and effects of mantle phase changes. In particular, improvements are needed in our knowledge of the thermal diffusivities of mafic and ultramafic minerals and rocks, in the mechanisms and kinetic laws for transition zone and lower mantle transformations, and in the inelastic behavior of those transformations at pressures approaching 25 GPa.

Modeling studies also offer the prospects for improved understanding of metastability, for its consequence for slab processes, and for larger-scale geodynamics. We see opportunities to integrate thermokinetic models with simulations of the deformation states of deep slabs and with equation-of-state predictions of the seismic velocity and density structures of slabs. We also anticipate improvements in simulations of the temperature, kinetics, and deformation state in slabs with spatially variable plate age (and hence initial thermal structure) and with laterally varying descent rates. These improvements should facilitate comparisons of modeling results with real slabs, whose geometries are being clarified by tomographic studies.

GLOSSARY

Clapeyron slope: The slope in pressure-temperature space (dP/dT) of an equilibrium phase boundary separating the regions in which different phases are thermodynamically stable. The Clapeyron slope is defined thermodynamically by the ratio of the differences in entropy and volume between the product and reactant phases at equilibrium. Transformations of the $\alpha - \beta - \gamma$ polymorphs of $(Mg,Fe)_2SiO_4$ (Figure 6) have positive Clapeyron slopes (negative volume change and negative entropy change), whereas the spinel → magnesiowüstite + perovskite reaction has a negative Clapeyron slope (negative volume change but positive entropy change), as do most reactions producing perovskite at equilibrium.

Deep earthquakes: Defined conventionally as earthquakes with source depths greater than 300 km [e.g., *Gutenberg and Richter*, 1954]. The depth distribution of earthquakes shows a minimum near 300–325 km and an increase at deeper depths, suggesting that the deeper earthquakes are a distinct population caused by a different failure process than the shallower intermediate-depth earthquakes. In many Wadati-Benioff zones, clusters of intermediate-depth earthquakes extend to depths as great as 350 km. We thus consider the deeper population as deep earthquakes, such that the upper limit of deep seismicity can vary between arcs. The average global onset of deep earthquakes is at about 325–350 km.

Diopside: A member of the pyroxene group of minerals having a monoclinic structure and composition $Ca(Mg_xFe_{1-x})Si_2O_6$ with $x \geq 0.9$. Diopside is an essential mineral in lherzolites, an important type of rock in the upper mantle.

Divariant transformation: In mineralogical applications, a reaction in which a pair of mineral solid solutions with different compositions coexist in equilibrium over a range of pressures and temperatures. An example is the $(Mg,Fe)_2SiO_4$ olivine → spinel transformation in which olivine and spinel solid solutions with different Mg/Fe ratios coexist in equilibrium over a range of pressure and temperature in the $\alpha + \gamma$ two-phase stability field (Figure 6a).

Enstatite (orthoenstatite and clinoenstatite): A member of the pyroxene group of minerals having composition $(Mg_xFe_{1-x})SiO_3$ with $x \geq 0.9$. This mineral typically has orthorhombic structure at pressures below 6–10 GPa (orthoenstatite) and monoclinic structure at higher pressures (clinoenstatite). Orthoenstatite is a primary constituent of most peridotites in the upper mantle.

Harzburgite: A peridotite containing at least 10% enstatite in addition to the chief mineral olivine.

Ilmenite: As employed in the geophysical literature, the compound with composition $(Mg,Fe)SiO_3$ when it has the structure of the mineral ilmenite, an iron-titanium oxide. With increasing pressure at low temperatures, metastable clinoenstatite ($(Mg,Fe)SiO_3$) transforms directly to the ilmenite structure (Figure 10).

Kinetic hindrance: A condition under which chemical reactions take place sufficiently slowly that metastability occurs. For example, because reaction rates decrease with decreasing temperature, a phase can persist metastably outside its stability field if temperatures are sufficiently low.

Lower mantle: The deepest portion of the mantle where seismic velocities increase slowly with depth. The upper boundary, originally defined to be at a depth of 1000 km [*Bullen*, 1940], is now placed by most investigators at the depth of the global seismic velocity discontinuity near 660 km. The lower mantle is thought to be dominated by perovskite mineralogy.

Martensitic transformation: An isochemical transformation in which the product phase (the martensite or martensitic polymorph) is distorted by transformation of the host phase principally by shear but maintains a structurally continuous, nearly strain-free interface with its host. Shear stress favors the stability of the martensitic polymorph. Mineralogical examples include the orthoenstatite → clinoenstatite transformation and, under high stress, the olivine → spinel transformation [e.g., *Kirby and Stern*, 1993].

Metastability: A condition where a material is not in its most stable (lowest energy) form. Under near-equilibrium conditions at high temperatures, one phase cannot exist significantly into the pressure-temperature stability field of another polymorph, so reactions are closely reversible across the phase boundaries. However, because reaction rates decrease with decreasing temperature, a phase can persist metastably for an indefinite time well outside its stability field if temperatures are sufficiently low. For example, diamonds created at very high pressures deep in the mantle can persist indefinitely in a metastable state at Earth's surface conditions even though they are grossly outside their stability field.

Peridotite: The dominant rock type of the upper mantle, composed mostly of the mineral olivine and accompanied by at least 10% pyroxene.

Perovskite: As employed in the geophysical literature, the high-pressure compound $(Mg,Fe)SiO_3$ having the perovskite structure. Similarly, $Ca(Mg,Fe)Si_2O_6$ is called "Ca perovskite."

Polymorphic transformation: An isochemical transformation of one crystalline phase into another with different structure (a polymorph). Examples of mineral pairs that are polymorphs include graphite-diamond, calcite-aragonite, quartz-coesite, and olivine-spinel in the spinel stability field.

Pyroxenes: A major group of upper mantle silicates with structures characterized by straight and parallel chains of silica tetrahedra. The pyroxenes enstatite and diopside are primary minerals in peridotites that make up the bulk of the upper mantle.

Seismic moment and seismic magnitude: Earthquake sizes are quantified in two ways. Seismic moment for a faulting earthquake source is the product of the fault area, the average slip displacement, and the shear modulus of the surrounding rocks and has the physical units of a torque. Seismic moment is also the scalar amplitude of the seismic moment tensor, a directional property of an earthquake source measured from its radiated seismic waves [*Aki and Richards*, 1980]. Earthquake magnitude is derived from the logarithm of the amplitude of ground motion as measured on standard seismometers. Because the seismic moment is directly related to the amount of deformation associated with the faulting process, it is considered the most reliable measure of earthquake size. The moment magnitude M_w is a magnitude scale related directly to the logarithm of the seismic moment [*Geller and Kanamori*, 1977; *Kanamori*, 1977].

Seismic moment tensor: A representation of the geometry and strength of a seismic source by a tensor whose components are related to the strain changes at the source [*Aki and Richards*, 1980]. The tensor can represent slip on a planar fault (i.e., shear faulting) in terms of a double-couple force system, or more complex source geometries. The isotropic component of this tensor describes the part of the source producing a net volume change.

Spinel: As employed in the geophysical literature, the compound with composition $(Mg,Fe)_2SiO_4$ having the structure of the mineral spinel. With increasing pressure, the mineral olivine (the α phase of

$(Mg,Fe)_2SiO_4$) transforms to β-$(Mg,Fe)_2SiO_4$ (the mineral wadsleyite, with a modified spinel structure) and then γ-$(Mg,Fe)_2SiO_4$ (the mineral ringwoodite with a spinel structure).

Stishovite: A dense, high-pressure polymorph of SiO_2 thought to exist in the transition zone and possibly in the lower mantle.

Transformational faulting: A form of faulting found in some mineral systems that exhibit polymorphism. If the low-pressure polymorph is pressurized at low enough temperature that it persists metastably and is subsequently deformed, it may fault suddenly without essential loss of cohesion by localization of transformation to its denser polymorph in a fine-grained shear zone [*Kirby*, 1987; *Kirby et al.*, 1991]. "Anticrack" faulting is another term occasionally used for transformational faulting [*Green and Burnley*, 1989; *Green*, 1994]. This term emphasizes the nucleation of transformational faults by the creation and interactions of "crack-like" inclusions of the high-pressure phase under stress. We prefer the term "transformational faulting" because it emphasizes the connection of the faulting process with mineralogical changes of state.

Transition zone: That portion of the mantle where seismic velocity increases rapidly with depth. The upper boundary is placed at the depth of the seismic velocity discontinuity at about 410 km. The lower boundary, originally defined to be at about 1000 km depth [*Bullen*, 1940], is currently placed at the depth of the global seismic velocity discontinuity at about 660 km. These rapid seismic velocity increases are thought to reflect the presence of minerals (such as spinel, modified spinel, ilmenite, and garnet) that are stable at pressures existing at depths of 410–660 km. The transition zone probably occurs over a broader range of depths in slabs because they are colder than normal mantle (Figure 2c).

Upper mantle: Traditionally defined as that portion of the mantle above the lower mantle, i.e., including the transition zone. It is sometimes more useful to think of the upper mantle as overlying the transition zone, such that the transition zone contains minerals transitional between those stable in the upper and lower mantles.

Wadati-Benioff zone: An inclined zone of seismicity at a convergent plate boundary marking the presence of cold subducting lithosphere. This structure was first noted in Japan by *Wadati* [1935] and recognized elsewhere by *Visser* [1936] and *Berlage* [1937]. *Benioff* [1949] proposed that the inclined seismic zone was due to large-scale thrust faulting. With the discovery of plate tectonics, it was recognized that although many shallow earthquakes in subduction zones result from interplate thrusting, others, especially at depths exceeding about 50 km, result from deformation within the slab. We follow *Uyeda* [1978] and *Frohlich* [1987a] in using the term "Wadati-Benioff zone."

ACKNOWLEDGMENTS. Dedicated to the memories of Kiyoo Wadati and Roger Burns, two recently deceased pioneers of deep earthquake seismology and mineral physics. We have benefited from helpful discussions, reviews, and sharing of results prior to publication from many scientists, including Doug Wiens, Jeff McGuire, Paul Lundgren, Charles Wicks, Mark Richards, Cliff Frohlich, Heidi Houston, John Vidale, Wei-Chuang Huang, Bob Engdahl, Stuart Sipkin, George Choy, Norman Sleep, Craig Bina, George Helffrich, Pamela Burnley, Eric Bergman, Ken Creager, Wang-Ping Chen, Mary Ann Glennon, Takashi Iidaka, David Engebretson, Rob van der Hilst, Ming Liu, and Elizabeth Campbell. Cliff Frohlich, Ming Liu, and Peter Molnar provided helpful reviews and guidance. Laura Stern helped edit the manuscript. We also thank E. Robert Engdahl for permission to use unpublished earthquake hypocenter data. Stein thanks the Laboratory for Terrestrial Physics, NASA Goddard Space Flight Center, for hospitality during portions of this study. Additional support was provided to Okal by NSF grant EAR-93-16396.

Peter Molnar was the editor responsible for this paper. He wishes to thank Ming Liu, Cliff Frohlich, and Charles Meade for their technical reviews. He also wishes to thank John Hildebrand and another anonymous reviewer for their cross-disciplinary reviews.

REFERENCES

Akaogi, M., E. Ito, and A. Navrotsky, Olivine-modified spinel-spinel transitions in the system Mg_2SiO_4-Fe_2SiO_4: Calorimetric measurements, thermochemical calculation, and geophysical application, *J. Geophys. Res.*, *94*, 15,671–15,685, 1989.

Aki, K., and P. G. Richards, *Quantitative Seismology*, 2 vols., 934 pp., W. H. Freeman, New York, 1980.

Anderson, O. L., and P. C. Perkins, Runaway temperatures in the asthenosphere resulting from viscous heating, *J. Geophys. Res.*, *79*, 2136–2138, 1974.

Beck, S. L., P. Silver, T. C. Wallace, and D. James, Directivity analysis of the deep Bolivian earthquake of June 9, 1994, *Geophys. Res. Lett.*, *22*, 2257–2260, 1995.

Benioff, H., Seismic evidence for the fault origin of oceanic deeps, *Geol. Soc. Am. Bull.*, *60*, 1837–1856, 1949.

Berlage, H. P., A provisional catalogue of deep-focus earthquakes in the Netherlands East Indies 1918–1936, *Gerlands Beitr. Geophys.*, *50*, 7–17, 1937.

Bevis, M., Seismic slip and downdip strain rates in Wadati-Benioff zones, *Science*, *240*, 1317–1319, 1988.

Bevis, M., et al., Geodetic observations of very rapid convergence and back-arc extension at the Tonga arc, *Nature*, *374*, 249–251, 1995.

Billington, S., and B. L. Isacks, Identification of fault planes associated with deep earthquakes, *Geophys. Res. Lett.*, *2*, 63–66, 1975.

Bina, C. R., Mantle discontinuities, *U.S. Natl. Rep. Int. Union Geod. Geophys. 1987–1990*, *Rev. Geophys.*, *29*, 783–793, 1991.

Bina, C. R., and G. R. Helffrich, Phase transition Clapeyron slopes and transition zone seismic discontinuity topography, *J. Geophys. Res.*, *99*, 15,853–15,860, 1994.

Blanco, M. J., and W. Spakman, The *P*-wave velocity structure of the mantle below the Iberian Peninsula: Evidence for subducted lithosphere below southern Spain, *Tectonophysics*, *221*, 13–34, 1993.

Boland, J. N., and R. C. Liebermann, Mechanism of the olivine-to-spinel phase transformation in Ni_2SiO_4, *Geophys. Res. Lett.*, *10*, 87–90, 1983.

Boley, B. A., and J. H. Weiner, *Theory of Thermal Stresses*, 586 pp., John Wiley, New York, 1960.

Brearley, A. J., and D. C. Rubie, Transformation mechanisms of San Carlos olivine to β-phase under subduction zone conditions, *Phys. Earth Planet. Inter.*, *86*, 45–67, 1994.

Brearley, A. J., D. C. Rubie, and E. Ito, Mechanisms of the transformations between the α, β and γ polymorphs of Mg_2SiO_4 at 15 GPa, *Phys. Chem. Miner.*, *18*, 343–358, 1992.

Bridgman, P. W., Polymorphic transition and geological phenomenon, *Am. J. Sci.*, *243A*, 90–97, 1945.

Brodholt, J., and S. Stein, Rheological control of Wadati-Benioff zone seismicity, *Geophys. Res. Lett.*, *15*, 1081–1084, 1988.

Buforn, E., A. Udias, and R. Madariaga, Intermediate and deep earthquakes in Spain, *Pure Appl. Geophys.*, *136*, 375–393, 1991.

Bullen, K. E., The problem of the Earth's density variation, *Bull. Seismol. Soc. Am.*, *30*, 235–250, 1940.

Burbach, G., and C. Frohlich, Intermediate and deep seismicity and lateral structure of subducted lithosphere in the Circum-Pacific regions, *Rev. Geophys.*, *24*, 833–874, 1986.

Burnley, P. C., The effect of nonhydrostatic stress on the olivine-spinel transformation in Mg_2GeO_4, Ph.D. thesis, 187 pp., Univ. of Calif., Davis, 1990.

Burnley, P. C., The fate of olivine in subducting slabs: A reconnaissance study, *Am. Mineral.*, *80*, 1293–1301, 1995.

Burnley, P. C., and H. W. Green, Stress dependence of the mechanism of the olivine-spinel transformation, *Nature*, *338*, 753–756, 1989.

Burnley, P., and S. H. Kirby, Pressure-induced embrittlement of polycrystalline tremolite $Ca_2Mg_5Si_8O_{22}(OH_2, F)_2$ (abstract), *Eos Trans. AGU*, *63*, 1095, 1982.

Burnley, P. C., H. W. Green, and D. Prior, Faulting associated with the olivine to spinel transformation in Mg_2GeO_4 and its implications for deep-focus earthquakes, *J. Geophys. Res.*, *96*, 425–443, 1991.

Cahill, T., and B. Isacks, Seismicity and shape of the subducted Nazca plate, *J. Geophys. Res.*, *97*, 17,503–17,529, 1992.

Cahn, J. W., The kinetics of grain boundary nucleated reactions, *Acta Metall.*, *4*, 449–459, 1956.

Cande, S. C., J. L. LaBrecque, R. L. Larson, W. C. Pitman III, X. Golovchenko, and W. F. Haxby, Magnetic lineations of the world's ocean basins, map, Am. Assoc. of Pet. Geol., Tulsa, Okla., 1989.

Chen, W.-P., En echelon ruptures during the great Bolivian earthquake of 1994, *Geophys. Res. Lett.*, *22*, 2261–2264, 1995.

Choy, G. L., and J. Boatwright, The rupture characteristics of two deep earthquakes inferred from broadband GDSN data, *Bull. Seismol. Soc. Am.*, *71*, 691–711, 1981.

Choy, G. L., and J. L. Boatwright, Global patterns of radiated energy release and apparent stress, *J. Geophys. Res.*, *100*, 18,205–18,228, 1995.

Christian, J. W., *The Theory of Transformations in Metals and Alloys*, vol. I, *Equilibrium and General Kinetic Theory*, 586 pp., Pergamon, Tarrytown, N. Y., 1975.

Chung, W.-Y., and H. Kanamori, Source process and tectonic implication of the Spanish deep-focus earthquake of March 29, 1954, *Phys. Earth Planet. Inter.*, *13*, 85–96, 1976.

Chung, W.-Y., and H. Kanamori, Variation of seismic source parameters and stress drops within a descending slab and its implications in plate mechanics, *Phys. Earth Planet. Inter.*, *23*, 134–159, 1980.

Cormier, V. F., Slab diffraction of *S* waves, *J. Geophys. Res.*, *94*, 3006–3024, 1989.

Coveny, P., and R. Highfield, *The Arrow of Time*, pp. 189–200, Fawcett Columbine, New York, 1990.

Creager, K. C., and T. H. Jordan, Slab penetration into the lower mantle, *J. Geophys. Res.*, *89*, 3031–3049, 1984.

Creager, K. C., and T. H. Jordan, Slab penetration into the lower mantle beneath the Mariana and other island arcs of the northwest Pacific, *J. Geophys. Res.*, *91*, 3573–3589, 1986.

Daessler, R., and D. A. Yuen, The effects of phase transition kinetics on subducting slabs, *Geophys. Res. Lett.*, *20*, 2603–2606, 1993.

Dainton, F. S., *Chain Reactions: An Introduction*, 226 pp., Methuen, New York, 1966.

Davies, G. F., Mechanics of subducted lithosphere, *J. Geophys. Res.*, *85*, 6304–6318, 1980.

Davies, J. H., and D. Stevenson, Physical model of source region of subduction zone volcanics, *J. Geophys. Res.*, *97*, 2037–2070, 1992.

Dell'Angelo, L., Defect structures in a quartz-tremolite rock under high stresses: Evidence for amorphization, in *Defects and Processes in the Solid State: Geoscience Applications, The McLaren Volume*, edited by J. N. Boland and J. D. FitzGerald, pp. 99–119, Elsevier, New York, 1993.

DeMets, C., R. G. Gordon, D. F. Argus, and S. Stein, Current plate motions, *Geophys. J. Int.*, *101*, 425–478, 1990.

Durham, W., H. Heard, and S. H. Kirby, Experimental deformation of polycrystalline ice: Preliminary results, *J. Geophys. Res.*, *88*, 377–392, 1983.

Dziewonski, A. M., A. Friedman, D. Giardini, and J. H. Woodhouse, Global seismicity of 1982: Centroid moment tensor solutions for 308 earthquakes, *Phys. Earth Planet. Inter.*, *33*, 76–90, 1983.

Dziewonski, A. M., G. Ekström, and M. P. Salganik, Centroid moment tensor solutions for April–June 1994, *Phys. Earth Planet. Inter.*, *88*, 69–78, 1995.

Ekstrom, G., Teleseismic analysis of the great 1994 Bolivia earthquake, *Eos Trans. AGU*, *75*(44), Fall Meet. Suppl., 465, 1994.

Ekström, G., and A. M. Dziewonski, Evidence of bias in estimations of earthquake size, *Nature*, *332*, 319–323, 1988.

Engdahl, E. R., R. D. van der Hilst, and J. Berrocal, Imaging of subducted lithosphere beneath South America, *Geophys. Res. Lett.*, *22*, 2317–2320, 1995.

Engebretson, D., and S. Kirby, Deep Nazca slab seismicity: why is it so anomalous?, *Eos Trans. AGU*, *73*(43), Fall Meet. Suppl., 379, 1992.

Fischer, K. M., T. H. Jordan, and K. C. Creager, Seismic constraints on the morphology of deep slabs, *J. Geophys. Res.*, *93*, 4773–4784, 1988.

Forsyth, D. W., and S. Uyeda, On the relative importance of the driving forces of plate motion, *Geophys. J. R. Astron. Soc.*, *43*, 163–200, 1975.

Frohlich, C., Kiyoo Wadati and early research on deep focus earthquakes: Introduction to special section on deep and intermediate focus earthquakes, *J. Geophys. Res.*, *92*, 13,777–13,788, 1987a.

Frohlich, C. H., Aftershocks and temporal clustering of deep earthquakes, *J. Geophys. Res.*, *92*, 13,944–13,956, 1987b.

Frohlich, C., The nature of deep focus earthquakes, *Annu. Rev. Earth Planet. Sci.*, *17*, 227–254, 1989.

Frohlich, C., Earthquakes with non-double-couple mechanisms, *Science*, *264*, 804–809, 1994a.

Frohlich, C., A break in the deep, *Nature*, *368*, 100–101, 1994b.

Frost, H. J., and M. F. Ashby, *Deformation-Mechanism Maps*, 166 pp., Pergamon, Tarrytown, N. Y., 1982.

Fukao, Y., Source process of a large deep-focus earthquake and its tectonic implication: The western Brazil earthquake of 1963, *Phys. Earth Planet. Inter.*, *5*, 61–76, 1972.

Fukao, Y., M. Obayashi, and H. Inoue, Subducting slabs stagnant in the mantle transition zone, *J. Geophys. Res.*, *97*, 4809–4822, 1992.

Furumoto, M., and Y. Fukao, Sesimic moments of great deep earthquakes, *Phys. Earth Planet. Inter.*, *11*, 352–357, 1976.

Geller, R. J., Scaling relations for earthquake source parame-

ters and magnitudes, *Bull. Seismol. Soc. Am.*, *66*, 1501–1523, 1976.

Geller, R. J., and H. Kanamori, Magnitudes of great shallow earthquakes from 1904 to 1952, *Bull. Seismol. Soc. Am.*, *67*, 587–598, 1977.

Giardini, D., and J. H. Woodhouse, Deep seismicity and modes of deformation in Tonga subduction zone, *Nature*, *307*, 505–509, 1984.

Giardini, D., and J. H. Woodhouse, Horizontal shear flow in the mantle beneath the Tonga arc, *Nature*, *319*, 551–555, 1986.

Gilbert, F., and A. M. Dziewonski, An application of normal mode theory to the retrieval of structural parameters and source mechanisms from seismic spectra, *Philos. Trans. R. Soc. London A*, *278*, 187–269, 1975.

Glennon, M. A., and W.-P. Chen, Ruptures of deep-focus earthquakes in the northwestern Pacific and their implications on seismogenesis, *Geophys. J. Int.*, *120*, 706–720, 1995.

Goto, K., Z. Suzuki, and H. Hamaguchi, Stress distribution due to olivine-spinel phase transition in descending plate and deep focus earthquakes, *J. Geophys. Res.*, *92*, 13,811–13,820, 1987.

Grand, S. P., Mantle shear structure beneath the Americas and surrounding oceans, *J. Geophys. Res.*, *99*, 11,591–11,621, 1994.

Green, H. W., II, Solving the paradox of deep earthquakes, *Sci. Am.*, *271*(3), 64–71, 1994.

Green, H. W., II, and P. C. Burnley, A new self-organizing mechanism for deep-focus earthquakes, *Nature*, *341*, 733–737, 1989.

Green, H. W., II. and H. Houston, The mechanics of deep earthquakes, *Annu. Rev. Earth Sci.*, *23*, 169–213, 1995.

Green, H. W., II, T. E. Young, D. Walker, and C. H. Scholz, Anti-crack associated faulting at very high pressure in natural olivine, *Nature*, *348*, 720–722, 1990.

Griggs, D. T., High-pressure phenomena with applications to geophysics, in *Modern Physics for the Engineer*, edited by L. N. Ridenour, pp. 272–305, McGraw-Hill, New York, 1954.

Griggs, D., The sinking lithosphere and the focal mechanism of deep earthquakes, in *The Nature of the Solid Earth*, edited by E. C. Robertson, pp. 361–384, McGraw-Hill, New York, 1972.

Griggs, D. T., and D. W. Baker, The origin of deep-focus earthquakes, in *Properties of Matter Under Unusual Conditions*, pp. 23–42, John Wiley, New York, 1968.

Griggs, D., and J. Handin, Observations on fracture and a hypothesis of earthquakes, *Mem. Geol. Soc. Am.*, *79*, 347–373, 1960.

Griggs, D. T., F. J. Turner, and H. C. Heard, Deformation of rocks at 500° to 800°C, in *Rock Deformation (A Symposium)*, edited by D. T. Griggs and J. Handin, *Mem. Geol. Soc. Am.*, *79*, 39–104, 1960.

Grimison, N. L., and W.-P. Chen, The Azores-Gibraltar plate boundary: Focal mechanisms, depths of earthquakes, and their tectonic implications, *J. Geophys. Res.*, *91*, 2029–2047, 1986.

Grunfest, I. J., Thermal feedback in liquid flow: Plane shear at constant stress, *Trans. Soc. Rheol.*, *7*, 195–207, 1963.

Gutenberg, B., The energy of earthquakes, *Q. J. Geol. Soc. London*, *112*, 1–14, 1956.

Gutenberg, B., and C. F. Richter, *Seismicity of the Earth and Associated Phenomena*, 2nd ed., Princeton Univ. Press, Princeton, N. J., 1954.

Hacker, B. R., and S. H. Kirby, High-pressure deformation of calcite marble and its transformation to aragonite under non-hydrostatic conditions, *J. Struct. Geol.*, *15*, 1207–1222, 1993.

Hamburger, M. W., and B. L. Isacks, Deep earthquakes in the southwest Pacific: A tectonic interpretation, *J. Geophys. Res.*, *92*, 13,841–13,854, 1987.

Handin, J., R. V. Hager Jr., M. Friedman and J. N. Feather, Experimental deformation of sedimentary rocks under confining pressure: Pore pressure tests, *Am. Assoc. Pet. Geol. Bull.*, *47*, 717–755, 1963.

Hara, T., K. Kuge, and H. Kawakatsu, Determination of the isotropic component of the 1994 Bolivia deep earthquake, *Geophys. Res. Lett.*, *22*, 2265–2268, 1995.

Helffrich, G., S. Stein, and B. Wood, Subduction zone thermal structure and mineralogy and their relation to seismic wave reflections and conversions at the slab/mantle interface, *J. Geophys. Res.*, *94*, 753–763, 1989.

Hobbs, B. E., and A. Ord, Plastic instabilities: Implications for the origin of intermediate and deep focus earthquakes, *J. Geophys. Res.*, *93*, 10,521–10,540, 1988.

Hodder, A. P., Thermodynamic constraints on phase changes as earthquake source mechanisms in subduction zones, *Phys. Earth Planet. Inter.*, *34*, 221–225, 1984.

Hogrefe, A., D. C. Rubie, T. G. Sharp, and F. Seifert, Metastability of enstatite in deep subducting lithosphere, *Nature*, *372*, 351–353, 1994.

Honda, S., D. A. Yuen, S. Balachandar, and D. Reutler, Three-dimensional instabilities of mantle convection with multiple phase transitions, *Science*, *259*, 1308–1311, 1993.

Houston, H., The non-double-couple component of deep earthquakes and the width of the seismogenic zone, *Geophys. Res. Lett.*, *20*, 1687–1690, 1993.

Houston, H., Deep earthquakes shake up debate (News and Views), *Nature*, *372*, 724, 1994.

Houston, H., and J. Vidale, The temporal distribution of seismic rupture during deep earthquake rupture, *Science*, *265*, 771–774, 1994.

Houston, H., and Q. Williams, Fast rise times and the physical mechanism of deep earthquakes, *Nature*, *352*, 520–522, 1991.

Hsui, A. T., and M. N. Toksöz, The evolution of thermal structures beneath a subduction zone, *Tectonophysics*, *60*, 43–60, 1979.

Huang, W.-C., S. H. Kirby, and S. Stein, Mechanics of deep-focus earthquakes and the fluxes of subducting lithosphere (abstract), *Eos Trans. AGU*, *72*(44), Fall Meet. Suppl., 513, 1991.

Huang, W.-C., G. Ekström, E. A. Okal, and M. P. Salganik, Application of the CMT algorithm to analog recordings of deep earthquakes, *Phys. Earth Planet. Inter.*, *83*, 283–297, 1994.

Huang, W.-C., E. O Okal, G. Ekström and M. P. Salganik, Centroid-moment-tensor solutions for deep earthquakes predating the digital era: The WWSSN dataset (1962–1976), *Phys. Earth Planet. Inter.*, in press, 1996.

Hubbert, M. K., and W. W. Rubey, Role of fluid pressure in mechanics of overthrust faulting, 1, Mechanics of fluid-filled porous solids and its application to overthrust faulting, *Geol. Soc. Am. Bull.*, *70*, 115–166, 1959.

Iidaka, T., and D. Furukawa, Double seismic zone for deep earthquakes in the Izu-Bonin subduction zone, *Science*, *263*, 1116–1118, 1994.

Iidaka, T., and D. Suetsugu, Seismological evidence for metastable olivine inside a subducting slab, *Nature*, *356*, 593–595, 1992.

Isacks, B., and P. Molnar, Distribution of stresses in the descending lithosphere from a global survey of focal mechanism solutions of mantle earthquakes, *Rev. Geophys.*, *9*, 103–174, 1971.

Isacks, B., L. Sykes, and J. Oliver, Spatial and temporal clustering of deep and shallow earthquakes in the Fiji-Tonga-Kermadec region, *Bull. Seismol. Soc. Am.*, *57*, 935–958, 1967.

Isacks, B., J. Oliver, and L. R. Sykes, Seismology and the new global tectonics, *J. Geophys. Res.*, *73*, 5855–5899, 1968.

Ito, E., and T. Katsura, A temperature profile of the mantle transition zone, *Geophys. Res. Lett.*, *16*, 425–428, 1989.

Ito, E., and H. Sato, Aseismicity in the lower mantle by superplasticity of the descending slab, *Nature*, *351*, 140–141, 1991.

Jarrard, R. D., Relations among subduction parameters, *Rev. Geophys.*, *24*, 217–284, 1986.

Jordan, T. H., Lithospheric slab penetration into the lower mantle beneath the Sea of Okhotsk, *J. Geophys.*, *43*, 473–496, 1977.

Kanamori, H., The energy release in great earthquakes, *J. Geophys. Res.*, *82*, 2981–2987, 1977.

Katsura, T., and E. Ito, The system Mg_2SiO_4-Fe_2SiO_4 at high pressures and temperatures: Precise determination of stabilities of olivine, modified spinel, and spinel, *J. Geophys. Res.*, *94*, 15,663–15,670, 1989.

Kawakatsu, H., Insignificant isotropic component in the moment tensor of deep earthquakes, *Nature*, *351*, 50–53, 1991.

Kennett, B. L. N., and E. R. Engdahl, Travel times for global earthquake location and phase identification, *Geophys. J. Int.*, *105*, 429–465, 1991.

Kerschhofer, L., D. C. Rubie, T. G. Sharp, and S. Seifert, Kinetics of the transformation of San Carlos olivine to spinel under subduction zone conditions, *Eos Trans. AGU*, *76*(46), Fall Meet. Suppl., F564, 1995.

Kikuchi, M., and M. Ishida, Source retrieval for deep local earthquakes with broadband records, *Bull. Seismol. Soc. Am.*, *83*, 1855–1870, 1993.

Kikuchi, M., and H. Kanamori, The mechanism of the deep Bolivia earthquake of June 9, 1994, *Geophys. Res. Lett.*, *21*, 2341–2344, 1994a.

Kikuchi, M., and H. Kanamori, The mechanism of the deep Bolivia earthquake of June 9, 1994, *Eos Trans. AGU*, *75*(44), Fall Meet. Suppl., 465, 1994b.

Kirby, S. H., Localized polymorphic phase transitions in high-pressure faults and applications to the physical mechanism of deep earthquakes, *J. Geophys. Res.*, *92*, 13,789–13,800, 1987.

Kirby, S. H., Intraslab earthquakes and phase changes in subducting lithosphere, *U.S. Natl. Rep. Int. Union Geod. Geophys. 1990–1994*, *Rev. Geophys.*, *33*, 287–297, 1995.

Kirby, S. H., and S. Stein, Thermodynamic theory of the energetics of deep earthquakes based on transformational faulting in metastable peridotite (abstract), *Eos Trans. AGU*, *73*(43), Fall Meet. Suppl., 378, 1992.

Kirby, S. H., and L. A. Stern, Experimental dynamic metamorphism of mineral single crystals, *J. Struct. Geol.*, *15*, 1223–1240, 1993.

Kirby, S. H., W. B. Durham, and H. C. Heard, Rheology of ices Ih, II and III at high pressures: A progress report, in *Ices in the Solar System*, edited by J. Klinger et al., pp. 711–729, D. Reidel, Norwell, Mass., 1985.

Kirby, S. H., W. B. Durham, and L. A. Stern, Mantle phase changes and deep-earthquake faulting in subducting lithosphere, *Science*, *252*, 216–225, 1991.

Kirby, S., W. Durham, and L. Stern, The Ice I → II transformation: Mechanisms and kinetics under hydrostatic and nonhydrostatic conditions, in *Physics and Chemistry of Ice*, edited by N. Maeno and T. Hondoh, pp. 456–463, Hokkaido Univ. Press, Sapporo, Japan, 1992.

Kirby, S. H., E. A. Okal and R. Engdahl, The 9 June 1994 Bolivian deep earthquake: An exceptional event in an extraordinary subduction zone, *Geophys. Res. Lett.*, *22*, 2233–2236, 1995a.

Kirby, S. H., E. A. Okal and E. R. Engdahl, Ultralarge very deep earthquakes: Dynamical triggering of transformational faults in regions of grossly metastable peridotite?, *Eos Trans. AGU*, *76*(46), Fall Meet. Suppl., F606–F607, 1995b.

Kirby, S., E. R. Engdahl and R. Denlinger, Intraslab earthquakes and arc volcanism: Dual physical expressions of crustal and uppermost mantle metamorphism in subducting slabs, in *Dynamics of Subduction*, *Geophys. Monogr. Ser.*, edited by G. B. Bebout et al., AGU, Washington, D. C., in press, 1996.

Kostoglodov, V. V., Maximum depth of earthquakes and phase transformation within the lithospheric slab descending in the mantle, in *Physics and Interior Structure of the Earth*, edited by V. A. Magnitsky, pp. 52–57, Nauka, Moscow, 1989.

Kuge, K., and H. Kawakatsu, Significance of non-double-couple components of deep and intermediate-depth earthquakes: Implications from moment tensor inversions of long-period seismic waves, *Phys. Earth Planet. Inter.*, *75*, 243–266, 1993.

Liu, L.-G., Phase transformations, earthquakes and the descending lithosphere, *Phys. Earth Planet. Inter.*, *32*, 226–240, 1983.

Lomnitz-Adler, J., Are deep-focus earthquakes caused by a martensitic transformation?, *J. Phys. Earth*, *38*, 83–98, 1990.

Lundgren, P. R., and D. Giardini, Seismicity, shear failure, and modes of deformation in deep seismic zones, *Phys. Earth Planet. Inter.*, *74*, 63–74, 1992.

Lundgren, P. R., and D. Giardini, Isolated deep earthquakes and the fate of subduction in the mantle, *J. Geophys. Res.*, *99*, 15,833–15,842, 1994.

McGarr, A., Seismic moments of earthquakes beneath island arcs, phase changes, and subduction velocities, *J. Geophys. Res.*, *82*, 256–264, 1977.

McKenzie, D. P., Speculations on the consequences and causes of plate motions, *Geophys. J. R. Astron. Soc.*, *18*, 1–32, 1969.

McKenzie, D. P., Temperature and potential temperature beneath island arcs, *Tectonophysics*, *10*, 357–366, 1970.

Meade, C., and R. Jeanloz, Acoustic emissions and shear instabilities during phase transformation in Si and Ge at ultra-high pressures, *Nature*, *339*, 616–618, 1989.

Meade, C., and R. Jeanloz, Deep-focus earthquakes and recycling of water into the Earth's mantle, *Science*, *252*, 68–72, 1991.

Mendiguren, J. A., and K. Aki, Source mechanism of the deep Colombian earthquake of 1970 July 31 from the free oscillation data, *Geophys. J. R. Astron. Soc.*, *55*, 539–556, 1978.

Minear, J., and M. N. Toksöz, Thermal regime of a downgoing slab and new global tectonics, *J. Geophys. Res.*, *75*, 1379–1419, 1970.

Mitronovas, W., and B. Isacks, Seismic velocity anomalies in the upper mantle beneath the Tonga-Kermadec island arc, *J. Geophys. Res.*, *76*, 7154–7180, 1971.

Molnar, P., D. Freedman, and J. S. F. Shih, Lengths of intermediate and deep seismic zones and temperatures in downgoing slabs of lithosphere, *Geophys. J. R. Astron. Soc.*, *56*, 41–54, 1979.

Nicolis, G., and I. Prigogine, *Exploring Complexity*, pp. 15–26, W.H. Freeman, New York, 1989.

O'Connell, R. J., On the scale of mantle convection, *Tectonophysics*, *38*, 119–136, 1977.

Ogawa, M., Shear instability in a visco-elastic material as the cause of deep-focus earthquakes, *J. Geophys. Res.*, *92*, 13,801–13,810, 1987.

Okal, E. A., Use of the mantle magnitude Mm for the reassessment of the seismic moment of historical earthquakes, II, Intermediate and deep events, *Pure Appl. Geophys.*, *139*, 59–85, 1992.

Okal, E. A., Radial modes from the great 1994 Bolivian earthquake: No evidence for an isotropic component to the source, *Geophys. Res. Lett.*, *23*, 431–434, 1996.

Okal, E. A., and C. R. Bina, The deep earthquakes of 1921–1922 in northern Peru, *Phys. Earth Planet. Inter.*, *83*, 283–297, 1994.

Okal, E. A., and R. J. Geller, On the observability of isotropic seismic sources: The July 31, 1970 Colombian earthquake, *Phys. Earth Planet. Inter.*, *18*, 176–196, 1979.

Okal, E. A., and S. H. Kirby, Deep earthquakes beneath the North Fiji Basin: Faulting in a detached and recumbent slab transforming from metastable peridotite to the slab transition zone mineral assemblage (abstract), *Eos Trans. AGU*, *74*(43), Fall Meet. Suppl., 97, 1993a.

Okal, E. A., and S. H. Kirby, Quantitative reassessment of the intermediate and deep seismicity of the Indonesian arc: Preliminary results (abstract), *Seismol. Res. Lett.*, *64*, 14, 1993b.

Okal, E. A., and S. H. Kirby, Frequency-moment relations for deep earthquakes and implications for the seismogenic zone in slabs, *Phys. Earth Planet. Inter.*, *92*, 169–187, 1995.

Okal, E. A., S. H. Kirby, and S. Stein, The onset of deep earthquakes in the Indonesia subduction zone: Relation to slab thermal parameter and mantle phase changes (abstract), *Eos Trans. AGU*, *74*(16), Spring Meet. Suppl., 308, 1993.

Okino, K., M. Ando, S. Kaneshima, and K. Hirahara, The horizontally lying slab, *Geophys. Res. Lett.*, *16*, 1059–1062, 1989.

Oliver, J., and B. Isacks, Deep earthquake zones, anomalous structures in the upper mantle, and the lithosphere, *J. Geophys. Res.*, *72*, 4259–4275, 1967.

Orowan, E., Convection in a non-Newtonian mantle, continental drift, and mountain building, *Philos. Trans. R. Soc. London A*, *258*, 284–313, 1965.

Page, R., Focal depths of aftershocks, *J. Geophys. Res.*, *73*, 3897–3903, 1968.

Paterson, M. S., *Experimental Rock Deformation: The Brittle Field*, Springer-Verlag, New York, 1978.

Peltier, W. R. (Ed.), *Mantle Convection*, Gordon and Breach, New York, 1989.

Poirier, J.-P., *Creep of Crystals*, 260 pp., Cambridge Univ. Press, New York, 1985.

Post, R. L., Jr., High-temperature creep of Mt. Burnet dunite, *Tectonophysics*, *42*, 75–110, 1977.

Prigogine, I., and I. Strengers, *Order Out of Chaos*, pp. 140–153, Bantam, New York, 1984.

Raleigh, C. B., Tectonic implications of serpentinite weakening, *Geophys. J. R. Astron. Soc.*, *14*, 113–118, 1967.

Raleigh, C. B., and M. S. Paterson, Experimental deformation of serpentine and its tectonic implications, *J. Geophys. Res.*, *70*, 3965–3985, 1965.

Reasenberg, P. A., and L. M. Jones, California aftershock hazard forecast, *Science*, *247*, 345–346, 1990.

Rees, B. A., and E. A. Okal, The depth of the deepest historical earthquakes, *Pure Appl. Geophys.*, *125*, 699–715, 1987.

Remsberg, A. R., J. N. Boland, T. Gasparik, and R. C. Liebermann, Mechanism of the olivine-spinel transformation in Co_2SiO_4, *Phys. Chem. Miner.*, *15*, 498–506, 1988.

Richter, F. M., Focal mechanisms and seismic energy release of deep and intermediate earthquakes in the Tonga-Kermadec region and their bearing on the depth extent of mantle flow, *J. Geophys. Res.*, *84*, 6783–6795, 1979.

Ringwood, A. E, Phase tranformations and differentiation in subducted lithosphere: Implications for mantle dynamics, basalt petrogenesis, and crustal evolution, *J. Geol.*, *90*, 611–643, 1982.

Royden, L. H., Evolution of retreating subduction boundaries formed during continental collision, *Tectonics*, *12*, 629–638, 1993.

Rubie, D. C., Reaction-enhanced ductility: The role of solid-solid univariant reactions in deformation of the crust and mantle, *Tectonophysics*, *96*, 331–352, 1983.

Rubie, D. C., The olivine → spinel transformation and the rheology of subducting lithosphere, *Nature*, *308*, 505–508, 1984.

Rubie, D. C., Mechanisms and kinetics of reconstructive phase transformations in the Earth's mantle, in *Short Course Handbook on Experiments at High Pressure and Applications to the Earth's Mantle*, vol 21, edited by R. W. Luth, pp. 247–303, Mineral. Assoc. of Can., Edmonton, Alberta, 1993.

Rubie, D. C., and C. R. Ross II, Kinetics of the olivine-spinel transformation in subducting lithosphere: Experimental constraints and implications for deep slab processes, *Phys. Earth Planet. Inter.*, *86*, 223–241, 1994.

Rubie, D. C., and A. B. Thompson, Kinetics of metamorphic reactions at elevated temperatures and pressures: An assessment of available experimental data, in *Metamorphic Reactions: Kinetics, Textures and Deformation, Adv. Phys. Geochem.*, vol. 4, edited by A. B. Thompson and D. C. Rubie, pp. 27–79, Springer-Verlag, New York, 1985.

Rubie, D. C., Y. Tsuchida, T. Yagi, W. Utsumi, T. Kikegawa, O. Shimomura, and A. J. Brearley, An in situ X ray diffraction study of the kinetics of the Ni_2SiO_4 olivine-spinel transformation, *J. Geophys. Res.*, *95*, 15,829–15,844, 1990.

Savage, J. C., The mechanics of deep-focus faulting, *Tectonophysics*, *8*, 115–127, 1969.

Saxena, S. K., N. Chatterjee, Y. Fei, and G. Shen, *Thermodynamic Data on Oxides and Silicates*, Springer-Verlag, New York, 1993.

Schmidt, M. W., and S. Pili, The stability of lawsonite and zoisite at high pressures: Experiments in CASH to 92 kbar and implications for the presence of hydrous phases in subducted lithophere, *Earth Planet. Sci. Lett.*, *124*, 105–118, 1994.

Scott, S. K., *Chemical Chaos*, 454 pp., Oxford Univ. Press, New York, 1991.

Sharp, T. G., and D. C. Rubie, Catalysis of the olivine to spinel transformation by high-clinoenstatite, *Science*, *269*, 1095–1098, 1995.

Silver, P., R. W. Carlson, and P. Olson, Deep slabs, geochemical heterogeneity, and the large-scale structure of mantle convection, *Annu. Rev. Earth Planet. Sci.*, *16*, 477–541, 1988.

Silver, P. G., et al., Rupture characteristics of the deep Bolivian earthquake of 9 June 1994 and the mechanism of deep-focus earthquakes, *Science*, *268*, 69–76, 1995.

Sleep, N. H., Teleseismic *P*-wave transmission through slabs, *Bull. Seismol. Soc. Am.*, *63*, 1349–1373, 1973.

Spakman, W., S. Stein, R. van der Hilst, and R. Wortel, Resolution experiments for NW Pacific subduction zone tomography, *Geophys. Res. Lett.*, *16*, 1097–1110, 1989.

Stark, P. B., and C. Frohlich, The depths of the deepest deep earthquakes, *J. Geophys. Res.*, *90*, 1859–1869, 1985.

Stein, C. A., and S. Stein, A model for the global variation in oceanic depth and heat flow with lithospheric age, *Nature*, *359*, 123–129, 1992.

Stein, S., Deep earthquakes: A fault too big?, *Science*, *268*, 49–50, 1995.

Stein, S., and G. C. Kroeger, Estimating earthquake source parameters from seismological data, in *Solid Earth Geophysics and Geotechniques, AMD Symp. Ser.*, vol. 42, edited by S. Nemet-Nasser, pp. 61–71, Am. Soc. of Mech. Eng., New York, 1980.

Stein, S., and A. Pelayo, Seismological constraints on stress in the oceanic lithosphere, *Philos. Trans. R. Soc. London A*, *337*, 53–72, 1991.

Stern, L. A., S. H. Kirby, and W. B. Durham, Textual observations of H_2O ice II nucleation and growth processes during phase transformations under hydrostatic and nonhy-

drostatic stress, *Eos Trans. AGU*, *75*(44), Fall Meet. Suppl., 635, 1994.

Sung, C. M., and R. G. Burns, Kinetics of high-pressure phase transformations: Implications to the evolution of the olivine-spinel transition in the downgoing lithosphere and its consequences on the dynamics of the mantle, *Tectonophysics*, *31*, 1–32, 1976a.

Sung, C. M., and R. G. Burns, Kinetics of the olivine-spinel transition: Implications to deep-focus earthquake genesis, *Earth Planet. Sci. Lett.*, *32*, 165–170, 1976b.

Sykes, L. R., The seismicity and deep structure of island arcs, *J. Geophys. Res.*, *71*, 2981–3006, 1966.

Sykes, L. R., Deep earthquakes and rapidly-running phase changes: A reply to Dennis and Walker, *J. Geophys. Res.*, *73*, 1508–1510, 1968.

Tao, W. C., and R. J. O'Connell, Deformation of a weak subducted slab and variation of seismicity with depth, *Nature*, *361*, 626–628, 1993.

Toksöz, M. N., J. W. Minear, and B. R. Julian, Temperature field and geophysical effects of a downgoing slab, *J. Geophys. Res.*, *76*, 1113–1138, 1971.

Toksöz, M. N., N. H. Sleep, and A. T. Smith, Evolution of the downgoing lithosphere and mechanisms of deep focus earthquakes, *Geophys. J. R. Astron. Soc.*, *35*, 285–310, 1973.

Tullis, J. A., Preferred orientations in experimentally deformed quartzites, Ph.D. thesis, Univ. of Calif., Los Angeles, 1971.

Turcotte, D. L., and G. Schubert, Structure of the olivine-spinel boundary in the subducting lithosphere, *J. Geophys. Res.*, *76*, 7980–7987, 1971.

Turcotte, D. L., and G. Schubert, Frictional heating of the descending lithosphere, *J. Geophys. Res.*, *78*, 5876–5886, 1973.

Turnbull, D., Phase changes, *Solid State Phys.*, *3*, 225–306, 1956.

Ulmer, P., and V. Trommsdorff, Serpentine stability to mantle depths and subduction-related magmatism, *Science*, *26*, 858–861, 1995.

Utsu, T., Anomalies in seismic wave velocity and attenuation associated with a deep earthquake zone, *Hokkaido Univ. Fac. Sci. J., Ser. 7, Geophysics*, *3*, 1–25, 1967.

Utsu, T., Seismological evidence of anomalous structure of island arcs with special reference to the Japanese region, *Rev. Geophys.*, *9*, 839–890, 1971.

Uyeda, S., *The New View of the Earth*, W. H. Freeman, New York, 1978.

van der Hilst, R., Complex morphology of subducted lithosphere in the mantle beneath the Tonga trench, *Nature*, *374*, 154–157, 1995.

van der Hilst, R., R. Engdahl, W. Spakman, and G. Nolet, Tomographic imaging of subducted lithosphere below northwest Pacific island arcs, *Nature*, *353*, 37–43, 1991.

van der Hilst, R., R. Engdahl, and W. Spakman, Tomographic inversion of *P* and *pP* for aspheric mantle structure below the northwest Pacific region, *Geophys. J. Int.*, *115*, 264–302, 1993.

Vasco, D. W., and L. R. Johnson, Inversion of waveforms for extreme source models with an application to the isotropic moment tensor component, *Geophys. J.*, *97*, 1–18, 1989.

Vassiliou, M. S., and B. H. Hager, Subduction zone earthquakes and stress in slabs, *Pure Appl. Geophys.*, *128*, 547–624, 1988.

Vaughan, P. J., H. W. Green, and R. S. Coe, Anisotropic growth in the olivine-spinel transformation of Mg_2GeO_4 under nonhydrostatic stress, *Tectonophysics*, *108*, 299–322, 1984.

Veevers, J., Powell, C., and Roots, R., Review of seafloor spreading around Australia, I, Synthesis of the patterns of spreading, *Aust. J. Earth Sci.*, *38*, 383–390, 1991.

Viasnys, J. R., and C. C. Pilbeam, Deep earthquake initiation by phase transformations, *J. Geophys. Res.*, *81*, 985–988, 1976.

Vidale, J. E., Waveform effects of a high velocity subducted slab, *Geophys. Res. Lett.*, *14*, 542–545, 1987.

Vidale, J. E., and H. Houston, The depth dependence of earthquake duration and implications for rupture mechanisms, *Nature*, *365*, 45–47, 1993.

Visser, S. W., Some remarks on the deep-focus earthquakes in the International Seismological Summary, *Gerlands Beit. Geophys.*, *48*, 254–267, 1936.

Wadati, K., Shallow and deep earthquakes, *Geophys. Mag.*, *1*, 162–202, 1928.

Wadati, K., On the activity of deep-focus earthquakes in the Japanese Islands and neighborhoods, *Geophys. Mag.*, *8*, 305–325, 1935.

Widiyantoro, S., and R. van der Hilst, The slab of subducted lithosphere beneath the Sunda arc, Indonesia, *Science*, *271*, 1566–1570, 1996.

Wiens, D. A., and J. J. McGuire, The 1994 Bolivia and Tonga events: Fundamentally different types of deep earthquakes, *Geophys. Res. Lett.*, *22*, 2245–2248, 1995.

Wiens, D. A., J. J. McGuire, and P. J. Shore, Evidence for transformational faulting from a deep double seismic zone in Tonga, *Nature*, *364*, 790–793, 1993.

Wiens, D., et al., A deep earthquake aftershock sequence and implications for the rupture mechanism of deep earthquakes, *Nature*, *372*, 540–543, 1994.

Willemann, R. J., and C. Frohlich, Spatial patterns of aftershocks of deep focus earthquakes, *J. Geophys. Res.*, *92*, 13,927–13,943, 1987.

Woodward, D. J., Stresses due to phase changes in subduction zones and an empirical equation of state for the mantle, *Geophys. J. R. Astron. Soc.*, *50*, 459–472, 1977.

Wortel, M. J. R., Seismicity and rheology of subducted slabs, *Nature*, *296*, 553–556, 1982.

Wortel, M. J. R., and N. J. Vlaar, Subduction zone seismicity and the thermo-mechanical evolution of downgoing lithosphere, *Pure Appl. Geophys.*, *128*, 625–659, 1988.

Wortel, R., Deep earthquakes and the thermal assimilation of subducting lithosphere, *Geophys. Res. Lett.*, *13*, 34–37, 1986.

Wu, T. C., W. Bassett, P. Burnley, and M. Weathers, Shear-promoted phase transitions in Fe_2SiO_4 and Mg_2SiO_4 and the mechanism of deep earthquakes, *J. Geophys. Res.*, *98*, 19,767–19,776, 1993.

Wysession, M. E., E. A. Okal, and K. L. Miller, Intraplate seismicity of the Pacific Basin, 1913–1988, *Pure Appl. Geophys.*, *135*, 261–359, 1991.

Wyss, M., and P. Molnar, Source parameters of intermediate and deep focus earthquakes in the Tonga arc, *Phys. Earth Planet. Inter.*, *6*, 279–292, 1972.

Zhou, H.-W., How well can we resolve the deep seismic slab with seismic tomography?, *Geophys. Res. Lett.*, *15*, 1425–1428, 1988.

Zhou, H.-W., Observations on earthquake stress axes and seismic morphology of deep slabs, *Geophys. J. Int.*, *103*, 377–401, 1990.

S. H. Kirby, U.S. Geological Survey, Mail Stop 977, 345 Middlefield Road, Menlo Park, CA 94025. (e-mail: skirby@isdmnl.wr.usgs.gov)

E. A. Okal and S. Stein, Department of Geological Sciences, Northwestern University, Evanston, IL 60208. (e-mail: okal@earth.nwu.edu; seth@earth.nwu.edu)

D. C. Rubie, Bayerisches Geoinstitut, Universität Bayreuth, D-95440 Bayreuth, Germany.